FOUNDATION DESIGN OF A NEW HOSPITAL BUILDING IN KECSKEMÉT

LUÍS MIGUEL CUNHA E COSTA

Dissertação submetida para satisfação parcial dos requisitos do grau de

MESTRE EM ENGENHARIA CIVIL — ESPECIALIZAÇÃO EM GEOTECNIA

Orientador: Professor Doutor António Joaquim Pereira Viana da Fonseca

Coorientador: Professor Doutor András Mahler

JULHO DE 2013

MESTRADO INTEGRADO EM ENGENHARIA CIVIL 2012/2013
DEPARTAMENTO DE ENGENHARIA CIVIL

Tel. +351-22-508 1901

Fax +351-22-508 1446

✉ miec@fe.up.pt

Editado por

FACULDADE DE ENGENHARIA DA UNIVERSIDADE DO PORTO

Rua Dr. Roberto Frias

4200-465 PORTO

Portugal

Tel. +351-22-508 1400

Fax +351-22-508 1440

✉ feup@fe.up.pt

http://www.fe.up.pt

Ao meu avô Bernardino

ACKNOWLEDGMENTS

The author would like to express his appreciation and gratitude to some people who contributed decisively to the final result of the current dissertation.

To Professor António Viana da Fonseca, firstly, for having made possible the current work in Budapest and after for all the help and valuable suggestions during the work, despite the physical distance.

To Professor András Mahler, for accepting the co-supervision proposal, for suggesting the thesis subject and for all the recommendations and help provided during my stay in Budapest.

To Structural Engineer Gábor Schnierer, for the help provided during the model implementation in AxisVM.

To my Friends, for the friendship during all these years, for the bohemian moments, for the good conversations and for the care. We are *Bon Vivants*!

To my Brother Gonçalo, for the great friendship and for the unthinkable moments of humor shared.

To my girlfriend Catarina, for all the motivation, support and specially for the selfless love.

Finally and most importantly to my Parents, for believing in me and for the unconditional love and support.

ABSTRACT

The goal of the current work was the design of a new hospital building located in Kecskemét, Hungary, focusing essentially geotechnical aspects. In this way, the calculation procedure took into account both the ultimate limit state and the serviceability limit state.

Initially, it was treated the CPTU data collected in the site, which permitted the correct definition of soil stratigraphy, resistance and deformability properties and subsequently the accurate assessment of the most effective foundation system.

After opting for a deep foundation solution, an ultimate state calculation was performed in order to determine the capacity of a single pile, clearly identifying the influence of each of its components, base resistance and shaft resistance. The obtained results led to a possible piled raft system.

The stress-strain analysis was carried out by a computer program based on the finite element method, AxisVM, and compared with a simplified hand calculation method. As usual in deformation problems analysis, associated to less severe consequences for the structure, a serviceability limit state is defined.

The reinforcement of both piles and raft was performed under the ultimate limit state assuring moderate concrete pressures to avoid cracking. AxisVM was used to perform the referred calculations.

Finally, a drainage system solution was proposed considering the initial high level of the water table. To run this calculation the Flow Mode of the program Plaxis 2D was selected and the solution found was compared with an empirical hand calculation method.

KEYWORDS: Bearing Capacity, CPTU test, Deep Foundations, Drainage, Piles, Raft, Settlement.

RESUMO

O objetivo do presente trabalho foi o dimensionamento de um edifício de um novo hospital localizado em Kecskemét, Hungria, focado essencialmente nos aspectos da Engenharia Geotécnica. Neste sentido, no processo de cálculo foram tidos em conta os estados limite último e de serviço.

Inicialmente, foi tratada a informação relativa aos ensaios CPTU efetuados *in situ* que permitiram a correta definição da estratigrafia do solo, das características de resistência e deformabilidade e consequentemente a avaliação mais eficaz do sistema de fundações.

Depois da opção por um sistema de fundações profundas, foi determinada a capacidade de carga de uma única estaca em estado limite último, evidenciando claramente a influência de cada uma das suas componentes, resistência de ponta e resistência lateral. Os resultados obtidos permitiram obter uma possível solução de estacas.

A análise tensão-deformação foi elaborada através de um programa baseado no Método dos Elementos Finitos, AxisVM e comparado com o método simplificado de cálculo manual. Tal como é habitual na análise de problemas de deformação, o dimensionamento é condicionando pelo estado limite de serviço.

O cálculo da armadura das estacas e do maciço de encabeçamento obedeceu ao estado limite último assegurando de tal modo tensões moderadas no betão evitando a fendilhação deste. O programa AxisVM foi de novo utilizado para este cálculo.

Por fim, foi proposta uma solução de drenagem tendo em conta a posição inicial elevada do nível freático. Este cálculo foi efetuado no programa Plaxis 2D através da opção *Flow* e mais uma vez a solução obtida foi confrontada com um método mais simplificado, desta feita de natureza empírica.

PALAVRAS-CHAVE: Assentamento, Capacidade de Carga, Drenagem, Ensaio CPTU, Estacas, Fundações profundas, Maciço de Encabeçamento.

ÖSSZEFOGLALÓ

A diplomamunka célja egy Kecskeméten létesítendő új kórházépület geotechnikai vonatkozású terveinek elkészítése volt. A tervezést mind a használhatósági mind a teherbírási határállapotok figyelembe vételével kellett végezni.

Elsőként, a területen mélyített CPT eredmények alapján került meghatározásra a talajrétegződés valamint a talajrétegek nyírószilárdsági és alakváltozás jellemzői. Ezen eredmények alapján választottam ki az épület szempontjából megfelelő alapozási módot.

A mélyalapozás kiválasztását követően számítással meghatároztam egy egyedi cölöp törőterhét, illetve annak komponenseit a köpenymenti és a talpellenállást. A kapott eredmények alapján a vizsgált épülethez a lemezzel kombinált cölöpalapozást választottam.

A lemez igénybevételeinek meghatározását az AxisVM, véges elemes számítógépes programmal végeztem, majd a kapott eredményeket összehasonlítottam az egyszerűsített számítási módszer eredményeivel. Ahogy az megszokott az alakváltozási problémák esetén a használhatósági határállapotot vettem figyelembe a számítás során.

A lemez és a cölöpök vasalásának méretezése a teherbírási határállapot figyelembe vételével készült. Ezekhez a számításokhoz az AxisVM programot használtam.

Végezetül a munkagödör víztelenítésének tervezést végeztem el. Ennek során a kezdeti magas talajvízszintet tekintettem kiindulási állapotnak. A számítások elvégzéséhez a Plaxis 2D véges elemes program „flow” számítási módozatát használtam. A kapott eredmények itt is tapasztalati, kézi módszerekkel meghatározott eredményekkel vetettem össze.

KULCSSZAVAK: Cölöpök, CPTu vizsgálat, lemezalap, mélyapaozás, süllyedés, teherbírás, víztelenítés.

TABLE OF CONTENTS

LIST OF FIGURES

LIST OF TABLES

NOMENCLATURE

Latin Characters

A – coefficient to determine the pile interaction factor (α)

A_b – pile cross-sectional area (m^2)

A_c – projected area of the cone (m^2)

A_c – pile cross-sectional concrete area (m^2)

A_N – projected area associated to cone inner diameter (m^2)

A_S – area of friction sleeve (m^2)

A_s – longitudinal reinforcement area (m^2)

$A_{s;bpmin}$ – minimum longitudinal reinforcement area (m^2)

A_{si} – shaft area associated to soil layer "i" (m^2)

A_T – projected area associated to cone outer diameter, equal to A_c (m^2)

B – smaller width of a rectangular foundation (m)

B – coefficient to determine the pile interaction factor (α)

B_q – pore pressure parameter

C – coefficient to determine the pile interaction factor (α)

C_s – linear correction factor

D – cone outer diameter (m)

D – pile diameter (m)

D – coefficient to determine the pile interaction factor (α)

D_b – diameter of pile base (m)

D_{eq} – equivalent pile diameter (m)

d – cone inner diameter (m)

eZ – displacement in vertical (z) direction

E – Young's modulus (MPa)

E_b – soil Young's modulus below foundation base (kPa, MPa)

E_p – pile modulus (kPa, MPa)

E_{sL} – Young's Modulus at the pile tip (kPa, MPa)

E_{sm} – soil Young's modulus at mid-depth of pile shaft (kPa, MPa)

$F_{c;d}$ – design load applied to a certain column, at the ultimate limit state (kN)

$F_{k;max}$ – maximum characteric load applied to a pile (kN)

f_{cj} – characteristic compressive cylinder strength of concrete at j days (MPa)

f_{clim} – limit strength of concrete depending on pile foundation type (MPa)

f_{c28} – compressive cylinder strength of concrete at 28 days (MPa)

f_c* – concrete compressive strength (MPa)

F_s – total force acting on friction sleeve (kN)

f_s – unit sleeve friction resistance (kPa, MPa)

G_s – specific gravity of the soil

H – height of the static water table (m)

H_c – total height of clay strata (m)

h_D – maximum residual head (m)

h_j – thickness of stratum “j” (m)

H_s – total height of sand strata (m)

h_0 – height of the water table in wells (m)

I_c – soil behaviour type index

I_ε – vertical strain influence factor

$I_{\varepsilon c}$ – continues foundation I_ε

$I_{\varepsilon p}$ – peak of I_ε

$I_{\varepsilon s}$ – axisymmetric foundation I_ε

I_ρ – displacement influence factor

K_c – pile tip bearing factor

k – modulus of subgrade reaction (kN/m^3)

k – soil coefficient of permeability (m/s)

k_c – clay coefficient of permeability (m/s)

k_{eq} – equivalent soil coefficient of permeability (m/s)

k_s – sand coefficient of permeability (m/s)

k_x – horizontal soil coefficient of permeability (m/s)

k_y – vertical soil coefficient of permeability (m/s)

k_p – pile flexibility (kN/m)

k_s – soil modulus of subgrade reaction (kN/m^3)

k_1 – coefficient that takes into account the execution method of the pile

k_2 – coefficient that takes into account the difficulty related to the concrete casting of the pile

L – pile length (m)

L – greater width of a rectangular foundation (m)

M – constrained deformation modulus (MPa)

n – number of piles per column

p – raft distributed load (kN/m^2)

P_{av} – average load on a pile within the group (kN/m)

p_a – atmospheric stress (kPa, MPa)

p_l – Ménard Limit Pressure (kPa, MPa)

p_{LM} – Ménard Limit Pressure (kPa, MPa)

P_T – unit load applied on pile *I* (kN)

$p_{max;base}$ – maximum base resistance (kPa, MPa)

Q – flow (m^3/s/m, m^3/day/m, L/day/m)

Q_{avg} – average flow (m^3/s/m, m^3/day/m, L/day/m)

Q_b – pile end bearing capacity (kN)

q_b – pile unit end resistance (kPa, MPa)

Q_c – total force acting on the cone (kN)

q_c – measured cone resistance (MPa)

q_{ce} – cone resistance around the base (kPa, MPa)

$q_{c;I;mean}$ – component of $p_{max;base}$ formula (kPa, MPa)

$q_{c;i;avg}$ – the layer “i” average q_c (kPa)

$q_{c;II;mean}$ – component of $p_{max;base}$ formula (kPa, MPa)

$q_{c;III;mean}$ – component of $p_{max;base}$ formula (kPa, MPa)

q_E – effective cone resistance (kPa, MPa)

Q_s – pile shaft friction capacity (kN)

q_s – pile shaft friction resistance (kPa, MPa)

q_{si} – pile unit side friction (kPa, MPa)

$q_{si;c}$ – pile unit side friction in cohesive stratum (kPa)

$q_{si;g}$ – pile unit side friction in granular stratum (kPa)

$q_{s;max}$ – upper limit of shaft friction (kPa, MPa)

Q_{ult} – ultimate pile axial capacity (kN)

|q| – absolute mode of flow (m^3/s/m, m^3/day/m, L/day/m)

$|q|_{avg}$ – average absolute mode of flow (m^3/s/m, m^3/day/m, L/day/m)

R_b – pile end bearing resistance (kN)

$R_{b;cal}$ – pile base resistance, calculated from ground test results, at the ultimate limit state (kN)

$(R_{b;cal})_{mean}$ – average of $R_{b;cal}$ in the tests performed (kN)

$(R_{b;cal})_{min}$ – miminum of $R_{b;cal}$ in the tests performed (kN)

$R_{b;k}$ – characteristic value of the base resistance of a pile (kN)

R_c – compressive resistance of the ground against a pile, at the ultimate limit state (kN)

$R_{c;cal}$ – calculated value of R_c (kN)

$(R_{c;cal})_{mean}$ – average of $R_{c;cal}$ in the tests performed (kN)

$(R_{c;cal})_{min}$ – miminum of $R_{c;cal}$ in the tests performed (kN)

$R_{c;d}$ – design value of R_c (kN)

$(R_{c;d})_{gd}$ – design value of R_c of greater diameter pile

$(R_{c;d})_{sd}$ – design value of R_c of smaller diameter pile

$R_{cd;DTU}$ – design value of R_c calculated according DTU 13.2 norm (kN)

$R_{cd;EC7}$ – design value of R_c calculated according EC7 Approach (kN)

$R_{c;DTU}$ – value of R_c calculated according DTU 13.2 norm (kN)

$R_{c;k}$ – characteristic value of R_c (kN)

R_f – friction ratio

$R_{s;cal}$ – ultimate shaft friction, calculated using ground parameters from test results (kN)

$(R_{s;cal})_{mean}$ – average of $R_{s;cal}$ in the tests performed (kN)

$(R_{s;cal})_{min}$ – miminum of $R_{s;cal}$ in the tests performed (kN)

$R_{s;k}$ – characteristic value of the shaft resistance of a pile (kN)

R_s – pile shaft friction resistance (kN)

R_o – distance of the line source (m)

R^2 – coefficient of determination

s – pile shape factor

s – spacing between piles (m)

s – pile settlement (mm)

s_{avg} – average pile settlement (mm)

s_{max} – maximum pile settlement (mm)

s_i – immediate settlement by Schmertmann method (m)

s_1 – settlement of a single pile under unit load (m)

u – pore water pressure (kPa, MPa)

u_0 – *in situ* pore pressure (kPa, MPa)

u_1 – pore pressure measured on the cone (kPa, MPa)

u_2 – pore pressure measured behind cone (kPa, MPa)

u_3 – pore pressure measured behind friction sleeve (kPa, MPa)

x – length of the trench (m)

w – raft settlement (m)

w_i – global settlement of the pile i within a group of n piles (m)

w_t – equal to s_1 (m)

z – depth (m)

Greek Characters

α – modulus factor for estimating Young's modulus

α – pile interaction factor

α – angular distortion (%)

α_{avg} – average angular distortion (%)

α_{max} – maximum angular distortion (%)

α_E – modulus factor for estimating Young's modulus from net cone resistance

α_{ij} – pile interaction factor

$\alpha_{ij;avg}$ – average pile interaction factor

α_M – constrained modulus cone factor

α_p – pile class factor;

$\alpha_{s;c}$ – shaft friction factor in cohesive stratum

$\alpha_{s;g}$ – shaft friction factor in granular stratum

β – pile shape factor

β – correlation factor

γ – total unit weight (kN/m^3)

γ_G – partial factor for permanent actions, G

γ_Q – partial factor for variable actions, Q

γ_t – partial factor for total resistance of a pile

Δq_s – net foundation pressure (kPa)

Δs – differential settlement (mm)

Δs_{avg} – average differential settlement (mm)

Δs_{max} – maximum differential settlement (mm)

ζ – zeta factor

η_1 – eta factor

λ – lambda factor

μ_L – mu factor

v – Poisson's ratio

v_s – Poisson's ratio

ξ – correlation factor depending on the number of piles tested or of profiles of tests

ξ – xi factor

ξ_3 – correlation factor to derive the pile resistance from ground investigation results

ξ_4 – correlation factor to derive the pile resistance from ground investigation results

ρ – rho factor

$\sigma_{c,max}$ – maximum compressive strength of concrete (MPa)

$\sigma_{c,mean}$ – average compressive strength of concrete (MPa)

σ_{vo} – total overburden stress (kPa)

σ'_{vb} – effective vertical stress at foundation level (kPa)

σ'_{vo} – effective overburden stress (kPa)

Φ – pile diameter (m)

Φ – rebar diameter (mm)

Abbreviations and Acronyms

ASTM – American Society for Testing and Materials

BAEL – *Béton Armé aux Etats Limites*

CFA – Continuous flight auger

CPT – Cone penetration test

CPT1 – CPT log number 1

CPT2 – CPT log number 2

CPT3 – CPT log number 3

DD – drilled-displacement

DTU – *Document technique unifié*

EC2 – Eurocode 2

EC7 – Eurocode 7

Ft – Hungarian Forints

IFM – Interaction Factor Method

LCPC – *Laboratoire Central des Ponts et Chausées*

mBf – *méter Balti felett* (Hungarian for meters above Baltic Sea)

OCR – overconsolidation ratio

PMT – Pressuremeter Test

SBT – Soil behaviour type

SBTn – Normalized soil behaviour type

SPT – Standard penetration test

1 INTRODUCTION

1.1. PROLOGUE

The foundations design is one of the basic elements of a Civil Engineering project since it assures the global stability of the superstructure. In order to achieve the required level of safety, the Geotechnical Engineer has to assess the most efficient foundation system, by choosing between a shallow or a deep foundation solution and then the subsequent design.

In the scope of this work, a mixed direct and indirect foundation system was selected, defined by the interaction of piles with a mat slab. The lack of soil strength at shallow depths demands the use of piles, which transmit the vertical loads to a certain depth where the soil bearing capacity is sufficient to absorb the given design loads.

The design of deep foundations is based on empirical and/or semi-empirical methods. These methods are based on experimental data obtained from tests performed in specific locations. The developed methods tend to be as much accurate as possible for that particular site. In order to adapt them for other soil types, it is necessary to evaluate its feasibility and define proper correlations regarding the involved soil and the structural foundation elements (piles and slab).

Nowadays, numerical methods are an essential tool in foundations design. These are often compared with the solutions obtained with empirical methods, which will be directly by their validation from the calibration of their results.

1.2. SCOPE AND OBJECTIVES

The subject of the current thesis, under the supervision of Professor António Viana da Fonseca, was proposed by Professor András Mahler, who was the co-supervisor during the period (dedicated to the development of this thesis) in Budapest. The objective was the geotechnical foundation design of a new hospital located in Kecskemét, a city in central Hungary, 86 km from Budapest.

Considering the scope of a master thesis, the author sought to show different approaches to solve the same type of problem evidencing at the same time the wide range of proposals and consequent solutions that dominate Geotechnics at the present time.

The proposed objectives are part of the normal geotechnical project issues. Starting with the description of soil conditions based on existing soil investigation (CPTu tests), a fully characterization of the ground conditions from a geotechnical point of view was conducted. After the complete interpretation of the *in situ* tests, it was necessary to calculate the pile bearing capacity (for different pile types) to define a possible foundation system and to calculate the concrete steel reinforcement.

The assessment of the piled raft settlements was also carefully discussed and analysed. Finally, considering the site water conditions, a dewatering system in the excavation pit was also designed.

1.3. ORGANIZATION OF THE THESIS

The present dissertation is divided in eight chapters and one appendix. The defined structure was considered adequate to cover all the proposed subjects, starting with more general chapters (2 and 3), where initial considerations are addressed and the methodologies are described, followed by the calculation and the respective result presented in chapters 4, 5, 6 and 7.

In Chapter 1, a brief introduction of the present work is made, including the scope and objectives and the organization of the thesis.

In Chapter 2, the geological and geotechnical framework of the construction site is defined, including the foundations type choice, the adopted soil stratigraphy and the estimation of soil strength and deformability parameters.

Chapter 3 presents all the methodologies used to perform the calculation of both the pile single bearing capacity and piled raft settlements.

In Chapter 4, the results regarding pile single capacity are summarized, as well as the choice between the two execution methods studied for piles (CFA and OMEGA), leading to a possible piled foundation system.

Chapter 5 presents the settlements estimation, where a numerical method is confronted with an empirical methodology.

In Chapter 6 all the reinforcement calculations are included, for the both the piles and the slab. The same numerical program referred in the previous chapter was used to perform the reinforcement slab calculation. The pile reinforcement was calculated according to Eurocode 2.

Chapter 7 presents a possible dewatering solution for the executed excavation. Again, a numerical calculation was performed and compared with an empirical method.

Finally, in Chapter 8, the final observations are made, regarding the main conclusions of the present work.

In Appendix A is presented the characteristic and design loads applied on the piles as well as a plan view of the design loads over the columns.

2
GEOLOGICAL AND GEOTECHNICAL FRAMEWORK OF THE CONSTRUCTION SITE

2.1. PROJECT DETAILS

The object of study of this work is the "A Building" foundations design, where area is highlighted in Figure 2.1 with a red contour.

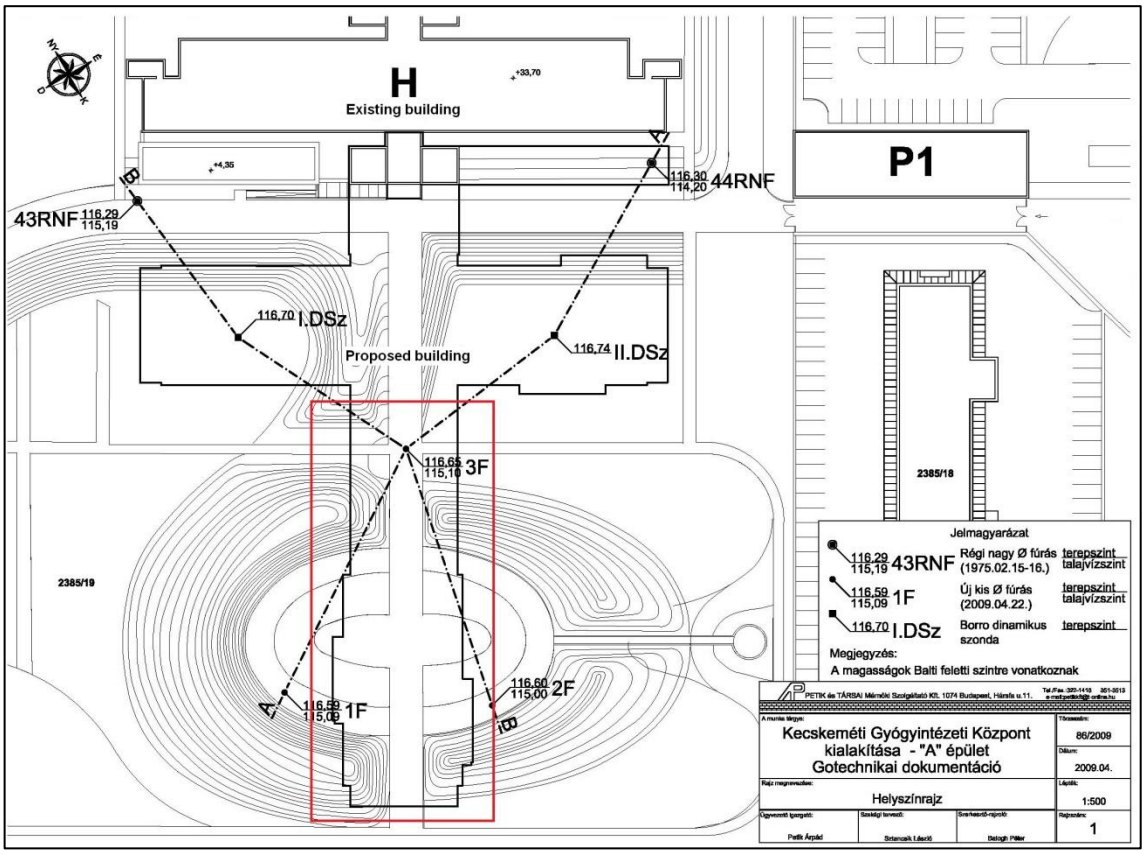

Figure 2.1 – Detail of the construction area (Petik and Partners Engineering Service Ltd)

The hospital's working platform is at the 112.400 mBf level from an initial ground level ranging from 116.29 mBf (drilling 43RNF) to 116.82 mBf, meaning an excavation varying from 3.89 m to 4.42 m. The inclination of the slopes is 3:2.

As it was referred previously, the objective was the geotechnical foundation design of a new hospital located in Kecskemét, constructed in 2009 (Figure 2.2).

Figure 2.2 – Overview of the constructed building

2.2. GEOLOGY

The hospital's construction area, represented on the geological map (Figure 2.3), is located in formations deposited during different phases of the Quaternary Period, being some of them relatively recent. The initial letter of the abbreviators in the legend of Figure 2.3, 'Q', represents the referred geological period.

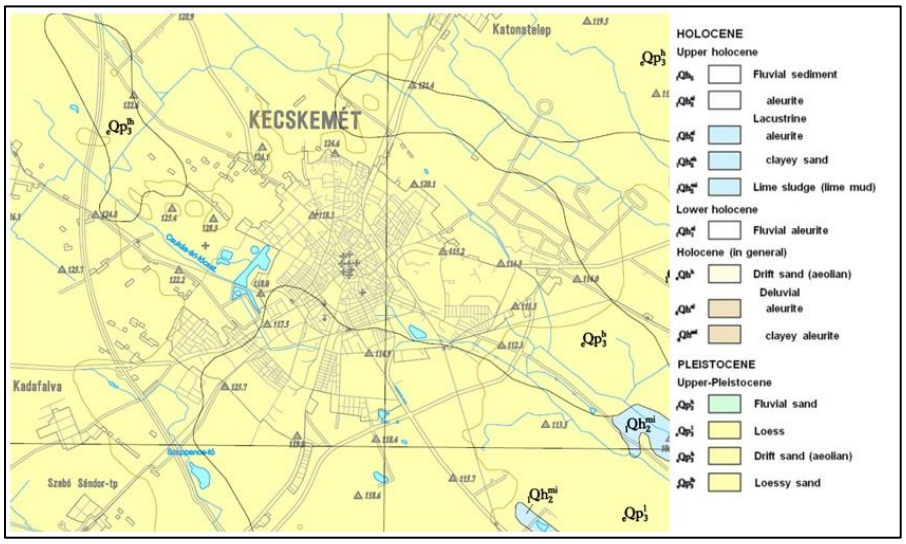

Figure 2.3 – Geological Map of Kecskemét, Bács-Kiskun County, scale 1:100000 (Gyalog, 2005)

The sediments of the Quaternary form a thin superficial layer of approximately 10 m, being composed essentially by coarse grained deposits. The older subsequent stratum consists of compact clayey layers and alluvial sediments, which are loose and formed by the mixture of sand and clay. Underlain a thousand meters thick Upper Pannonian lacustrine sequence, arises Fluvial Quaternary deposits.

2.3. GEOTECHNICAL OVERVIEW AND CHARACTERIZATION

During the survey, several boreholes were executed that allowed the definition of soil stratigraphy associated to the working area. In the plan view shown in Figure 2.1 are represented the respective locations of the seven drilling holes, that allowed the definition of two cross sections, A-A and B-B. The depth of drillings are twelve meters (1F, 2F and 3F) and sixteen meters (I.DSz, II.DSz and 44RNF), with dynamic probing heavy (DPH) tests – not used in the further geotechnical interpretation – performed alongside the boreholes I.DSz and II.DSz.

The cross section A-A (Figure 2.4) shows an embankment of an anthropic clayey deposit 1.5 m thick, followed by a slightly organic silt-clay stratum with two meters thickness. Around the four meters depth, the drillings performed distinguished two different soil types, on the left the predominance of sandy silt ground and on the right silty sand.

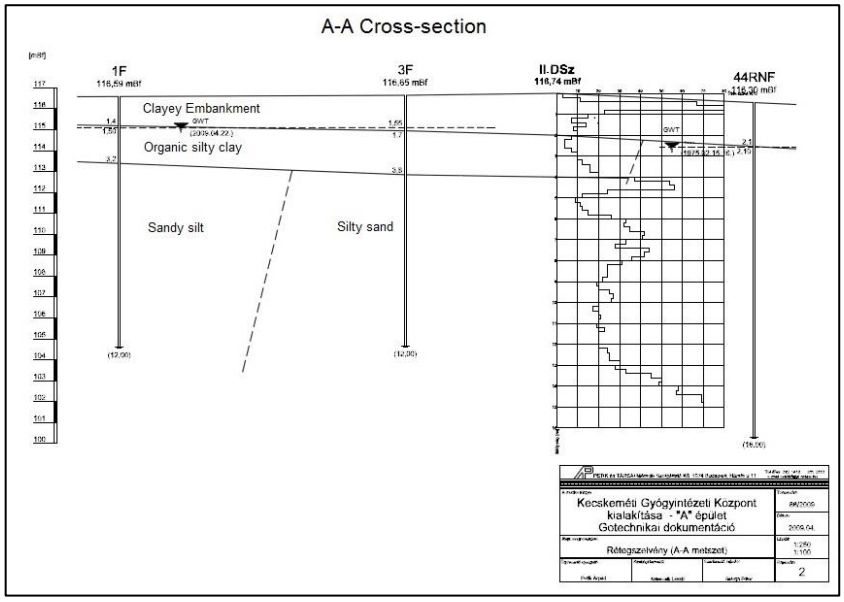

Figure 2.4 – Cross section A-A (Petik and Partners Engineering Service Ltd)

The cross section B-B (Figure 2.5) presents a very identical geotechnical sequence when compared with cross section A-A. The first two layers have the same characteristics and the last sequence, starting also around four meters depth, is a silty sand stratum.

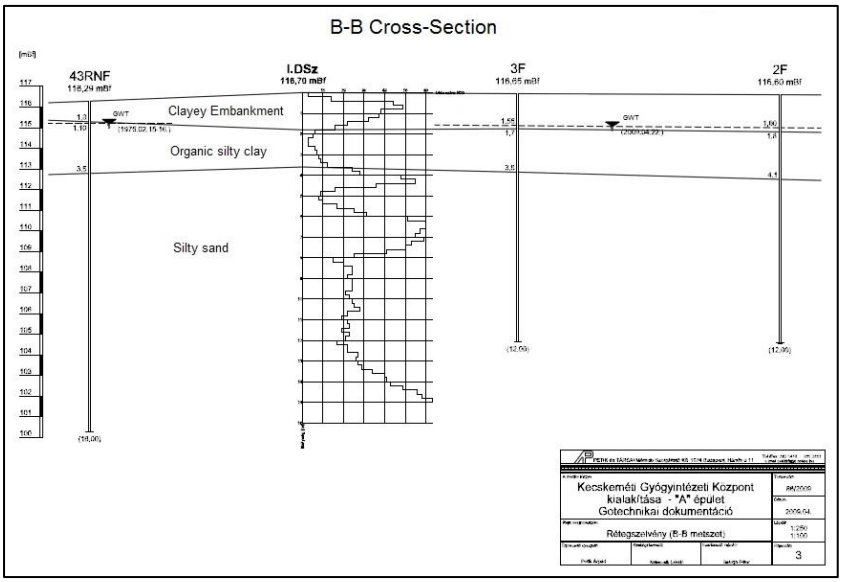

Figure 2.5 – Cross section B-B (Petik and Partners Engineering Service Ltd)

In both cases, the determined phreatic level position is 1.55 m depth. The evaluation of the groundwater levels is made in depth in all the boreholes, through the installation of a piezometer connected to the surface, where the results can be read when the sensor reaches the water level.

In order to determine the soil behaviour, regarding resistance, stiffness and deformability, 3 CTP/CPTU tests were performed, one the most renowned characterization ground tests in the current geotechnical practice, further outlined in this work (Subchapter 2.5).

The logs (unit sleeve friction resistance, f_s, cone resistance, q_c, friction ratio, R_f) of the three CPT tests are shown in Figure 2.7, Figure 2.9 and Figure 2.11, alongside with the respective soil behaviour type classification chart (Figure 2.8, Figure 2.10 and Figure 2.12). The colours in the R_f log correspond to one of the zones identified in the classification chart, whereas the colours in the q_c log must associated with either relative density (D_r) or consistency index (I_c) in the case of sands or clays, respectively (Figure 2.6).

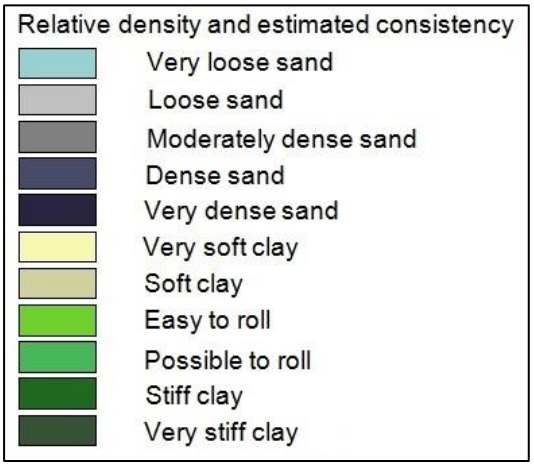

Figure 2.6 – Relative density and consistency index (FUGRO Consult KFT)

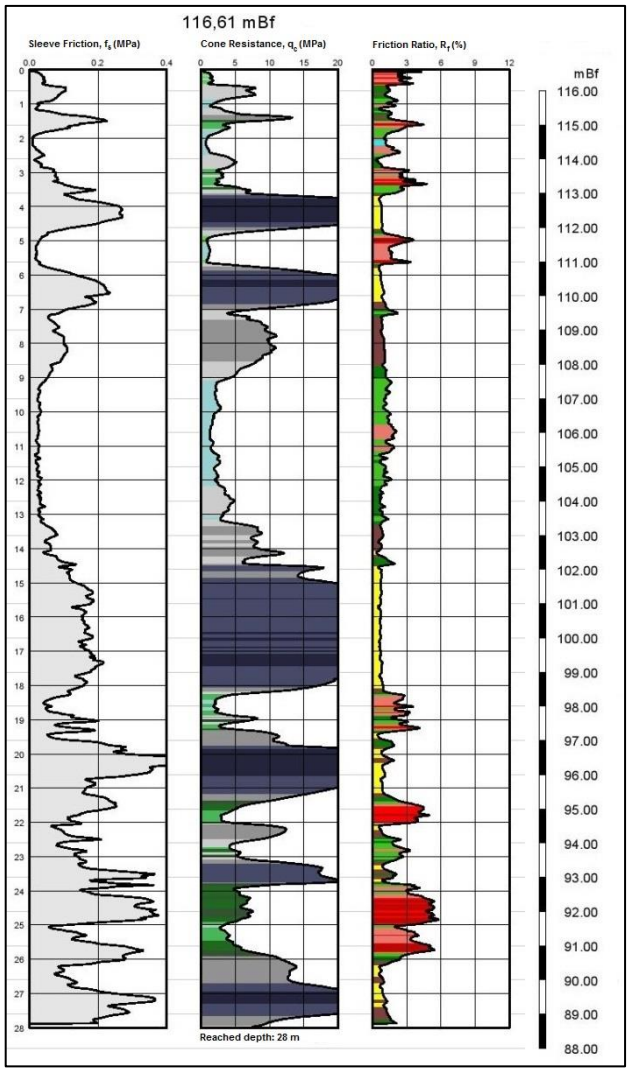

Figure 2.7 – CPT1 reported data (FUGRO Consult KFT)

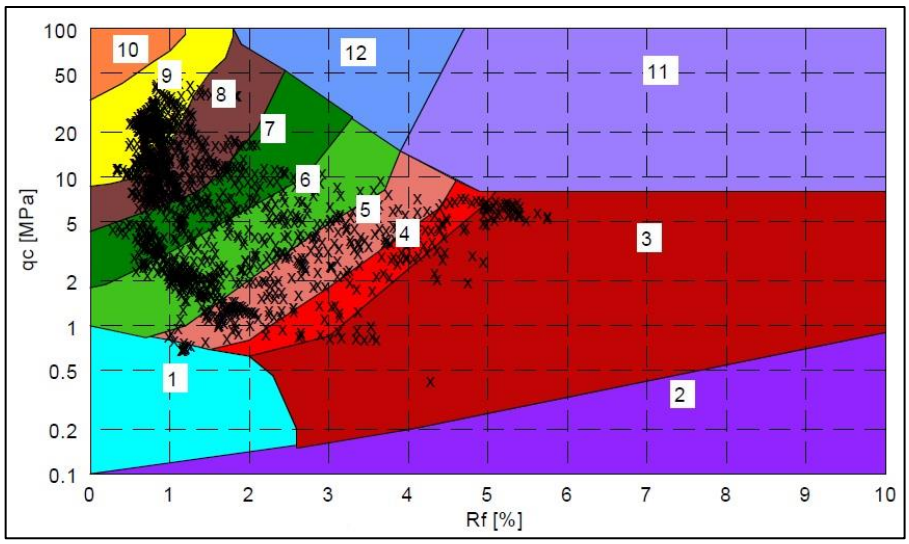

Figure 2.8 – CPT1 reported data within the adopted classification chart (FUGRO Consult KFT)

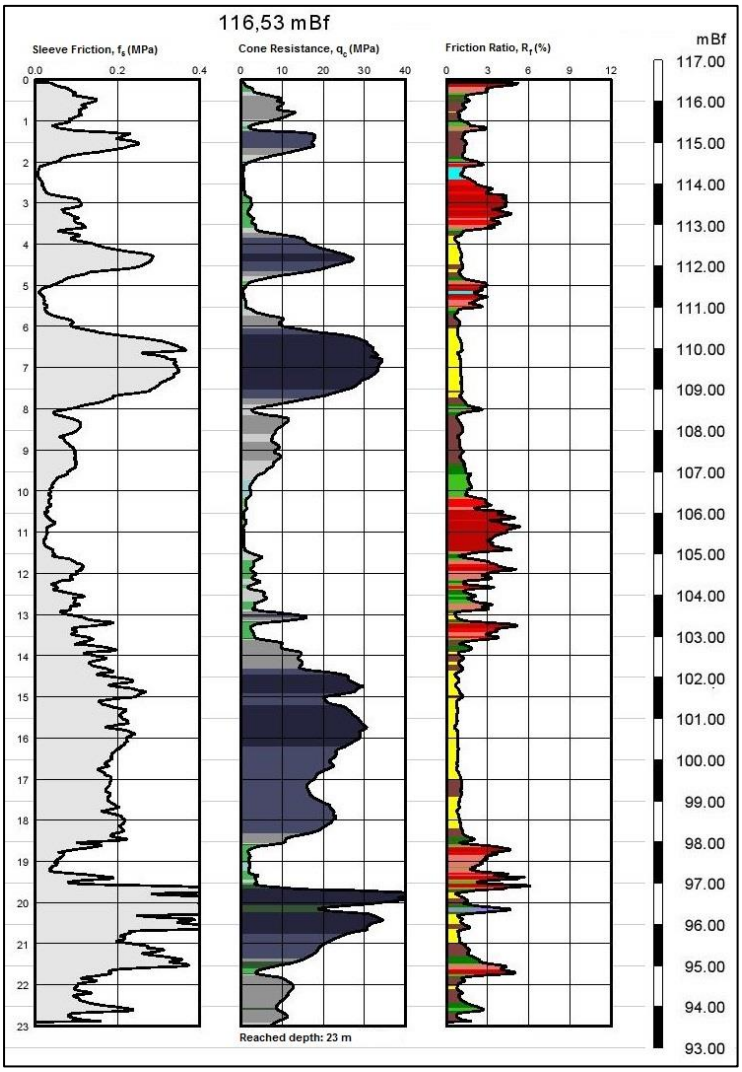

Figure 2.9 – CPT2 reported data (FUGRO Consult KFT)

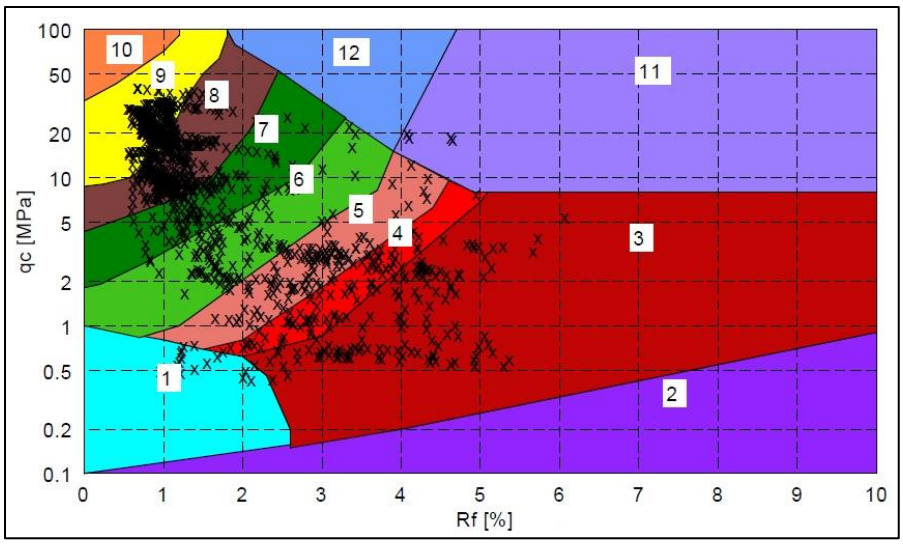

Figure 2.10 – CPT2 reported data within the adopted classification chart (FUGRO Consult KFT)

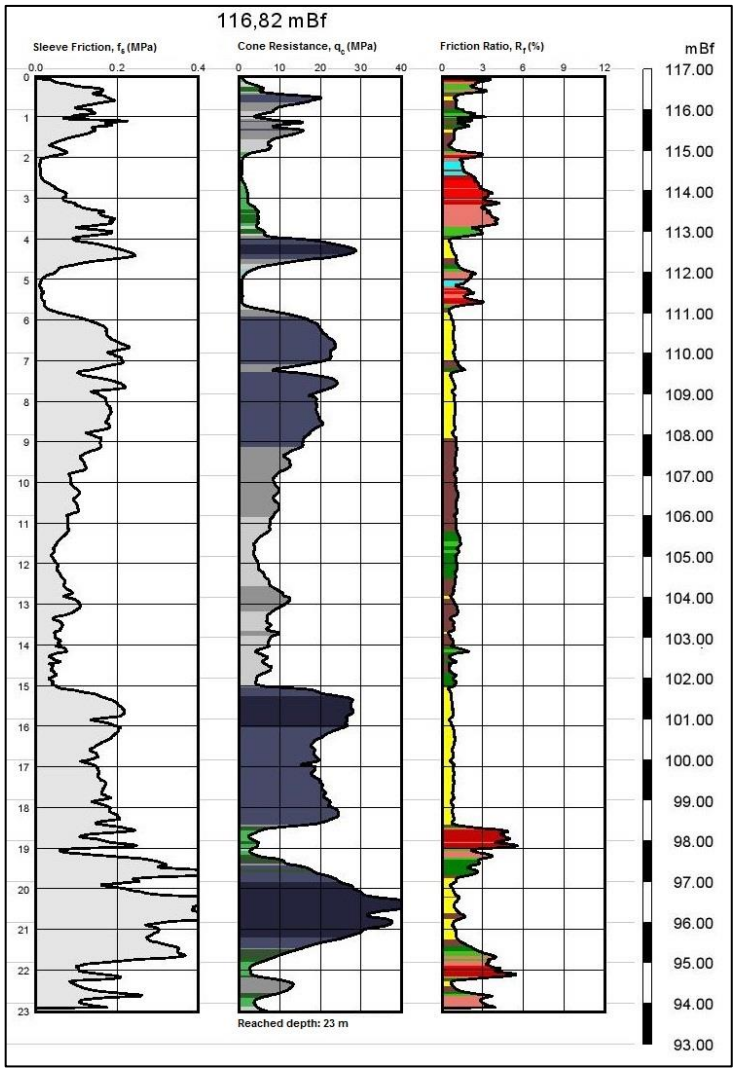

Figure 2.11 – CPT3 reported data (FUGRO Consult KFT)

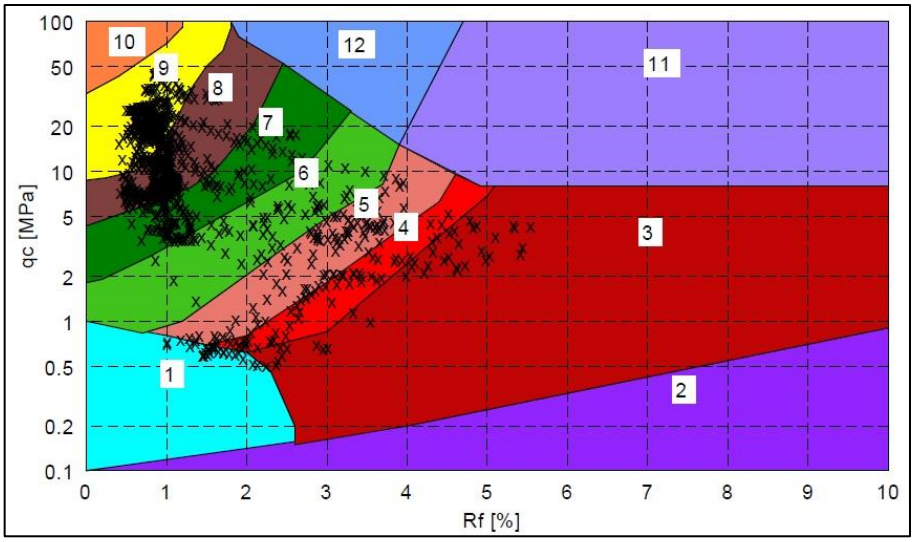

Figure 2.12 – CPT3 reported data within the adopted classification chart (FUGRO Consult KFT)

2.4. ASSESSMENT OF THE FOUNDATIONS TYPE

In foundation design, the consideration of a shallow foundation as a first approach is the most common solution, taking into account the lower costs involved and the simpler implantation complexity when compared to the adoption a deep foundation system. The two basic types of shallow foundations are isolated footings, working independently, and mat foundations, i.e., a concrete slab assuring a redistribution of the loads. The deep foundations can be associated to a basement slab (frequently called raft) by integrating a group of piles into a system, called piled raft.

The choice of the foundations type is based mainly in the following aspects:

- Soil stiffness;
- Soil strength;
- Structural loads;
- Foundation dimensions

In the specific case of this work, considering the reduced average q_c values immediately below the working ground level (112.400 mBf) and the dimensions the building object of this design (around 1000 m^2), a piled raft foundation system was adopted. Some advantages of this option are the greater settlement control due to the interaction between the piles and the slab and a more reduced stress level in the concrete slab, consequence of an uniform load distribution.

Another conclusion that can also be taken regards to pile length, a primary input of any ultimate pile capacity method. Again recalling the CPT data on Figure 2.7, Figure 2.9 and Figure 2.11, the q_c values are relatively high between 15 m and 18 m depth below the initial ground surface, which appeared to be an adequate position to set the piles tip. Therefore, the pile tip position was chosen to be 16 m (100.53 mBf) depth meaning a 11.87 m pile length, based on the defined working ground level (112.40 mBf). In practice, the considered pile length can be said to be 12 m.

2.5. THE CPT TEST FOR THE DESIGN OF DEEP FOUNDATIONS

2.5.1. GENERAL DESCRIPTION OF THE CPT TEST

The Cone Penetration Test is one of the most significant *in situ* tests used in the common geotechnical practice (Lunne *et al.*, 1997). Considering that the first developments of the mechanical CPT started in the first half of the 20th century, it is logically a very well-founded test, used by many researchers for ground characterization. The CPT test answers to central questions of the soil characterization being the one the most important tests used in the geotechnical design practice. The main advantages of the CPT are the continuous profiling, the reliable data registered and the strong theoretical background developed through the years which permits reliable correlations. On the other hand, this test requires skilled operators, relatively high investment and also does not provide soil sample.

Although the Standard Penetration Test (SPT) remains the most widely *in situ* test used in the world (Matos Fernandes, 2011), due to the its simplicity in operation and low cost, the CPT proved to be a much more reliable test, since it provides the measurement of three physical quantities, cone tip resistance, q_c, sleeve friction, f_s, and pore pressure, u_2, the latter register giving a new designation to the test, CPTU as it is going to be referred further. One of the biggest limitations of the SPT is the measurement of only one parameter (in the case, the number of blows, N) for the purpose of assuring a full characterization of the soil in study. The CPT has filled that lack by using different physical parameters which at the same time might converge to confirm a certain soil behaviour.

The first cone penetrometer tests were made in 1932, as referred above, with a cone tip attached to the steel rod, with 10 cm^2 of projected area and an apex angle of 60º and were performed by the Dutch engineer Pieter Barentsen in Netherlands.

In 1953, Begemann improved considerably the Dutch cone penetration test with the measurement of the local sleeve friction, possible with the introduction of an "adhesion jacket" behind the cone. Thus, it was possible to register not only the cone tip resistance but also the sleeve friction, which leaded to the first soil type classification based on CPT (Begemann, 1965).

An electric cone was developed in 1965 by Fugro with the dimensions and shape that were adopted as basis for the modern cones and also for the normalized test procedures (e.g. ASTM). The main advantages of the electric penetration relative to the mechanical part were the elimination of the incorrect readings of the sleeve friction, the continuous soil profiling possible the continuous penetration ratio and also the more accurate measurements provided by an electric device.

Regarding the evolution of the equipment, the year of 1974 brought eventually the most remarkable introduction in the history of the test. The cones started featuring a filter ring (*piezocones*), where it was possible to measure the pore water pressure. This innovation consequently led to an effective stress analysis, instead of the erroneous total stress interpretation hitherto used.

The procedure of the test consists on the penetration of a cone placed at the end of a series of rods that is pushed into the ground at a constant rate and provides simultaneously continuous measurements of the cone resistance, sleeve friction and even, when it is used the "piezocone", the pore pressure. The measurement of the pore pressure is nowadays very common in the geotechnical practice considering the advantages that it brings regarding the full characterization of the soil. The use of the piezocone instead of the original electric CPT implied also the introduction of a correction in the measured values for the cone resistance, being used a parameter called q_t. The ring filter located between the end of the friction sleeve and the cone creates an unequal area effect (Campanella *et al*., 1982), generating water pressures in descendent direction in the upper part of the cone. This pressure added to the measured cone resistance, q_c, correspond to the total resistance of the soil, q_t. Thus,

$$q_t = q_c + u_2(A_C - A_N)/A_C = q_c + u_2(1 - A_N/A_C) = q_c + u_2(1 - a) \quad (2.1)$$

where,

$A_C = 0.25\pi D^2$

$A_N = 0.25\pi d^2$

The second part of equation 2.1 will be greater the smaller the inner diameter, d, is. Currently, the equipment used to perform the piezocone has values for the parameter *a* between 0.70 and 0.85. From equation 2.1, it can be also concluded that the unequal area effect could be very significant in the total cone tip resistance, mainly when the parameter assumes the lower limit of the range. It still must be understood that this correction is only pertinent for cohesive soils, as result of the excess pore water pressure induced by the penetration. In granular soils, the value of q_c can be considered equal to q_t, regarding the drained behaviour that dominates in this type of materials. A similar correction must also be applied to the sleeve friction values when the cross sectional areas on the top and the bottom of the

sleeve are different. At the same time, now it is required to be assured the equal end area of the sleeve which avoids the use of such adjustment.

In Figure 2.13, a detailed illustration of the cone penetrometers and their terminology is presented, as well. The interpretation of the CPT/CPTU is done considering the values of the cone resistance, q_c, and the sleeve friction, f_s, as pressures although the measure is done as a force. Hence, the cone resistance is the total force acting on the cone, Q_c, divided by the projected area of the cone, A_c, whereas the sleeve friction is the force acting on the friction sleeve, F_s, divided by the surface area of the friction sleeve, A_s. Usually the pore pressure, u, is measured behind the cone in the u_2 position, instead of the less common on the cone (u_1) and on the friction sleeve (u_3) positions, as shown in Figure 2.14. The software associated to the equipment also computes the friction ratio, R_f, which is going to be discussed later and is express on equation 2.2.

$$R_f = \frac{f_s}{q_c} \tag{2.2}$$

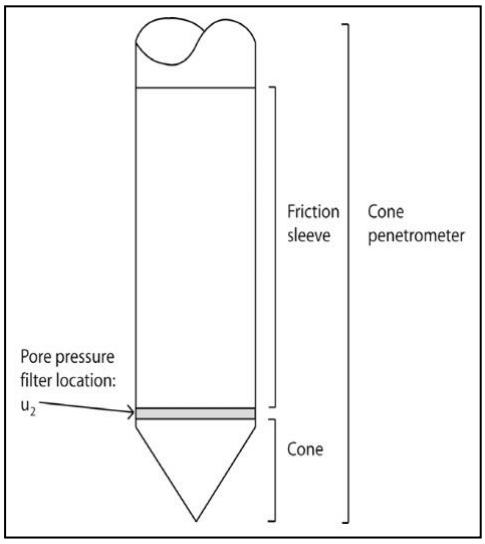

Figure 2.13 – Detail of a typical CPT probe (Robertson, 2012)

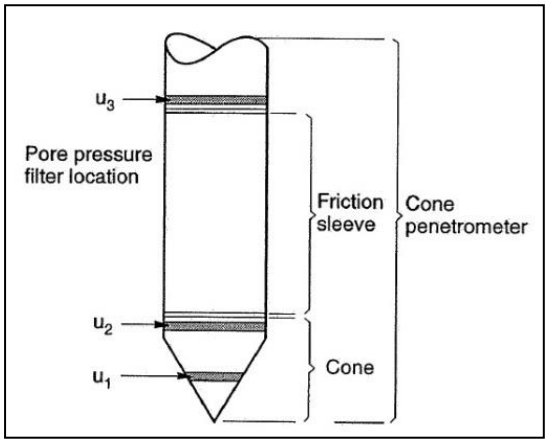

Figure 2.14 – Pore pressure filter locations (Lunne *et al*.,1997)

The diameter of the cone penetrometers is defined by the soil properties, being mainly used the 10 cm^2 (D= 35.7 mm) and the 15 cm^2 (D=43.70 mm) CPT probes. Only in very soft clays and shallow investigations are used smaller diameters and the greater ones are only used in the case of gravels. The standardized length of the friction sleeve is usually 13.4 cm corresponding to a 150 cm^2 of skin friction area, in the case of 10 cm^2 cone penetrometer. The normalized apex angle of the cone is 60º.

According to Robertson (2012), as an *in situ* test used for subsurface investigation, CPT/CPTU must answer some central questions, such as:

- Stratigraphy of the tested soil based on the interpretation of the physical quantities measured, which might be complemented with other tests that provide soil sample;
- Groundwater conditions, which is accomplished with the use of the piezocone through the measurement of the pore water pressure;
- Mechanical properties of the soil in study through the interpretation of the measured quantities (q_c or q_t, f_s, u_2).

The equipment used to perform the CPT/CPTU is nowadays very sophisticated (stronger pushing equipment and more robust cones) which allows the application of the test to a very wide range of soils. In addition to this fact, the measurement of three different physical quantities referred above will provide the estimation of many geotechnical parameters, via theoretical or empirical interpretation.

2.5.2. CPT INTERPRETATION

As it was referred previously, the CPT does not provide soil sample and consequently is not possible to identify the soil type directly. Alternatively the test can be completed by other borings that will lead to the soil classification based on the collected samples. The indirect way is an association between the tendency of the measured physical quantities and the soil characteristics. Naturally this procedure only became possible to be done separately after been done alongside with borings. The use of the second method is increasing as the accuracy of the correlations between CPT/CPTU and the soil characteristics are raising. Hence, it is comprehensible that CPT does not permit a very precise estimation of the physical characteristics of the soil, for example the grain size distribution, but correlations to determine the mechanical characteristics, such as resistance and deformability. In other words, the CPT predicts the *soil behaviour type* (SBT).

The experience showed that low values of cone resistance (q_c) might be associated to soft clay and, on the other hand, high values of this parameter are normally related to granular soils. The opposite happens with the value of the friction ratio (R_f) which tends to high in the first and low in the second.

After the introduction of the piezocone, it was possible to compute the evolution of the water pressure in depth, normally drawn in the same plot as the hydrostatic pressure (u_o) line. Thus, when the pore pressure (u_2) values are higher than u_o the soil crossed must be soft or medium clay, with undrained behaviour. The granular soils display a drained behaviour when bored so the water pressure line would nearly overlap the equilibrium pore pressure (u_o) line. The last interpretation from the water pressure computed data is related to overconsolidated and cracked soils or even very dense sands in which the penetration causes the generation of negative pore pressure excesses and consequently the pore water pressure line appears below u_o. This enhanced version of the test is particularly relevant when it is performed in soft clays, where the detection of a thin layer of sand is very important for the correct hydraulic analyses and further drainage system design.

As mentioned before, the introduction of the sleeve friction measurements leads to the first interpretation chart developed by Begemann (1965), relating the values of cone tip resistance and the

sleeve friction. Naturally, the chart (Figure 2.15) showed to be very limited since it is based on results of tests performed at shallow depths (less than 30 m). In normally consolidated clays, at great depths, the values of q_c tend to be high, even in the same range as the sands.

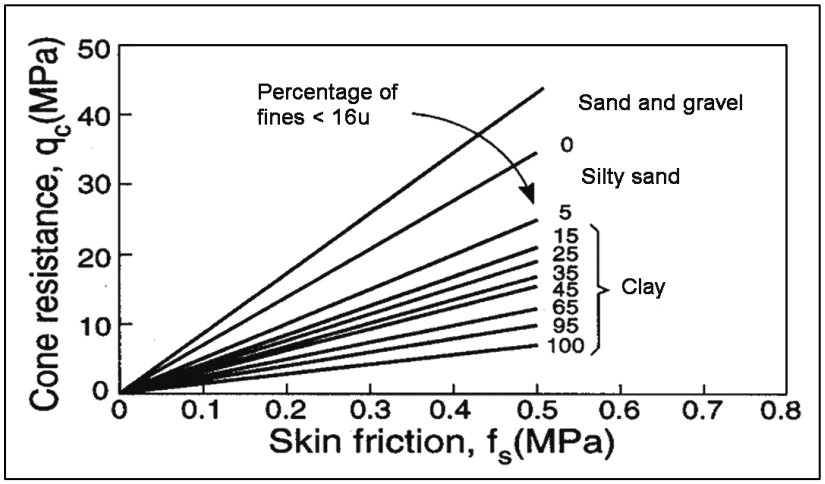

Figure 2.15 – First chart based on CPT test (Begemann, 1965)

Another chart (Figure 2.16) that deserves a reference is the one developed by Robertson and Campanella (1983) that correlates q_c and R_f and in which the borders between each soil type are no longer linear but rather curvilinear. Notwithstanding the previous fact, the chart was not very reliable as well lacking exactly in the same point as the first one since it was also developed based on shallow CPT tests.

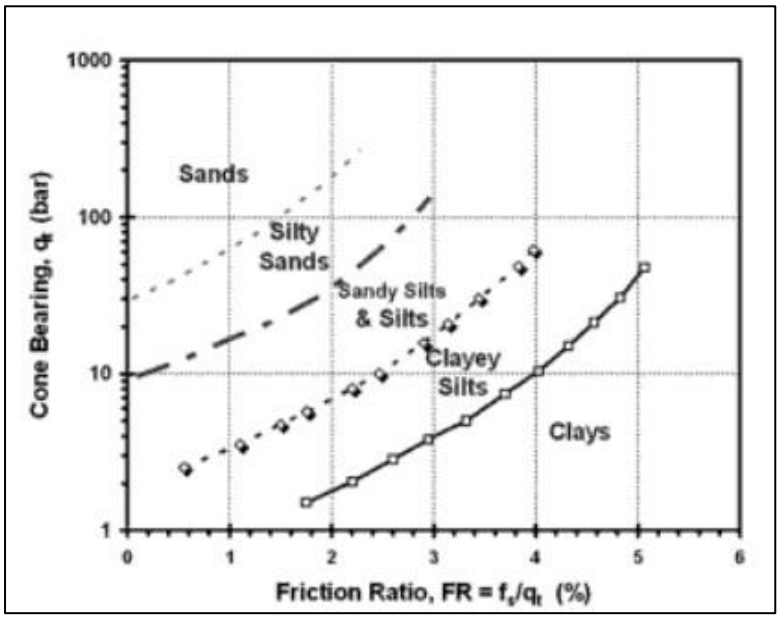

Figure 2.16 – Simplified soil type classification chart (Robertson and Campanella, 1983)

In 1986, Robertson *et al.* developed the first soil classification chart based on all the data provided by CPTU (q_t, f_s, u) which at same time proved to be the first high reliable CPT-based results interpretation. In addition, Robertson used a dimensionless quantity called pore pressure parameter, B_q, introduced by Senneset and Janbu (1985). This parameter takes into account the influence of the overburden stress (σ_{vo}) as shown in equation 2.3:

$$B_q = \frac{u_2 - u_0}{q_t - \sigma_{v0}} \tag{2.3}$$

Robertson *et al.* (1986) proposed two charts, depending whether the test is performed with or without pore pressure measurements, as it can be seen in Figure 2.17. Robertson *et al.* identified twelve soil behaviour types that can be divided in two main groups:

- From 1 to 6, cohesive soils;
- From 7 to 12, granular soils.

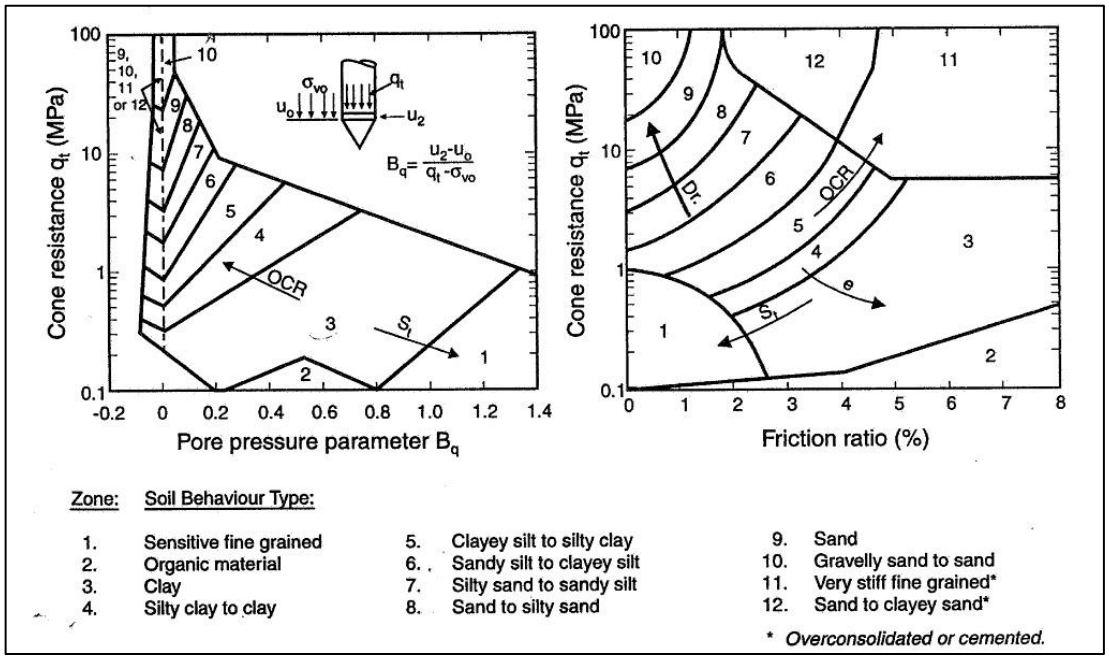

Figure 2.17 – Soil behaviour type classification chart based on CPTU data (Lunne *et al.*, 1997)

The influence of the effective overburden stress both in the cone tip resistance and sleeve friction, the increase of the first implies the same in the second, led to the development of a new interpretation approach (Robertson, 1990) based on normalized parameters. This way, the depth of the CPT drilling would no longer affect the results obtained. The normalized parameters are the normalized cone resistance, Q_t, normalized friction ratio, F_r, and the pore pressure ratio, B_q, given by the equation 2.4, 2.5 and 2.6, respectively:

$$Q_t = \frac{q_t - \sigma_{v0}}{\sigma'_{v0}} \tag{2.4}$$

$$F_r = \frac{f_s}{q_t - \sigma_{v0}} \tag{2.5}$$

$$B_q = \frac{\Delta u}{q_t - \sigma_{v0}} \tag{2.6}$$

where,

$\sigma'_{vo} = \sigma_{v0} - u_0$ is the effective vertical stress;

$\Delta u = u_2 - u_0$ is the pore pressure excess.

Once again Robertson created two charts (SBTn charts), one for the CPTU and one for the CPT (Figure 2.18) and naturally the boundaries were adjusted to fit the normalized parameters effect. There were identified nine zones based on a wide range of factors, such as void ratio, age, cementation in the case of granular soils and overconsolidation ratio (OCR) and soil sensitivity for cohesive soils. The zones can be included again in two main groups:

- From 1 to 4, cohesive soils;
- From 5 to 9, granular soils.

The previous experience and the referred extensive research made these SBTn charts very popular and widely used in common geotechnical practice.

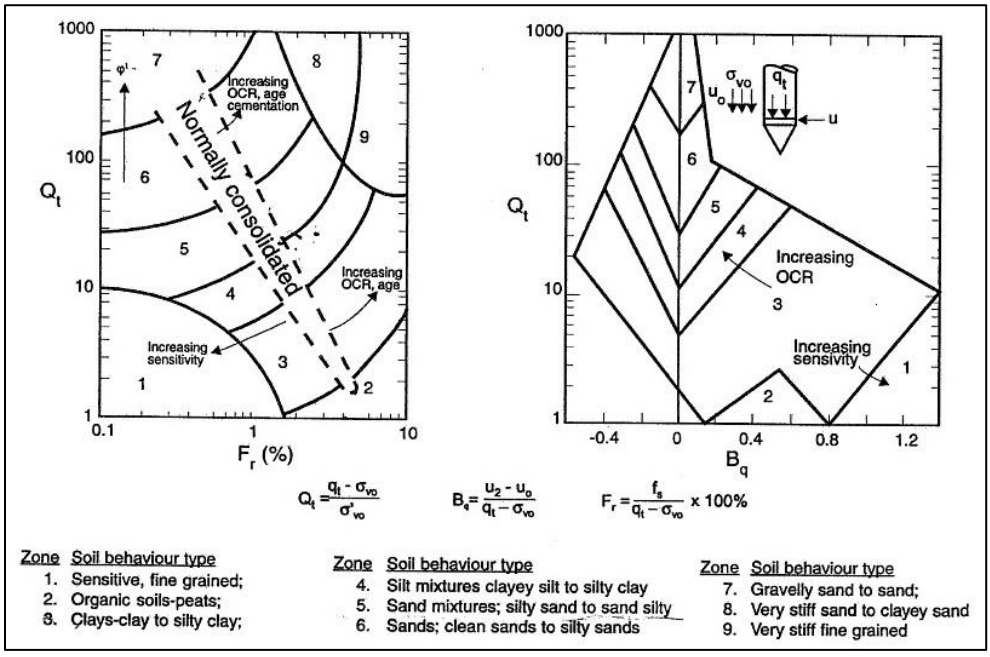

Figure 2.18 – Normalized soil behaviour type classification chart based on CPTU data (Lunne *et al.*, 1997)

In order to avoid any kind of mistake using the non-normalized chart (Robertson *et al.*, 1986) or the normalized chart (Robertson, 1990), Robertson (2009, 2012) proposed a unified approach based on both. This enhanced review pointed out nine consistent SBT zones (Table 2.1) plotted in only one chart (Figure 2.19) which relates the normalized cone resistance (Q_{tn}) and the normalized friction ratio (F_r). The first dimensionless parameter (equation 2.7) was modified from the original Q_t, now taking into account not only the vertical stress effects but also the horizontal stress influence, leading to a full normalized interpretation.

$$Q_{tn} = \left(\frac{q_t - \sigma_{v0}}{p_a}\right) \left(\frac{p_a}{\sigma'_{v0}}\right)^n \tag{2.7}$$

where,

n is the stress exponent that varies with soil type and stress level;

p_a is the atmospheric pressure.

Another important addition was the soil behaviour type index, I_c (equation 2.8), which provides the necessary input to define the soil behaviour type, since the index was also plotted in the chart as contours. The parameter is based on Q_{tn} and F_r and should be calculated based on an iterative process, suggested by Zhang *et al*. (2002), in which the stress exponent, n, could be estimated using I_c and the latter should be determined using Q_{tn}.

$$I_c = \sqrt{(3.47 - \log Q_t)^2 + (\log F_r + 1.22)^2} \tag{2.8}$$

Besides the index I_c and the stress exponent, n, the unified approach brought a much more embracing CPT interpretation, with correlations between the SBTn charts and a wide range of soil properties such as the state parameter (ψ), peak friction angle (Φ'_p), shear-wave velocity (V_{s1}), small strain shear modulus (G_o), Young's modulus (E'), constrained modulus (M) and the tendency of the soil to be dilative-contractive and drained-undrained.

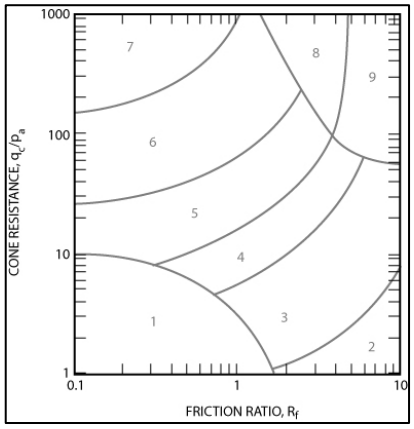

Figure 2.19 – Normalized soil behaviour type classification chart (Robertson, 2012)

Table 2.1 – Soil Behaviour Type zones defined in the Unified Approach (Robertson, 2012)

Zone	Soil Behaviour Type	I_c
1	Sensitive, fine grained	N/A
2	Organic soils – clay	> 3.60
3	Clays – silty clay to clay	2.95 – 3.60
4	Silt mixtures – clayey silt to silty clay	2.60 – 2.95
5	Sand mixtures – silty sand to sandy silt	2.05 – 2.60
6	Sands – clean sand to silty sand	1.31 – 2.05
7	Gravelly sand to dense sand	< 1.31
8	Very stiff sand to clayey sand*	N/A
9	Very stiff, fine grained*	N/A

* Heavily overconsolidated or cemented

The zones can be included once more in two main groups:

- From 1 to 4, cohesive soils;
- From 5 to 9, granular soils.

2.5.3. ADOPTED SOIL STRATIFICATION

In the scope of this work, the CPT interpretation data provided by the responsible company was made through the SBT charts developed by Robertson *et al.* (1986). Using the friction ratio (R_f) log in Figure 2.7, Figure 2.9 and Figure 2.11 and associating its colours to the ones in the respective classification charts (Figure 2.8, Figure 2.10 and Figure 2.12), it was possible to define two main soil behaviour types:

- Granular;
- Cohesive.

This distinction is very common and important, since almost every CPT based design method suggests different coefficients whether the soil is sand or clay. The adopted soil stratification is presented in Table 2.2, Table 2.3 and Table 2.4.

Table 2.2 – CPT1 results for the soil behaviour type (SBT)

SBT	Layer	h_i (m)	h_f (m)	H (m)
Granular	1	112.40	112.00	0.40
Cohesive	2	112.00	110.70	1.30
Granular	3	110.70	106.50	4.20
Cohesive	4	106.50	105.50	1.00
Granular	5	105.50	100.53	4.97

Table 2.3 – CPT2 results for the soil behaviour type (SBT)

SBT	Layer	h_i (m)	h_f (m)	H (m)
Granular	1	112.40	112.00	0.40
Cohesive	2	112.00	111.00	1.00
Granular	3	111.00	106.50	4.50
Cohesive	4	106.50	103.00	3.50
Granular	5	103.00	100.53	2.47

Table 2.4 – CPT3 results for the soil behaviour type (SBT)

CPT3	Layer	h_i (m)	h_f (m)	H (m)
Granular	1	112.40	111.80	0.60
Cohesive	2	111.80	111.00	0.80
Granular	3	111.00	100.53	10.47

Associated to each of the layers defined previously, corresponds an average value of the cone tip resistance (q_c) and the sleeve friction (f_s) as follows in Table 2.5, Table 2.6 and Table 2.7:

Table 2.5 – CPT1 average q_c and f_s values

Layer	$q_{c,mean}$ (MPa)	$f_{s,mean}$ (kPa)
1	26.34	218.2
2	3.92	39.8
3	9.89	94.9
4	1.52	24.3
5	10.00	76.3

Table 2.6 – CPT2 average q_c and f_s values

Layer	$q_{c,mean}$ (MPa)	$f_{s,mean}$ (kPa)
1	24.44	257.0
2	8.35	97.6
3	15.39	159.7
4	3.16	67.0
5	21.64	187.9

Table 2.7 – CPT3 average q_c and f_s values

Layer	$q_{c,mean}$ (MPa)	$f_{s,mean}$ (kPa)
1	7.83	89.6
2	1.92	18.9
3	13.39	116.3

2.6. ESTIMATION OF RESISTANCE AND DEFORMABILITY PARAMETERS

2.6.1. UNIT WEIGHT OF DEFINED STRATUM

The estimative of the unit weight (γ) was made based on the Figure 2.20, which correlates the parameter with the sleeve friction (f_s) and the specific gravity of the solid, G_s.

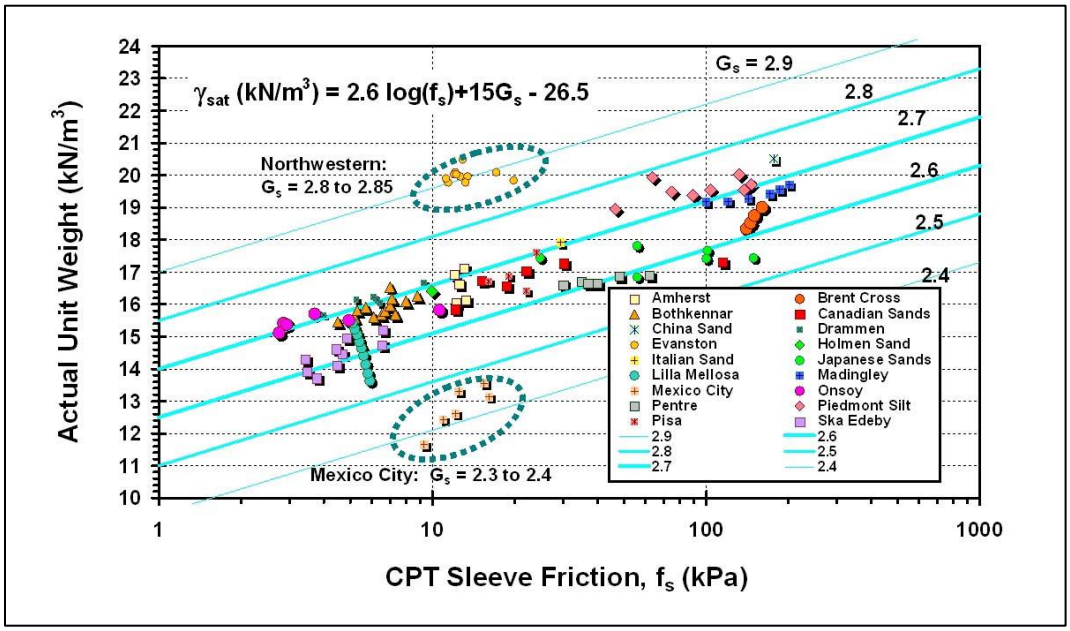

Figure 2.20 – Unit weight correlation chart with CPT data (Mayne, 2007)

According to Table 2.5, Table 2.6 and Table 2.7 a weighted average of f_s was defined, for both granular and cohesive soil types, taking into account the thickness of the layers. For example, the granular sleeve friction average value associated to the CPT1 was calculated as follows:

$$f_{s,CPT1}^{granular} = \frac{H_1 f_{s1} + H_3 f_{s3} + H_5 f_{s3}}{H_1 + H_2 + H_3} \quad (2.9)$$

Table 2.8 summarizes the weighted f_s values for both soil behaviour types in each of the CPT tests performed. The last column includes the adopted values.

Table 2.8 – Estimated f_s values

SBT	$f_{s,CPT1}$ (kPa)	$f_{s,CPT2}$ (kPa)	$f_{s,CPT3}$ (kPa)	$f_{s,average}$ (kPa)
Granular	90.4	174.4	114.9	126.6
Cohesive	33.1	73.8	18.9	41.9

Using the equation written in the Figure 2.20, it is possible to estimate the soil unit weight, as follows:

$$\gamma_{sat} = 2.6\log(f_s) + 15G_s - 26.5 \quad (2.10)$$

The value adopted for the G_s parameter was 2.6 for both soil types, leading to the respective unit weights presented in the Table 2.9:

Table 2.9 – Estimated unit weight values

SBT	$f_{s,average}$ (kPa)	γ (kN/m^3)
Granular	126.6	18.0
Cohesive	41.9	16.7

2.6.2. Adopted value for the Poisson's Ratio

Since there was no data regarding the estimative of the Poisson's Ratio (ν) in the scope of the geotechnical investigation, there were considered the average values concerning the both types of soils:

- Granular soils: ν=0.3;
- Cohesive soils: ν=0.2-0.3, considering a drained behaviour.

2.6.3. Estimation of Young's modulus

The most common correlation used to determine the Young's Modulus (E) via CPT test is expressed in equation 2.17.

$$E = \alpha . q_c \quad (2.11)$$

where,

α is the modulus factor.

The value of alpha (α) is, in this case, a coefficient related to the Young's modulus (E), being usually indicated in index the letter "E". The equation 2.12 was proposed by Robertson (2009), depending on the soil behaviour type index, I_c.

$$\alpha_E = 0.015\left[10^{(0.55I_c+1.68)}\right] \quad (2.12)$$

Considering the two dominant behaviours aforementioned, a value for I_c was defined for both granular and cohesive materials, based on the ranges defined in Table 2.1.

For granular soils, and using the classification charts on Figure 2.8, Figure 2.10 and Figure 2.12, it is possible to identify a concentration of points around the zone 8 and 9, meaning a soil behaviour type so-called silty sand to sand. Hence, correlating this classification with the data in Table 2.1, a value of 1.8 was defined for this material, corresponding to a silty sand.

For cohesive soils, the definition of a single soil behaviour type is not as simple as in the previous case, fact caused by the relative dispersion of points between the zones 3, 4, 5 and 6 (Figure 2.8, Figure 2.10 and Figure 2.12). Nevertheless, with the exception of the CPT2 results where there are a significant presence of marks in zone 3, in the other two tests the points belong mostly to border regions, 5 and 6. Hence, the cohesive soil behaviour type varies largely from silty clay to clayey silt, being defined for the SBT index the value of 3.0. In Table 2.10, the Young's modulus cone factor (α_E) values determined through equation 2.12 are summarized:

Table 2.10 – Proposed α_E values

SBT	I_c	α_E
Granular	1.8	7.02
Cohesive	3.0	32.07

The obtained value for the granular soils is consistent with the density of this sand (dense to very dense) based on the relative density, D_r, plotted alongside with q_c in each of the CPTU tests (Figure 2.8, Figure 2.10 and Figure 2.12). On the other hand, the calculated value for fine-grained soils exceeds largely the recommendations of several authors (Senneset, 1992; Kulhawy and Mayne, 1990), who indicate as upper limits for the constrained modulus cone factor (α_M) of 15 the first, and 14 for the last two.

In linear elasticity, the constrained modulus M is linked to the Young's modulus E via:

$$M = \frac{E(1-\nu)}{(1+\nu)(1-2\nu)} \tag{2.13}$$

Considering the Poisson's ratio adopted range ν=0.2-0.3, characteristic for cohesive soils with drained behavior, then:

$$E = (0.900 - 0.743)M$$

Conservatively adopting ν=0.3 and α_M=14, it can be written:

$$E \cong 10.\, q_c$$

It should be noted that the proposed formula presented on equation 2.12 is associated to the net cone resistance (q_t-σ_{vo}). However, this nuance was neglected having regarding the low influence (reducing the E value in 1.39%) of the total overburden stress when compared with q_c averages.

In accordance with the above, the adopted α_E values are resumed in the Table 2.11.

Table 2.11 – Adopted α_E values

SBT	α_E
Granular	7.02
Cohesive	10

Table 2.12, Table 2.13 and Table 2.14 resume the average Young's modulus in each layer.

Table 2.12 – Estimation of the E based on CPT1 results

CPT1	Layer	H (m)	$q_{c,mean}$ (MPa)	E (MPa)
Granular	1	0.40	26.34	184.8
Cohesive	2	1.30	3.92	39.2
Granular	3	4.20	9.89	69.4
Cohesive	4	1.00	1.52	15.2
Granular	5	4.97	10.00	70.1

Table 2.13 – Estimation of the E based on CPT2 results

CPT2	Layer	H (m)	$q_{c,mean}$ (MPa)	E (MPa)
Granular	1	0.40	24.44	171.5
Cohesive	2	1.00	8.35	83.5
Granular	3	4.50	15.39	108.0
Cohesive	4	3.50	3.16	31.6
Granular	5	2.47	21.64	151.8

Table 2.14 – Estimation of the E based on CPT3 results

CPT3	Layer	H (m)	$q_{c,mean}$ (MPa)	E (MPa)
Granular	1	0.60	7.83	54.9
Cohesive	2	0.80	1.92	19.2
Granular	3	10.47	13.39	93.9

After setting these coefficients, it is important to define a tendency or in other words to assign a law for the Young's modulus evolution in depth. Thus, it was considered a linear evolution of the modulus starting in the surface with a nonzero value, considering the obtained results through the ground tests.

The obtained values for the Young's modulus, associated to the midpoint of each layer, are represented in Figure 2.21.

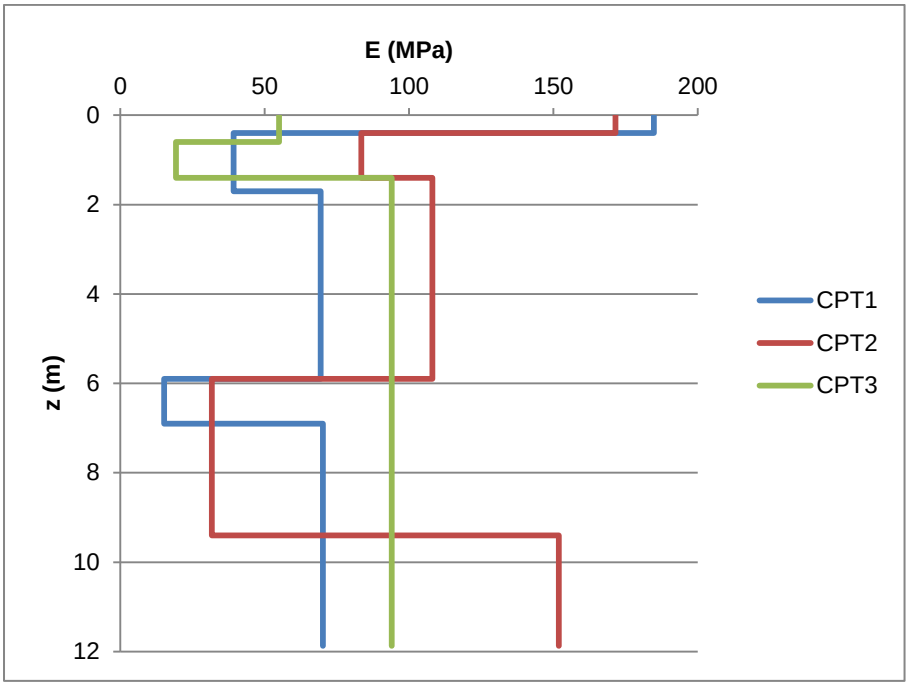

Figure 2.21 – Young's Modulus vs. depth

As can be seen, the evolution with depth shows to be very inconstant as result of the measured q_c variability. Despite that, it shall be mentioned that some of those results are influencing too much considering their global importance for the geotechnical behaviour of the foundation, such as:

- The extremely high q_c values in the first layer are justified by the presence of gravels or even rocks that must be neglected considering its low thickness (0.20 m, 0.20 m, 0.30 m for CPT1, CPT2, CPT2, respectively);
- In CPT1 test, around the 6 m depth, the specific average q_c value (1.52 MPa) for the cohesive stratum affects excessively the linear results, considering it is only 1 m thick. Thus, the referred data should not be considered in the weighing.

In relation to CPT2, the low average value in the cohesive layer (4) at 7.65 m depth must also be removed from the trend line calculation, adjusting *a posteriori* the equation by introducing a factor that takes into account the relevance of the mentioned stratum. Figure 2.22 shows the simplified Young's modules curves and the respective linear correlation, an equation of the type y=mx+b.

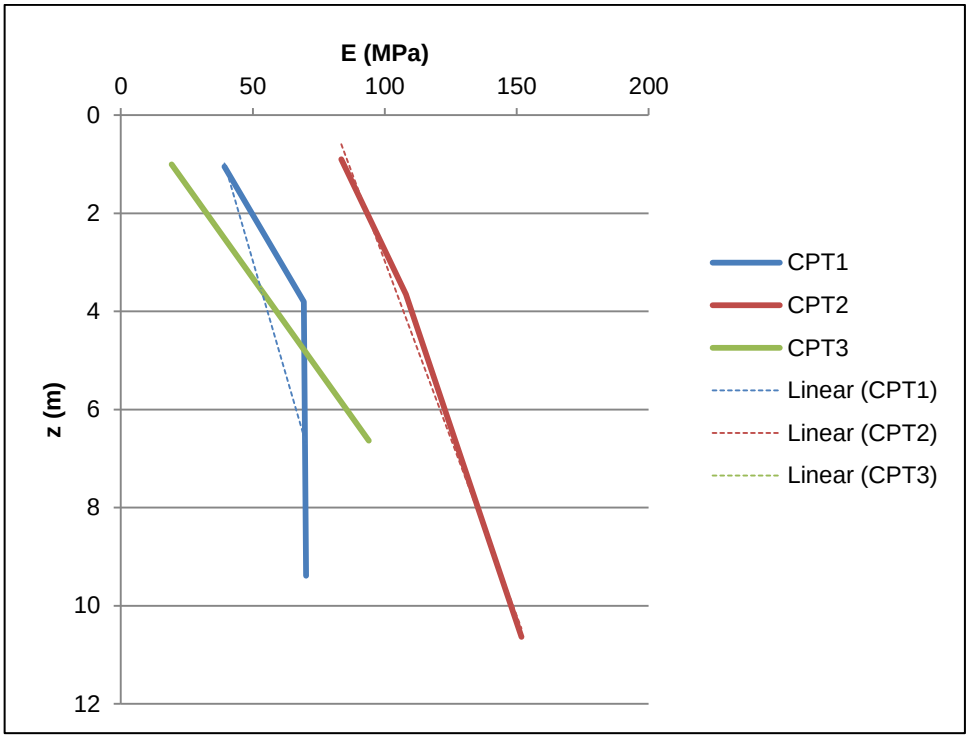

Figure 2.22 – Linear trend lines adjusting the Young's Modulus evolution

The equations related to each ground test are as follows:

$$E_{CPT1} = 33.93 + 5.40z \tag{2.24}$$

$$E'_{CPT2} = 80.66 + 6.93z \tag{2.35}$$

$$E_{CPT3} = 5.96 + 13.26z \tag{2.16}$$

Regarding the equation 2.15, it should also be applied a correction due to the exclusion of the layer 4 from the previous calculations. The factor is equal to:

$$f_{CPT2} = 1 - \frac{H_{layer\,4}}{H_{total}} = 1 - \frac{3.50}{11.87} \cong 0.70$$

where,

$H_{layer\,4}$ is the thickness of layer 4;

H_{total} is the total depth of analysed CTP data.

Hence, the equation 2.15 is now written as follows:

$$E_{CPT2} = f_{CPT2}.E'_{CPT2} = 56.46 + 4.85z \quad (2.17)$$

The adopted equation is the average of the previous three, as follows:

$$E = 32.12 + 7.84z, (MPa, m) \quad (2.18)$$

2.7. APPLICATION OF THE CPT/CPTU RESULTS IN DEEP FOUNDATIONS DESIGN

One of the major applications of the test was, since its beginning, and continues to be the determination of the bearing capacity of piles. The continuous soil profiling in depth allows the pile surrounding ground definition. However, the prediction of the pile capacity is not easily obtained since it depends on different factors, such as:

- Type of the pile;
- Installation method, related to the previous one;
- Type of the soil crossed.

The empirical CPT/CPTU design methods developed through the years tend to integrate all these effects, but the difficulty in quantifying them requires the introduction of factors of safety, through the reduction of the calculated values. All the design calculations were made following the Eurocode 7 (EC7) regulations, that preconizes the use of resistance and correlation factors, being the first ones applied to determine the characteristic value and followed by the calculation of the design values. This issue will be resumed in the next chapter.

Regarding the adequacy of the CPT/CPTU data in design problems, Lunne *et al.* (1997) compiled the gained experience to develop the Table 2.15:

Table 2.15 – Reliability ratings regarding design with CPTU data (adapted from Lunne *et al.*, 1997)

Soil Type	Pile Design	Bearing Capacity
Sand	1-2	1-2
Clay	1-2	1-2
Intermediate soils	1-2	2-3

*Reliability ratings: 1- High; 2- High to moderate; 3- Moderate; 4- Moderate to Low; 5-Low

According to Table 2.15, it can be confirmed the good reliability provided by the CPT/CPTU data in geotechnical design, specifically in deep foundations design. Moreover, Robertson (2012) stated that the CPT test is the most accurate in pile design.

3
METHODS OF ANALYSIS FOR SINGLE PILE CAPACITY AND STRESS-STRAIN BEHAVIOUR OF THE PILED RAFT

3.1. INTRODUCTION

In geotechnical design project, the prediction of the resistance and deformability of the soil are the main goal. Hence, the calculation approaches must be carefully chosen, based essentially on its theoretical premises consistency, suitability to the case study and applicability in common practice. Considering the high uncertainty that surrounds geotechnical problems, the design approaches must be verified based on comparisons with other methods, avoiding unsafe solutions and framing the range of results. Thus, there were considered two static approaches for the single pile capacity prediction, both hand calculation methods. For the deformation analysis of the piled raft two approaches of different nature were considered, the first using a structural program based on finite element method (FEM) and the second based on an geotechnical hand calculation method. During the chapter the adopted methodologies are described in a general way, which will then be adapted to the specific case study.

3.2. CALCULATION OF THE BEARING CAPACITY OF A SINGLE PILE

The value of the bearing capacity of a single pile (Q_{ult}) comprises two components:

- End bearing load (point resistance), Q_b (kN);
- Side friction load (shaft resistance), Q_s (kN).

Thus,

$$Q_{ult} = Q_b + Q_s \tag{3.1}$$

The equation 3.1 can also be written in terms of resistance (R), as follows:

$$R_c = R_b + R_s = A_b q_b + \sum A_{si} q_{si} \tag{3.2}$$

where,

A_b, cross-sectional area of the pile (m^2);

q_b, pile unit end resistance (kPa)

A_{si}, shaft area of the soil layer i (m^2);

q_{si}, pile unit side friction (kPa).

In the scope of the geotechnical design, ruled by the Eurocode 7 (EC7), the obtained results are the calculated values, so the equation 3.2 should be written as follows:

$$R_{c;cal} = R_{b;cal} + R_{s;cal} \tag{3.3}$$

where,

$R_{b;cal}$, ultimate pile base resistance, calculated from ground test results;

$R_{s;cal}$, ultimate shaft friction, calculated from ground test results.

According to EC7, the determination of pile foundations design value depends on different factors which must be applied to the characteristic value, reducing it:

- The approach used to determine the characteristic values (normally ground or load tests);
- The number of tests performed (n), in order to predict the variability of the results;
- The type of pile used and consequently the execution method.

Hence the characteristic value, when the number of tests is greater than one, is obtained as follows:

$$R_{c;k} = R_{b;k} + R_{s;k} = \frac{R_{b;cal} + R_{s;cal}}{\xi} = \frac{R_{c;cal}{}'}{\xi} \tag{3.4}$$

where,

$R_{b;k}$, characteristic value of the base resistance of a pile;

$R_{s;k}$, characteristic value of the shaft resistance of a pile;

ξ, correlation factor depending on the number of piles tested or of profiles of tests.

Figure 3.1 illustrates the mobilization of the both shaft and base resistance and its relationship with the correspondent force.

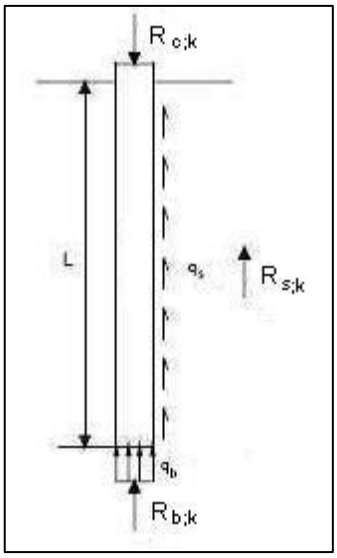

Figure 3.1 – Components of a pile bearing capacity

The design value $R_{c;d}$ is equal to:

$$R_{c;d} = \frac{R_{c;k}}{\gamma_t} \tag{3.5}$$

where,

$R_{c;k}$, characteristic compressive resistance of the ground against a pile, at the ultimate limit state;

γ_t, is the partial resistance factor on total/combined resistance for piles in compression.

3.2.1. METHOD TO DETERMINE THE COMPRESSIVE RESISTANCE OF A SINGLE PILE PROPOSED IN EUROCODE 7 BASED ON DE RUITER AND BERINGEN (1979) METHOD

This method is outlined in detail in EC7 Part 2, Annex D.7 (CEN, 2007), where geotechnical interpretation regarding cone and piezocone penetration tests is applied. The guideline suggests approaches for the calculation of the pile unit end resistance (q_b) and the pile side friction (q_s).

The determination of q_b, so called $p_{max;base}$, is given by the equation 3.6:

$$p_{max;base} = 0{,}5.\alpha_p.\beta.s.\left[\frac{q_{c;I;mean} + q_{c;II;mean}}{2} + q_{c;III;mean}\right] \leq 15\ MPa \tag{3.6}$$

where,

α_p is the pile class factor;

β is the factor which takes account of the shape of the pile;

s is the factor which accounts for the shape of the pile base given by the equation 3.7:

$$s = \frac{1 + \frac{\sin \varphi}{L/B}}{1 + \sin \varphi} \tag{3.7}$$

$q_{c;I;mean}$ is the mean of the $q_{c;I}$ values over the depth running from the pile base level to a level which is at least 0.7 times and at most 4 times the equivalent pile base diameter D_{eq} deeper (Figure 3.2);

$q_{c;II;mean}$ is the mean of the lowest $q_{c;II}$ values over the depth going upwards from the critical depth to the pile base (Figure 3.2);

$q_{c;III;mean}$ is the mean value of the $q_{c;III}$ values over a depth interval running from pile base level to a level of 8 times the pile base diameter above the pile base. This procedure starts with the lowest $q_{c;II}$ value used for the computation of $q_{c;II;mean}$. The upper limit for this component is 2 MPa (Figure 3.2).

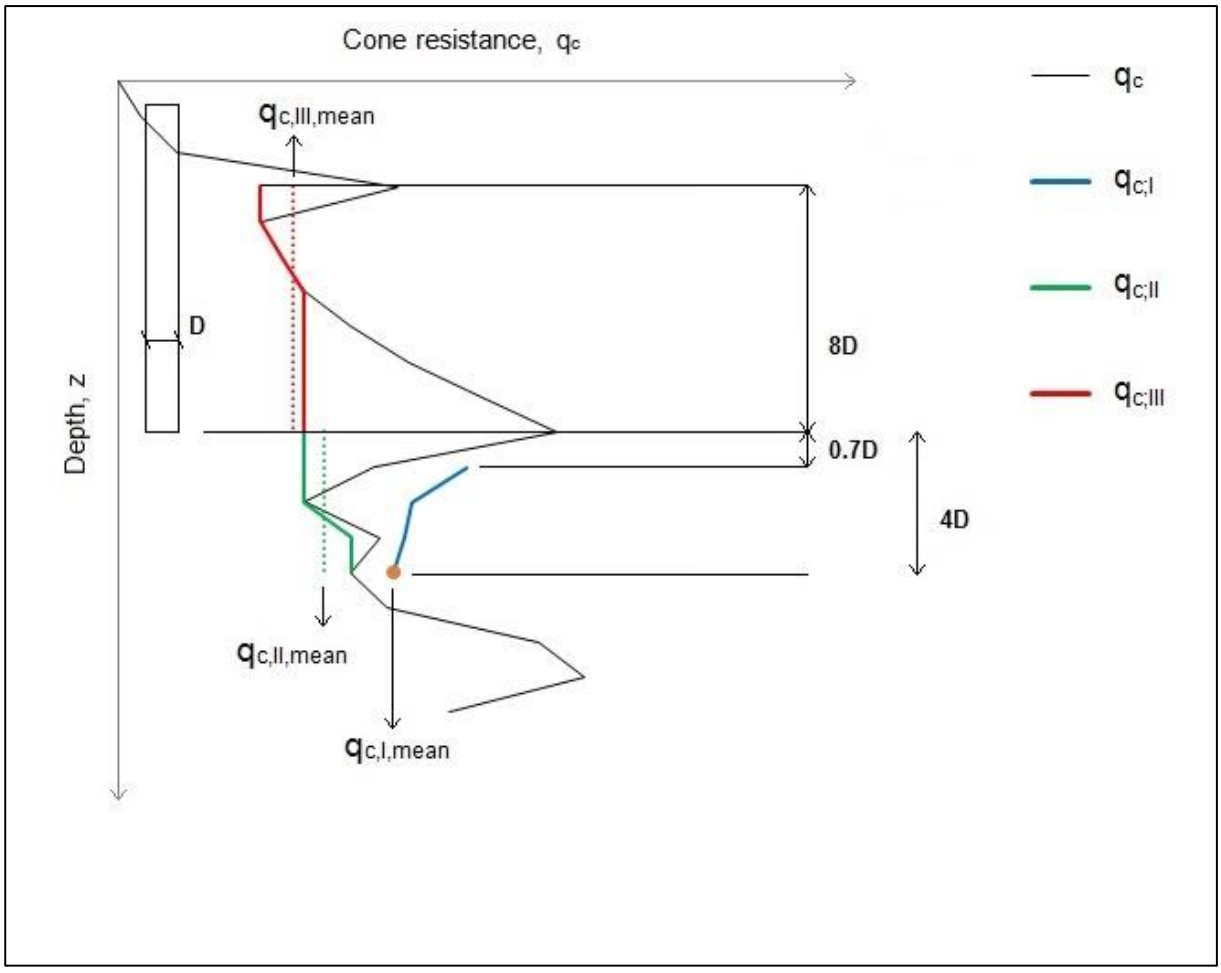

Figure 3.2 – Components of the pile end resistance in EC7 approach

The values of the pile class factor (α_p) are summarized in Table 3.1, according to the results obtained by Lakatos (2011) in pile load tests conducted in Hungarian soil. The parameters are only valid for pile toes placed in granular strata.

Table 3.1 – α_p values (adapted from Lakatos, 2011)

Pile class or type	α_p
Soil displacement type piles	
▪ Driven (vibrated) precast reinforced concrete	1.0
▪ Driven (vibrated) precast steel pipe (close end)	1.0
▪ Closed end steel pile driven, removed and concreted *in situ*	1.0
▪ OMEGA Screw piles	0.80
Soil replacement type piles	
▪ CFA piles	0.70
▪ Bored pile (with slurry)	0.50
▪ Bored pile (with casing)	0.50

Actually, the computation of the $q_{c;I}$ and $q_{c;III}$ represents an envelope of the q_c values on the safety side, procedure firstly introduced by de Ruiter and Beringen (1979). Using the original nomenclature proposed by the authors, the equation 3.8 represents the q_b value proposed by de Ruiter and Beringen:

$$q_b = \frac{q_{c1} + q_{c2}}{2} \leq 15\ MPa \tag{3.8}$$

where,

q_{c1} is the same as $q_{c;I;mean}$;

q_{c2} is the same as $q_{c;III;mean}$.

Hence, it must be mentioned that the EC7 approach for the base resistance is an enhanced version based on the de Ruiter and Beringen Method (1979).

The determination of q_s, named $p_{max;shaft}$ according to EC7, can also be made following the approach proposed by Lakatos (2011). The author suggested two different equations (3.9 and 3.10) for the calculation of the unit side friction (q_{si}), one for granular ($q_{si;g}$) layers and other for cohesive layers ($q_{si;c}$), respectively, as follows:

$$q_{si;g} = min\left\{\alpha_{s;g}.\sqrt{q_{c;i;avg}}; q_{s;max}\right\}, \qquad q_{c;i;avg}\ [kPa] \tag{3.9}$$

where,

$\alpha_{s;g}$ is a factor defined according to Table 3.2;

$q_{c;i;avg}$ is the layer "i" average q_c;

$q_{s;max}$ is the upper limit of shaft friction.

$$q_{si;c} = min\{1{,}2.\alpha_{s;c}.\sqrt{q_{c;i;avg}}; q_{s;max}\}, \qquad q_{c;i;avg}\ [kPa] \tag{3.10}$$

where,

$\alpha_{s;c}$ is a factor defined according to Table 3.3;

$q_{c;i;avg}$ is the layer "i" average q_c;

$q_{s;max}$ is the upper limit of shaft friction.

In the following Table 3.2 and Table 3.3 are shown the values for the factors $\alpha_{s;g}$ and $\alpha_{s;c}$ and the respective upper limits for side friction resistance ($q_{s;max}$).

Table 3.2 – $\alpha_{s;g}$ values (adapted from Lakatos, 2011)

Pile class or type	$\alpha_{s;g}$	$q_{s;max}$ (kPa)
Soil displacement type piles		
▪ Driven (vibrated) precast reinforced concrete	0.90	150
▪ Driven (vibrated) precast steel pipe (close end)	0.75	120
▪ Closed end steel pile driven, removed and concreted *in situ*	1.10	160
▪ OMEGA Screw piles	0.75	160
Soil replacement type piles		
▪ CFA piles	0.55	120
▪ Bored pile (with slurry)	0.55	100
▪ Bored pile (with casing)	0.45	80

Table 3.3 – $\alpha_{s;c}$ values (adapted from Lakatos, 2011)

Pile class or type	$\alpha_{s;c}$	$q_{s;max}$ (kPa)
Soil displacement type piles		
▪ Driven (vibrated) precast reinforced concrete	1.05	85
▪ Driven (vibrated) precast steel pipe (close end)	0.80	70
▪ Closed end steel pile driven, removed and concreted *in situ*	1.10	90
▪ OMEGA Screw piles	1.25	100
Soil replacement type piles		
▪ CFA piles	1.00	80
▪ Bored pile (with slurry)	1.00	80
▪ Bored pile (with casing)	1.00	80

3.2.2. LCPC METHOD (BUSTAMANTE AND FRANK, 1999)

The method proposed by Bustamante and Frank (1999) is a static method based on correlations between the results of geotechnical characterization tests and results of piles load test, being therefore very popular. Firstly introduced by Bustamante and Gianeselli (1982), the method was enhanced in 1999 using the gathered data provided by *Laboratoire central des ponts et chausses* (LCPC).

These data is based on more than 400 load tests performed on piles which allowed the definition of solid correlations for a wide range of different types of soils and piles (in materials and construction processes). The large number of site investigation lead to refined values for the correct assessment of the skin friction and the end bearing capacity. Additionally, it is possible to establish correlations between the measured CPT and SPT data with Pressuremeter Test (PMT) when the latter is not performed during the investigation works.

The penetrometer (CPT) approach defines q_b as follows in equation 3.11:

$$q_b = K_c q_{ce} \tag{3.11}$$

where,

q_{ce} is the cone resistance around the base;

K_c is the pile tip bearing factor.

The pile unit skin friction (q_{si}) is given by the equation 3.12:

$$q_{si} = min\{q_c/\beta\,;q_{s;max}\} \tag{3.12}$$

where,

q_c is the average CPT cone resistance in each assumed layer;

β is a correlation factor;

$q_{s;max}$ is the upper limit of shaft friction.

3.3. STRESS-STRAIN BEHAVIOUR ANALYSIS

The deformation analysis continues to be one the hardest issues to solve in the scope of the geotechnical project regarding the high non-linearity of the soil behaviour. Specifically, the soil stiffness, perhaps the most important parameter involved in the serviceability of the structures, tends to have a rather inconstant evolution with depth (2.6.3) being at the same time impossible to reflect all this variability. Thus, the pile group settlements assessment is achieved assuming some simplifications, in any case conservative, of the behaviour of not only the soil but also the piled raft and its interaction.

As defined in Eurocode 7 (CEN, 2004), "*a limiting value for a particular deformation is the value at which a serviceability limit state, such as unacceptable cracking, is deemed to occur in the supported structure*".

3.3.1. THEORETICAL LOAD-SETTLEMENT CURVES

Considering the difficulties, mainly logistics, in relation to the execution of a considerable and representative number of pile load tests in the construction site, several projects assume idealized load-settlement curves (see Figure 3.3) based on registers obtained in instrumented piles, namely in static load tests.

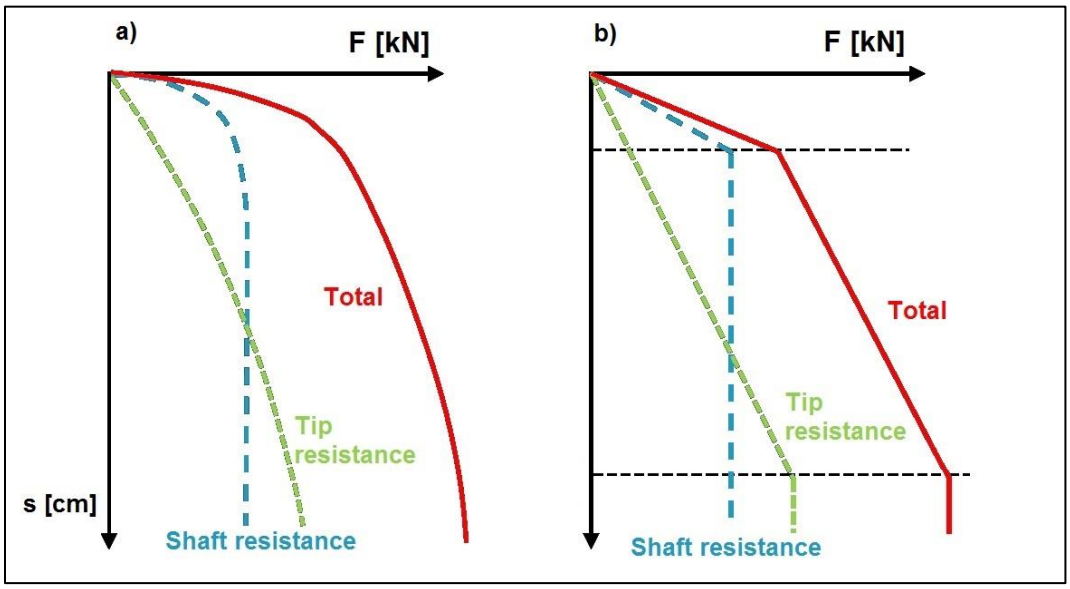

Figure 3.3 – Load settlement curves: a) Observed curve based on a load test; b) Theoretical curve

The theoretical curves are constructed by overlaying the shaft resistance, so called t-z curves and the base resistance, named as q-z curves, if both are expressed in stress along depth (z). Through the observation of results of load tests performed in CFA piles (as the one plotted in Figure 3.4, in an experimental site in residual soils), it is possible to establish a relation between the developed settlement at the ultimate base or shaft resistance with pile diameter.

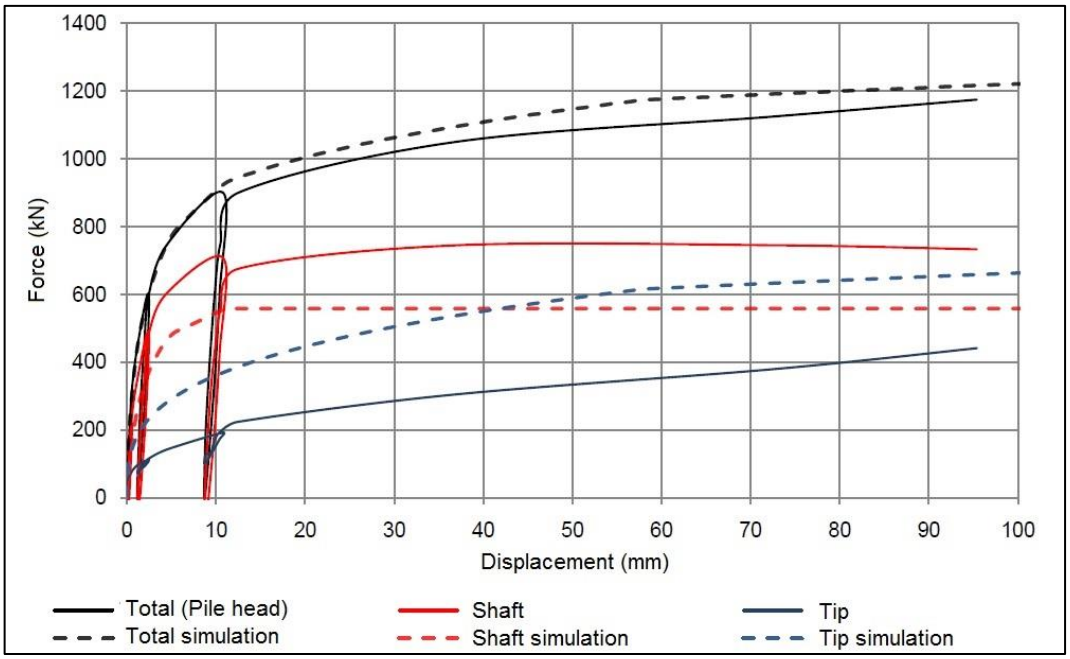

Figure 3.4 – Example of results obtained in CEFEUP/ISC'2 Experimental Site (Viana da Fonseca and Santos, 2008) modelled by Fernandes (2011)

A common and simplified method is to assume that the mobilization of each of the components occurs for a certain deformation level, expressed as function of the pile diameter. Obviously, the generated settlement depends on the pile diameter, as referred above, but also on the execution method. Hence, shaft resistance is generally fully mobilized for values around 1.5% to 2.0% (Figure 3.5) of the pile diameter (D_1), developing a minor settlement and not depending significantly on the piles execution method.

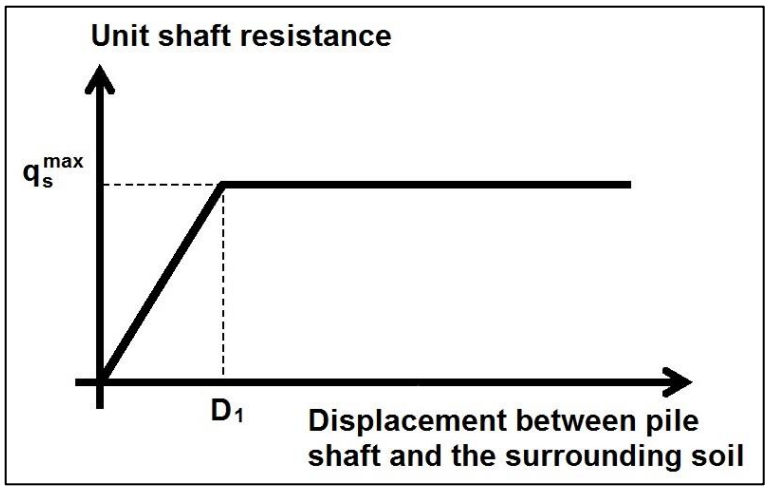

Figure 3.5 – Theoretical unit shaft resistance curve

On the other hand, the mobilization of the base resistance (Figure 3.6) requires a larger settlement being in this case more dependent on the pile type, with the values ranging from 5% (displacement piles) to 10% (replacement piles) of the pile diameter (D_2).

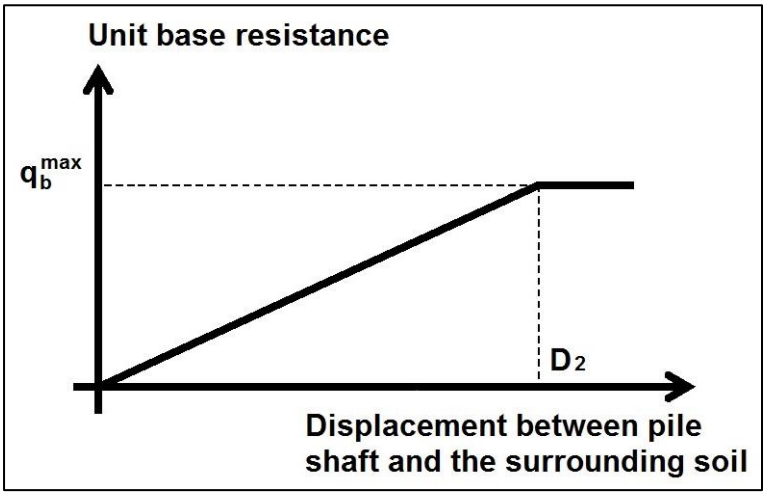

Figure 3.6 – Theoretical unit base resistance curve

Thus, the pile stiffness is essentially given by the portion of the base resistance considering the early mobilization of the shaft resistance.

3.3.2. Analysis of Raft Settlements

A raft can be compared to a footing of larger dimensions and its study can be done similarly. Thus, the settlement estimative of a raft can be done following the same assumptions adopted for the footings, where the elastic solutions are still used and valid unlike what happens in deep foundations considering this king of analysis. Notwithstanding, the empirical and semi-empirical methods are also accepted and well-recognized in geotechnical design practice mainly for the conservative solutions. The Schmertmann Method (1970) is an example of a semi-empirical method that derives from the theoretical elastic solutions and it was intended to narrow certain deviations observed between the referred solutions and real cases. The method is one of the most renowned in the scope of the settlement analysis of a shallow foundation regardless its remote introduction. A brief description of the method is done below.

The general expression of the immediate settlement proposed by Schmertmann (1970) is presented in the equation 3.13:

$$s_i = C_s \Delta q_s \int \left(\frac{I_\varepsilon}{E}\right) dz \tag{3.13}$$

where,

C_s is a dimensionless linear correction factor calculated according to equation 3.14;

Δq_s is the net foundation pressure;

I_ε is the vertical strain influence factor explained in Figure 3.7;

E is the Young's Modulus.

$$C_s = 1 - 0.5\left(\frac{\sigma'_{vb}}{\Delta q_s}\right) \tag{3.14}$$

where,

σ'_{vb} is the effective vertical stress at foundation level.

The equation 3.14 reflects the effect of the foundation embedment, logically favourable for the global settlement reducing it and a very significant enhancement introduced by the method. It must be referred that one of the causes for the deviation in the results of the elastic solution is related to non-consideration of C_s factor. Actually, the elastic solutions do not consider the influence of the effective vertical stress increase with the depth, which leads to increase of the Young's Modulus too.

The Figure 3.7 describes graphically the evolution with depth of the vertical strain influence factor, where the vertical strain grows until reaching a peak ($I_{\varepsilon p}$) depending on the stress level. Thereafter the influence factor starts to decrease, lowering until zero. The correspondent ordinate represents the vertical strain influence depth. The factor I_ε is calculated according to Table 3.4

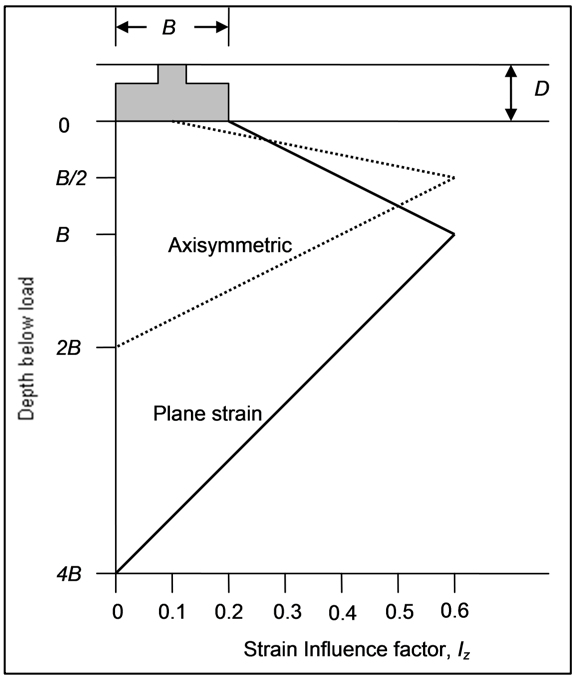

Figure 3.7 – Illustration of the vertical strain influence factor calculation (adapted from www.rocscience.com)

Table 3.4 – Vertical strain influence factor expressions (Matos Fernandes, 2011)

Foundation Shape	Depth	I_ε expression
Axisymmetric (square or circular)	0≤ z ≤B/2	$I_\varepsilon = 0.1+(z/B).(2.I_{\varepsilon p}-0.2)$
	B/2 ≤ z ≤ 2B	$I_\varepsilon = 0.667I_{\varepsilon p}.(2-z/B)$
Continues 10≤L/B	0≤ z ≤B	$I_\varepsilon = 0.2+(z/B).(I_{\varepsilon p}-0.2)$
	B ≤ z ≤ 4B	$I_\varepsilon = 0.333I_{\varepsilon p}.(4-z/B)$
1<L/B<10	$I_\varepsilon = I_{\varepsilon s}+0.111(I_{\varepsilon c}- I_{\varepsilon s})$ $I_{\varepsilon s}$ is the I_ε for an axisymmetric foundation $I_{\varepsilon c}$ is the I_ε for an continues foundation	

In practice, the integral presented generally in equation 3.13 is replaced by a sum of *n* sublayers in which the soil is divided (equation 3.15):

$$s_i = C_s \Delta q_s \sum_{j=1}^{n} \frac{I_{\varepsilon j}}{E_j} h_j \tag{3.15}$$

3.3.3. Estimation of pile group Settlements

The analysis of pile group settlements must focus the pile-soil interaction since each pile behaves itself not independently but rather interacting with the surrounding ones. In this way, the stress-strain behavior should assess not only the individual pile deformation due to the load application over its axis but also the effect that the group will induce in the global settlement. There are numerous approaches regarding the estimation of pile group settlements amongst them the well-recognized Interaction Factor Method proposed by Poulos and Davis (1980) which is described below.

The global settlement (w_i) of the pile *i* within a group of n piles is given by the equation 3.16:

$$w_i = \sum_{j=1}^{n} \left(P_{av}.S_1.\alpha_{ij}\right) \tag{3.16}$$

where,

P_{av} is the average load on a pile within the group;

S_1 is the settlement of a single pile under unit load;

α_{ij} is the interaction factor for pile *i* due to any other pile (j) within the group, corresponding to the spacing s_{ij} between piles i and j.

Analysing the equation 3.16, some considerations must be done regarding the determination of s_1 and α_{ij}, since the value of the first component (P_{av}) is consequence of direct application of the project serviceability load.

The settlement of a single pile under unit load (s_1) corresponds to the pile flexibility (FL^{-1}) and, assuming a continuous elastic behaviour of the soil, it can be determined as follows in the equation 3.17, as proposed by Poulos (1987):

$$s_1 = w_t = \frac{P_T I_\rho}{D.E_{sL}} \tag{3.17}$$

where,

P_T is the unit load applied on pile *I*;

I_ρ is the displacement influence factor and is calculated according to equation 3.18:

D is the pile diameter;

E_{sL} is the Young's Modulus at the pile tip.

$$I_\rho = 4(1+\nu_s)\frac{\left[1+\frac{1}{\pi\lambda}.\frac{8}{1-\nu_s}.\frac{\eta_1}{\xi}.\frac{\tanh(\mu_L)}{\mu_L}.\frac{L}{D}\right]}{\left[\frac{4\eta_1}{(1-\nu_s)\xi}+\frac{4.\pi.\rho.\tanh(\mu_L).L}{\zeta.\mu_L.D}\right]} \tag{3.18}$$

where,

ν_s is the Poisson's ratio;

λ is the lambda factor calculated according to equation 3.19

η_1 is the eta factor according to equation 3.20;

ξ is the xi factor according to equation 3.21;

μ_L is the mu factor according to equation 3.22;

L is the pile length;

ρ is the rho factor according to equation 3.23;

ζ is the zeta factor according to equation 3.24.

$$\lambda = 2(1+\nu_s).E_p/E_{sL} \tag{3.19}$$

where,

E_p is the pile modulus.

$$\eta_1 = D_b/D \tag{3.20}$$

where,

D_b is the diameter of pile base.

$$\xi = E_{sL}/E_b \tag{3.21}$$

where,

E_b is the soil modulus below foundation base.

$$\mu_L = 2\sqrt{\frac{2}{\zeta.\lambda}}.\frac{L}{D} \tag{3.22}$$

$$\rho = E_{sm}/E_b \tag{3.23}$$

where,

E_{sm} is the soil modulus at mid-depth of pile shaft.

$$\zeta = ln\left[\frac{(0.25 + [2.5\rho(1-\nu_s) - 0.25]\xi).2L}{D}\right] \tag{3.24}$$

The Figure 3.8 represents graphically the concept of many of the above mentioned components and also the evolution in depth of the Young's modulus which is considered to increase linearly along the pile.

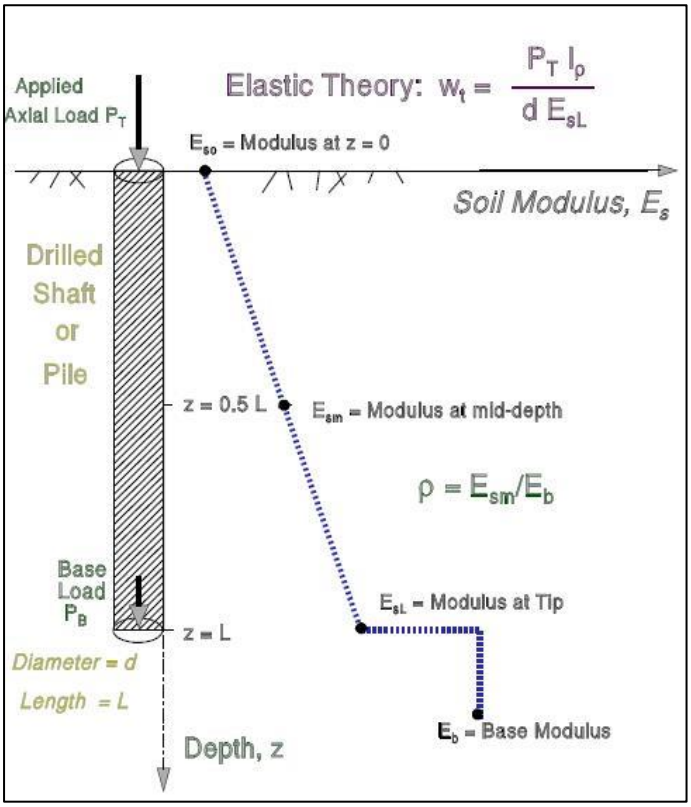

Figure 3.8 – Young's modulus vs. depth (Mayne, 2001)

The interaction factor (α_{ij}) represents the effect on the global settlement of the pile i due to the load application in another pile (j) within the group (Figure 3.9).

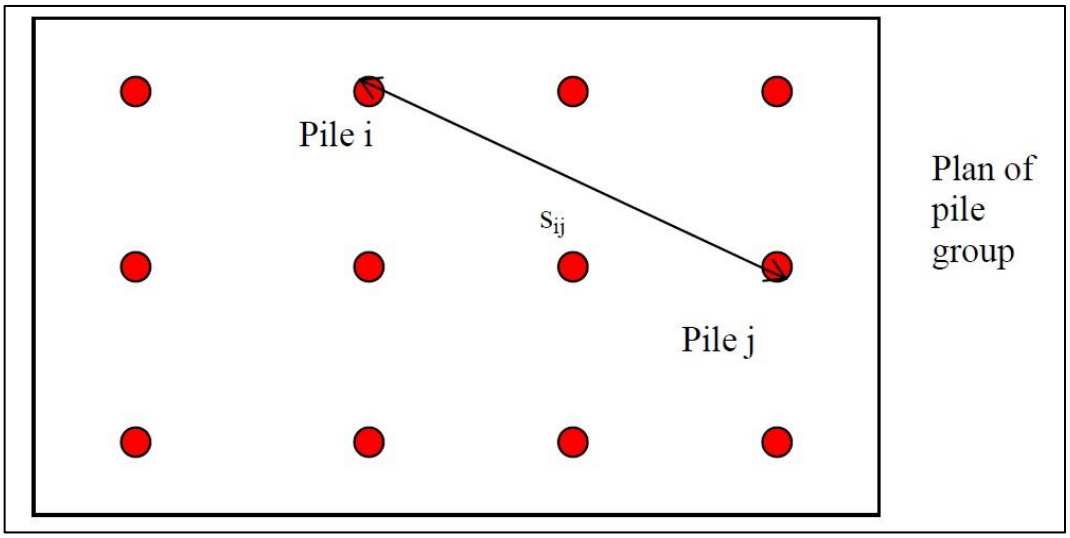

Figure 3.9 – Example of interaction factor method (Poulos, 2006)

The spacing between the piles (s) emerges, obviously, as the main factor to determine the interaction factor (α_{ij}), although the latter is not linearly proportional to the first. These correlations are the aim of the study of several researchers. One of the most recent approaches was proposed by Mandolini and Viggiani (1997). The authors suggested two expressions to define the interaction factor α, the first a polynomial function (3.25) and the second a natural logarithm function (3.26). In order to avoid scale effects, the pile spacing (s) component is normalized by the ratio with the pile diameter (D).

$$\alpha = A.(s/D)^B \tag{3.25}$$

$$\alpha = C + D.ln(s/D) \tag{3.26}$$

Where A, B, C and D are verified values tested by Mandolini and Viggiani. Regarding equation 3.25, A ranging between 0.57 to 0.98 whereas B ranges between -0.60 to -1.20. For the second equation (3.26) only one coefficient for each C (1.0) and D (-0.26) was computed.

4
DESIGN OF THE STUDIED PILED RAFT FOUNDATION

4.1. INTRODUCTION

Figure 4.1 represents the detailed structural plan view of the basement of the building "A" which location is defined by the red contour in Figure 2.1.The area of the building is 1059.06 m^2 and structural solution is as follows:

- 64 columns with cross section of 40x40 cm;
- 4 columns with cross section of 55x55 cm;
- 6 columns with cross section of 65x65 cm;
- Walls of 0.3 m thick.

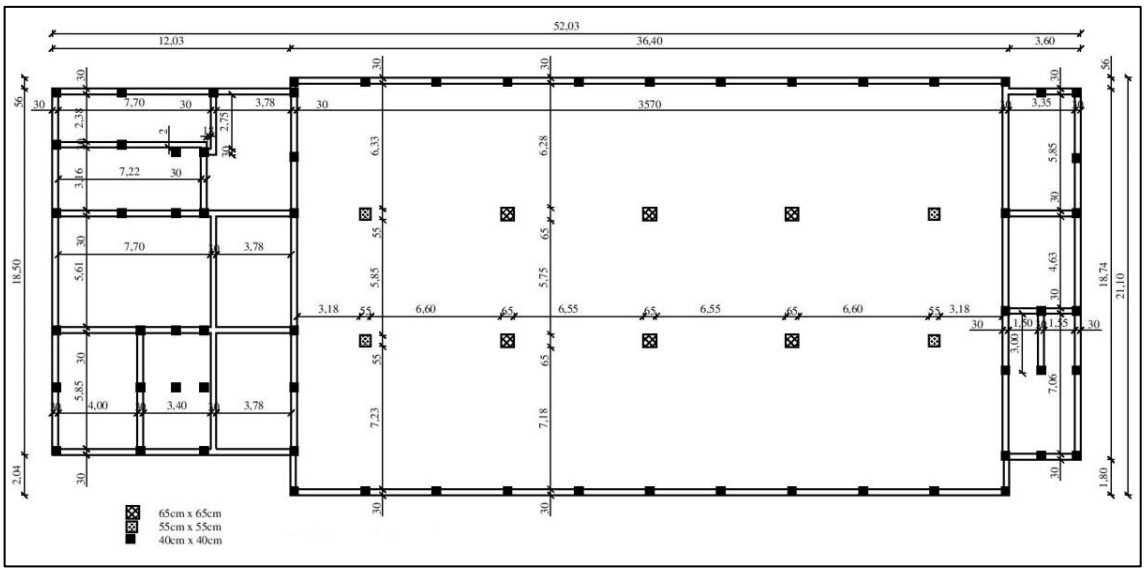

Figure 4.1 – Detail structural plan view (Bohn Deep Foundation Ltd)

The location of the piles was defined according to the given geometry (Figure 4.1). Consequently, in the case of a column receiving only one pile, the axis of the latter should overlap the axis of the first one. When the solution is more than one pile per column, the piles must have a distance between axis of three diameters (3D), centered on the column.

The foundations were designed considering exclusively vertical loads transmitted to the mat at the base of the columns, as given by the structural designer Bohn Deep Foundation Ltd (see Appendix A). In view of this action, the transversal loads will not be considered in the calculation that was developed in this thesis. The stresses (namely, the bending moments and the shear forces) induced by the differential settlements associated to the different vertical reactions of each pile(s) – simulated as springs – were exclusively supported by the mat slab. This was structurally designed accordingly.

The pile geotechnical design was done considering two different types of piles, CFA (replacement piles) and OMEGA (displacement piles) and for both of them were considered two different diameters. For CFA, there were used the ø 0.6 m and ø 0.8 m diameters whereas for the OMEGA were used the ø 0.4 m and ø 0.6 m diameters. A detailed analysis of both types is made in the Subchapter 4.2.

The calculation of a single pile bearing capacity (only axially loaded piles) was performed by two methods outlined in detail in the Subchapter 3.2.

- Method to determine the compressive resistance of a single pile proposed in Eurocode 7 Part 2, Annex D.7 (CEN, 2007), based on de Ruiter and Beringen (1979) method;
- LCPC Method (Bustamante and Frank, 1999).

It should also be referred that these methods determine the compressive ground resistance which may not be the most pernicious for the pile design when compared with compression strength limits of concrete indicated by the DTU 13.2 French standard, which were also calculated.

After reaching the design values for the single pile resistance, it was possible to determine the optimal pile group solution comparing them with the design loads. The final decision was made through the approximated calculation of the associated costs of both pile types.

4.2. CFA AND OMEGA PILES

The use of continuous flight auger (CFA) and the OMEGA piles (Figure 4.2) are common in the current day deep foundations solutions due to its high bearing capacity, notable productivity, absence of vibrations and noise during the works, being also possible to control the quality of the execution. The use of the CFA dates back to the year 1950, implemented first in the USA whereas the OMEGA piles are a most recent innovation in the deep foundations field being introduced in Europe during the last decade of the 20th century.

Figure 4.2 – On the left, a photo of a CFA pile and on the right, a photo of a OMEGA pile

4.2.1. CONTINUOUS FLIGHT AUGER PILES

The CFA piles diameters varies from 0.3 m to 1.0 m and pile tip can be located up to 30 meters deep, enabling the use of this solution in a very wide range of different geotechnical scenarios.

Regarding the execution method, the CFA piles are drilled foundations reaching the defined depth using a continuous flight auger and the installation process comprises three steps (Brown *et al.*, 2007):

- Drilling execution. the borehole stability is assured as the flights of the auger are filled with soil as the drilling goes on, avoiding the use of temporary casing or bentonite slurry;
- Casting of the pile. after reaching the required depth, the concrete starts being pumped and the auger, rotating in the same direction of the drilling, is slowly ejected, this procedure guarantees that the hole is never left open and the relation between pumped concrete pressure and the auger withdrawal rate will be decisive in the control of soil decompression;
- Placement of the reinforcement. after the withdrawal of the auger and with the concrete still fluid, the reinforcement should be placed.

Figure 4.3 illustrates the execution method of the CFA piles.

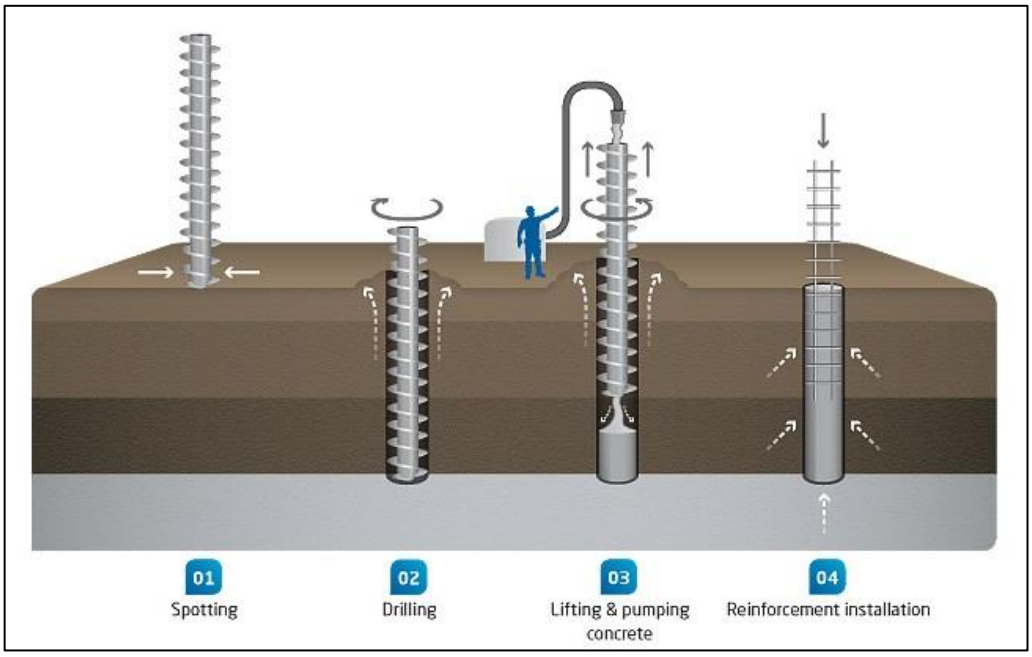

Figure 4.3 – Execution sequence of CFA piles (adapted from www.junttan.com)

Being excavated, and therefore non-displacement piles, the CFA are highly recommended in very confined construction areas with neighbouring foundations and underground structures, since there are no considerable induced movements of the surrounding soil. Another important advantage of CFA piles is the fact that their execution can be accompanied by registering electronically the involved parameters, such as penetration and uplift ratio, torque, auger depth, concrete injected volume at every step of the auger advance and subsequent withdrawal and the required pumping concrete pressure.

On the other hand, the great weakness of this solution continues to be the dependence of the operator performance, which will influence largely the geotechnical response of the pile (mainly the bearing capacity). The soil decompression resulting from the soil removal can also be a major problem in the

execution process, but at the same time it is also possible to reduce it considerably by using appropriately the monitoring equipment. Finally, the choice of CFA piles solution requires a minimum number of piles in order to justify the sophisticated equipment needed.

4.2.2. OMEGA PILES

The OMEGA piles are specific patented type of "screw piles" or, as it is called in the USA, drilled displacement piles (DD piles), belonging to the most recent enhancements in deep foundations solutions (Brown, 2005). The commercial diameters vary generally between 0.3 m and 0.6 m with increments of 50 mm and the maximum pile tip can be placed down to around 30 m.

The piles are executed by drilling a screw into the soil until the project defined depth is achieved without implying significant soil removal. The execution sequence is reasonably similar (Brown *et al.*, 2007) to the presented before in the case of the CFA piles:

- Drilling execution. the drilling advances as the auger penetrates forcing the soil to move laterally requiring therefore a greater torque than CFA, which has to be enough to mobilize the soil resistance; during the process both the torque and the penetration rate can be controlled in the operator's computer.
- Casting-on the pile. this step is very similar to the CFA, where the rotation is kept slow and in the same direction of the insertion as the auger is uplifted; alongside, the self-compacting concrete is pumped at a certain pressure.
- Placement of the reinforcement. the placement of the reinforcement cage can be made before, alongside or after the extraction of the auger; in the latter, it has to be lowered still with the concrete in a fluid state.

Figure 4.4 exemplifies the execution method of a general screw pile where the reinforcement is placed before the pile concrete casting.

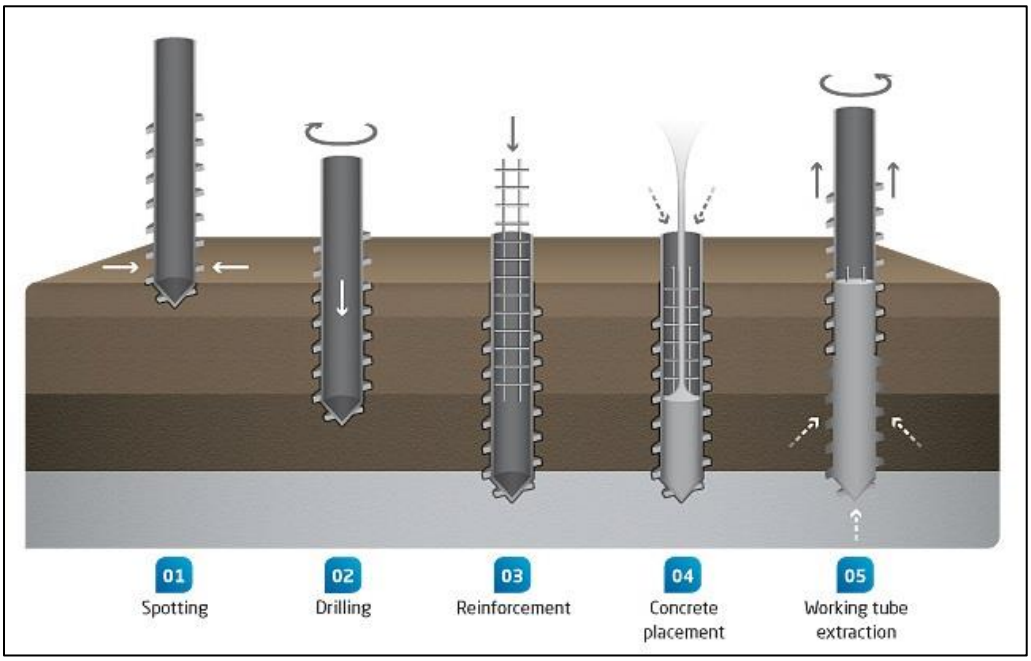

Figure 4.4 – Execution sequence of a general screw pile (adapted from www.junttan.com)

The induced soil lateral displacement densifies the surrounding soil allowing even, in some cases, a self-supporting phase between the drilling and the reinforcement placement. The increase of relative density is reflected in the increase of load bearing capacity, which proved to be one of major advantages of this technique. The absence of vibrations and the quiet installation makes this type of solutions even more recommendable than the CFA. Moreover, the non-replacement of the soil can also play an important role in the decision, considering the loss of high volume of material. Another notable advantage, directly associated to the previous, is the fact that transport trucks and earthworks machinery are not required. The complete monitoring of the process is also possible in the OMEGA piles execution.

The limited diameters range is the main disadvantage, must be pointed out mostly because of the required high torque (Almeida Neto, 2002). Thus, these piles are not commonly considered for the situation where high bending forces are induced, fitting well when receiving axial loads.

4.3. RESULTS FOR THE BEARING CAPACITY OF A SINGLE PILE

The determination of the bearing capacity design values was made from the interpretation of 3 CPTU tests, using only the cone resistance, q_c. The sleeve friction, f_s, does not take part of the pile capacity and the water pressure measurements were excluded due to the lack of reliance in the water pressure measurements (u). Consequently, the unequal area effect was not taken into account (using q_t instead of q_c), which in this case does not produce significant errors once the majority of the soil crossed shows a drained behaviour and also because the cohesive q_c values are significantly high.

In the specific case of this work, the calculated resistances were made through the analysis of ground test results (n=3), as referred. So, the correlation factors for this case are ξ_3 and ξ_4, as described in Annex A.3.3.3 of EC7 (CEN, 2007) and the characteristic values are calculated using the equation 4.1.

$$R_{c;k} = R_{b;k} + R_{s;k} = \frac{R_{b;cal} + R_{s;cal}}{\xi} = \frac{R_{c;cal}}{\xi} = min\left\{\frac{(R_{c;cal})_{mean}}{\xi_3}; \frac{(R_{c;cal})_{min}}{\xi_4}\right\} \quad (4.1)$$

where,

$(R_{c;cal})_{mean}$, is the average of the calculated resistance obtained in each of the tests performed;

$(R_{c;cal})_{min}$, is the minimum of the calculated resistance obtained in each of the tests performed;

ξ_3 and ξ_4 are correlation factors to derive the pile resistance from ground investigation results.

4.3.1. DESIGN BEARING CAPACITY ACCORDING TO THE METHOD PROPOSED IN EUROCODE 7

The obtained results for $p_{max;base}$ for both CFA and OMEGA piles are shown above as well as the calculation procedure.

Considering the equation 3.6, β=1 since the piles diameter is constant along its length for both CFA and OMEGA piles and s=1because the pile base is circular, being L/B=1.

To exemplify the calculation the of the $q_{c;I;mean}$, $q_{c;II;mean}$ and $q_{c;III;mean}$, consider the generic q_c values extracted from a CPT/CPTU log in Table 4.1. Assuming hypothetically that the pile tip is 4 m depth and the equivalent diameter (D_{eq}) is 0.4 m, then:

$$H_{-8D} = 4 - 8 \times 0.4 = 0.60 \cong 0.80\ m$$

$$H_{+0.7D} = 4 + 0.7 \times 0.4 = 4.28 \cong 4.40\ m$$

$$H_{+4D} = 4 + 4 \times 0.4 = 5.60\ m$$

Table 4.1 – Hypothetic q_c data

Depth (m)	q_c (MPa)	$q_{c;I}$ (MPa)	$q_{c;II}$ (MPa)	$q_{c;III}$ (MPa)
0.00	0.000			
0.40	2.479			
0.80	**4.349**			4.349
1.20	5.981			5.981
1.60	6.761			6.559
2.00	7.775			6.559
2.40	7.937			6.559
2.80	7.454			6.559
3.20	6.895			6.559
3.60	6.559			6.559
4.00	**6.881**		5.874	6.881
4.40	**7.102**	6.992	5.874	
4.80	6.645	6.876	5.874	
5.20	5.874	**6.626**	5.874	
5.60	**7.745**	6.849		
6.00	7.960			
6.40	7.850			
6.80	7.139			
7.20	6.419			

The yellow shaded value is $q_{c;I;mean}$ (6.626 MPa), the minimum average of $q_{c;I}$ and also the depth where the $p_{max;base}$ becomes minimum, being therefore called critical depth.

Starting at that point upwards to the pile tip, the $q_{c;II}$ is the minimum q_c value between the critical depth and its respective position. Thus, $q_{c;II;mean}$ is equal to 5.874 MPa (the average of all the $q_{c;II}$ values).

The algorithm to determine the $q_{c;III;mean}$ (6.285 MPa) is the same as the previous, changing the start and the ending point, being respectively the pile tip and a depth 8 diameters above it. In EC7, an upper limit of 2 MPa is defined for this value in the case of CFA piles. There is no specific reference to OMEGA piles in the referred code, for what it was decided to adopt the same value as maximum.

In Table 4.2, all the values of $q_{c;I;mean}$, $q_{c;II;mean}$, $q_{c;III;mean}$, α_p and $p_{max;base}$ are presented based on the CPT1, CPT2 and CPT3 for CFA and OMEGA piles calculated for both diameters. Lakatos (2011) suggests as well the adoption of an upper limit for the $p_{max;base}$ the resistance of 5 MPa for both cohesive and granular soils.

Table 4.2 – Pile end bearing capacity ($p_{max;base}$) according to EC7

	CPT1				CPT2				CPT3			
	OMEGA		CFA		OMEGA		CFA		OMEGA		CFA	
	0.40	0.60	0.60	0.80	0.40	0.60	0.60	0.80	0.40	0.60	0.60	0.80
$q_{c;I;mean}$ (MPa)	23.031	21.088	21.088	16.745	20.662	20.596	20.596	16.526	19.376	19.376	19.376	16.636
$q_{c;II;mean}$ (MPa)	22.550	2.297	2.297	1.904	16.315	12.325	12.325	1.725	15.897	15.897	15.897	2.400
$q_{c;III;mean}$ (MPa)	2.000	2.000	2.000	1.663	2.000	2.000	2.000	1.356	2.000	2.000	2.000	2.000
α_p	0.80	0.80	0.70	0.70	0.80	0.80	0.70	0.70	0.80	0.80	0.70	0.70
$p_{max;base}$ (MPa)	5.00	5.00	3.79	3.85	5.00	5.00	5.00	3.67	5.00	5.00	5.00	4.03

The imposition of an upper limit of 2 MPa for the $q_{c;III;mean}$ reduced significantly its influence in the final value, resulting that the $q_{c;I;mean}$ has the largest contribution, followed by the $q_{c;II;mean}$.

Finally, end bearing force values ($R_{b;cal}$) are shown in Table 4.3, as result of the multiplication of the $p_{max;base}$ values by the respective piles base area (A_b).

Table 4.3 – End bearing force ($R_{b;cal}$) according to EC7

$R_{b;cal}$ (kN)	CFA		OMEGA	
	0.6	0.8	0.4	0.6
CPT1	1354.99	1932.97	628.32	1413.72
CPT2	1413.72	1843.94	628.32	1413.72
CPT3	1413.72	2026.32	628.32	1413.72

The obtained results for $p_{max;shaft}$ for both CFA and OMEGA piles are shown in Table 4.4, Table 4.5 and Table 4.6, considering either the equations 3.9 or 3.10 depending on the crossed layer.

The outlined method detailed on 3.2.1 differs from the initial approach presented on Eurocode 7 basically on the evolution of the q_s with the increasing of the q_c. The chosen approach uses a square root function instead of a linear function according to EC7 guidelines. Moreover, Mahler (2007) showed that the square root function adjusts well the relation between skin friction and cone resistance (Figure 4.5). Using effective skin friction values registered on CFA pile load tests and plotting them alongside with cone resistance, a tendency was possible to define. The cohesive results grow faster than the granular and transitional soil, which justifies the factor of 1.2 in the equation 3.10. In this case, it was used the effective cone resistance, q_E, instead of using the total cone resistance measured on the CPTU test, which for the determination of a mathematical formula is not relevant.

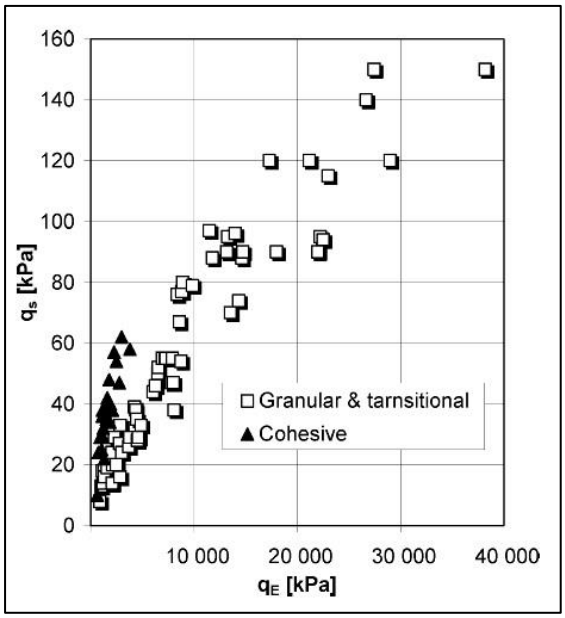

Figure 4.5 – Relation between the skin friction and the effective cone resistance (Mahler, 2007)

Using the $q_{c,mean}$ values indicated in Table 2.5, Table 2.6 and Table 2.7 and the respective layer thicknesses presented in Table 2.2, Table 2.3 and Table 2.4, it is possible to determine the unit side friction (q_{si}) as presented in Table 4.4, Table 4.5 and Table 4.6.

Table 4.4 – CPT1 q_s values for CFA and OMEGA piles

$q_{c,mean}$ (MPa)	CFA			OMEGA		
	α_s	$q_{s;max}$ (kPa)	q_{si} (kPa)	α_s	$q_{s;max}$ (kPa)	q_{si} (kPa)
26.34	0.55	120	89.3	0.75	160	121.7
3.92	1.00	80	75.2	1.25	100	94.0
9.89	0.55	120	54.7	0.75	160	74.6
1.52	1.00	80	46.7	1.25	100	58.4
10.00	0.55	120	55.0	0.75	160	75.0

Table 4.5 – CPT2 q_s values for CFA and OMEGA piles

$q_{c,mean}$ (MPa)	CFA			OMEGA		
	α_s	$q_{s;max}$ (kPa)	q_{si} (kPa)	α_s	$q_{s;max}$ (kPa)	q_{si} (kPa)
24.44	0.55	120	86.0	0.75	160	117.2
8.35	1.00	80	80.0	1.25	100	100.0
15.39	0.55	120	68.2	0.75	160	93.1
3.16	1.00	80	67.5	1.25	100	84.4
21.64	0.55	120	80.9	0.75	160	110.3

Table 4.6 – CPT3 q_s values for CFA and OMEGA piles

$q_{c,mean}$ (MPa)	CFA			OMEGA		
	α_s	$q_{s;max}$ (kPa)	q_{si} (kPa)	α_s	$q_{s;max}$ (kPa)	q_{si} (kPa)
7.83	0.55	120	48.7	0.75	160	66.4
1.92	1.00	80	52.6	1.25	100	65.8
13.39	0.55	120	63.6	0.75	160	86.8

The side friction loads ($R_{s;cal}$) values are shown in Table 4.7, as result of sum of the product of q_{si} by the respective shaft area (A_{si}) in each layer.

Table 4.7 – Side friction force ($R_{s;cal}$) according to EC7

$R_{s;cal}$ (kN)	CFA		OMEGA	
	0.6	0.8	0.4	0.6
CPT1	1287.62	1716.82	1149.94	1724.90
CPT2	1616.46	2155.28	1424.35	2136.53
CPT3	1390.35	1853.80	1257.95	1886.92

The average, $(R_{c;cal})_{mean}$, and the minimum, $(R_{c;cal})_{min}$, pile compressive resistance values are shown in the Table 4.8.

Table 4.8 – Average and minimum values of compressive resistance

[kN]	CFA		OMEGA	
	0.60	0.80	0.40	0.60
$(R_{c;cal})_{mean}$	2825.62	3843.04	1905.73	3329.83
$(R_{c;cal})_{min}$	2642.61	3649.79	1778.26	3138.62

Finally, in Table 4.9 the design values are calculated, as result of the application of the EC7 suggested method to determine the compressive resistance of a single pile.

Table 4.9 – Design total resistance of the piles after the correlation factors

[kN]	CFA		OMEGA	
	0.60	0.80	0.40	0.60
$(R_{c;cal})_{mean}$	2825.62	3843.04	1905.73	3329.83
ξ_3	1.33	1.33	1.33	1.33
$(R_{c;cal})_{min}$	2642.61	3649.79	1778.26	3138.62
ξ_4	1.23	1.23	1.23	1.23
$R_{c;k}$	2124.52	2889.51	1432.88	2503.63
γ_t	1.10	1.10	1.10	1.10
$R_{c;d}$	1931.39	2626.82	1302.62	2276.03

4.3.2. DESIGN BEARING CAPACITY ACCORDING TO LCPC METHOD (BUSTAMANTE AND FRANK, 1999)

The obtained results for q_b for both CFA and OMEGA piles are shown above according to the equation 3.11.

The q_{ce} values are summarized in Table 4.10. They represent the measured q_c between half a diameter (0.5D) above the pile tip and one and a half (1.5D) diameters below. It must be highlighted the high average q_c values registered around the base, validating the choice made regarding the pile tip position.

Table 4.10 – q_{ce} values for the different diameters considered

q_{ce} (MPa)	D=0.4 m	D=0.6 m	D=0.8 m
CPT1	23.302	23.597	23.930
CPT2	25.495	24.706	23.558
CPT3	21.350	21.597	21.284

The value of the K_c takes into account the pile type and the type of the surrounding soil. Bustamante and Frank (1999) suggested, for sand or silty sand, a value of K_c=0.15 for non-displacement (bored or excavated) piles and K_c=0.50 for displacement piles (driven). Since the piles tip is placed in every case in granular soil, the mentioned values were adopted, respectively for the CFA and OMEGA piles.

The q_b obtained values are presented in Table 4.11. No considerations regarding an upper limit for the pile end resistance were defined by the original authors. Hence, the results are largely influenced by the K_c and by the piles diameter. In fact, the OMEGA piles, in addition to the greater K_c, have a slightly larger average of q_{ce} value due to the smaller diameters and consequently more around the base influence.

Table 4.11 – Pile end bearing capacity (q_b) according to LCPC Method

q_b (MPa)	CFA		OMEGA	
	0.6	0.8	0.4	0.6
CPT1	3.540	3.589	11.651	11.799
CPT2	3.706	3.534	12.748	12.353
CPT3	3.240	3.193	10.675	10.799

The end bearing force values ($R_{b;cal}$) are shown in Table 4.12, as result of the multiplication of the q_b values by the respective base area (A_b) of the piles.

Table 4.12 – Pile end bearing force ($R_{b;cal}$) according to LCPC Method

$R_{b;cal}$ (kN)	CFA		OMEGA	
	0.6	0.8	0.4	0.6
CPT1	1000.80	1804.24	1464.14	3336.01
CPT2	1047.83	1776.24	1601.90	3492.77
CPT3	915.98	1604.75	1341.48	3053.25

The obtained results for q_s for both CFA and OMEGA piles are shown above according to the equation 3.12.

The average CPT cone resistance in each defined layer, so called $q_{c,mean}$, values are indicated in Table 2.5, Table 2.6 and Table 2.7. The β coefficient is a correlation factor to apply directly to average q_c values being defined only for 3 different types of piles (Table 4.13).

Table 4.13 – β correlation factor and $q_{s;max}$ based directly on CPT data (Viana da Fonseca *et al*., 2012)

Type of pile	Soils	Clays and Silts					Sands and Gravels		
	Range of q_c (MPa)	<3	3-6		>6		<5	8-15	>20
Bored without casing (dry method)	β	-	-	75			200	200	200
	$q_{s;max}$ (kPa)	15	40	80	40	80			120
Bored with temporary casing	β	-	100	100	-	100	250	250	300
	$q_{s;max}$ (kPa)	15	40	60	40	80	-	40	120
Driven precast concrete	β	-	75		-		150	150	150
	$q_{s;max}$ (kPa)	15	80		80		-	-	120

Considering that none of the pile types presented in Table 4.13 match the pile types chosen in the scope of this project, it was necessary the use of the correlation charts (Figure 4.6), converting the CPT q_c averages into an equivalent PMT p_l. This procedure allows the estimation of q_{si} based on Pressuremeter test results, wherewith were defined 10 curves relating p_l and q_s (Figure 4.7) depending on the type of piles (Table 4.17) and the crossed soil (Table 4.18).

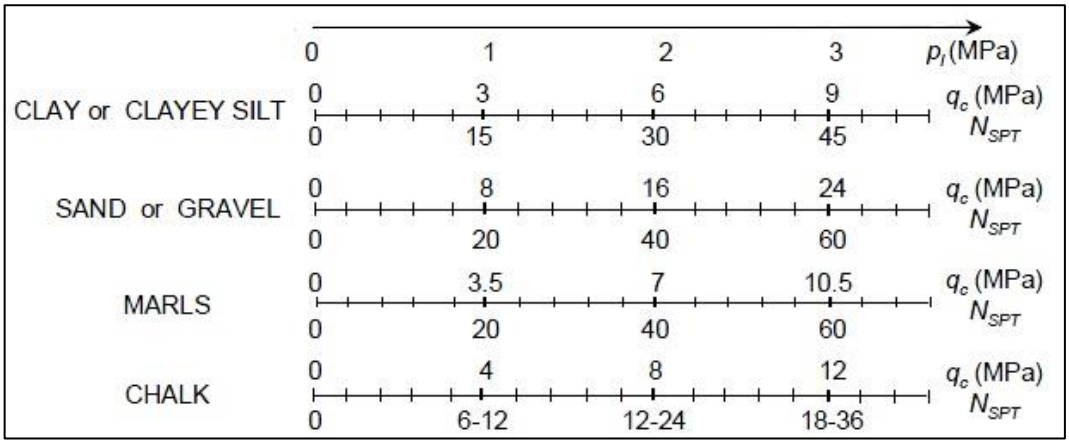

Figure 4.6 – Equivalent p_l depending on the soil type (Bustamante and Gianeselli, 1996)

According to Figure 4.6, the ratio q_c/p_l for clays or clayey silt is 3 and 8 for sand or gravels. In Table 4.14, Table 4.15 and Table 4.16 are presented the equivalent p_l associated to each of the identified strata, applying the correspondent ratio for granular and cohesive material.

Table 4.14 – CPT1 equivalent p_l values

Layer	h_i (m)	h_f (m)	$q_{c,mean}$ (MPa)	p_l (MPa)
1	112.40	112.00	26.338	3.29
2	112.00	110.70	3.923	1.31
3	110.70	106.50	9.885	1.24
4	106.50	105.50	1.515	0.51
5	105.50	100.53	9.997	1.25

Table 4.15 – CPT2 equivalent p_l values

Layer	h_i (m)	h_f (m)	$q_{c,mean}$ (MPa)	p_l (MPa)
1	112.40	112.00	24.438	3.05
2	112.00	11.00	8.348	2.78
3	111.00	106.50	15.394	1.92
4	106.50	103.00	3.164	1.05
5	103.00	100.53	21.640	2.71

Table 4.16 – CPT3 equivalent p_l values

Layer	h_i (m)	h_f (m)	$q_{c,mean}$ (MPa)	p_l (MPa)
1	112.40	111.80	7.827	0.98
2	111.80	111.00	1.922	0.64
3	111.00	100.53	13.389	1.67

As it was referred, the curve Q that connects the p_l to q_s must be chosen first based on the pile type and after on the soil crossed.

Table 4.17 – Description of the 418 analysed piles (Bustamante *et al.*, 2009)

Group Code	Type No.	Piles[2] Qty	D[3] (mm)	Depth[4] (m)	Pile Description
1	1	8	500-2000	11.5-23	Pile or Barrette Bored in the Dry
	2	64	270-1800	6-78	Pile or Barrette Bored with Slurry
	3	2	270-1200	20-56	Bored and Cased Pile (permanent casing)
	4	28	420-1100	5.5-29	Bored and Cased Pile (recoverable casing)
	5[1]	4	520-880	19-27	Dry Bored Piles or Slurry Bored Piles with Grooved Sockets or Piers (3 types)
2	6[1]	50	410-980	4.5-30	Bored Pile with a single or a double-rotation CFA (2 types)
3	7	48	310-710	5-19.5	Screwed Cast-in-Place
	8	1	650	13.5	Screwed Pile with Casing
4	9[1]	30	280-520	6.5-72.5	Pre-cast or Pre-stressed Concrete driven Pile (2 types)
	10	15	250-600	8.9-20	Coated Driven Pile (concrete, mortar, grout)
	11	19	330-610	4-29.5	Driven Cast-in Place Pile
	12	27	170-810	4.5-45	Driven Steel Pile, Closed Tip
5	13	27	190-1.22	8-70	Driven Steel Pile, Open End
6	14	23	260-600	6-64	Driven H Pile
	15	4	260-430	9-15.5	Driven Grouted[5 or 6] H Pile
7	16	15	-	3.5-2.5	Driven Sheet Pile
1	17		80-140	4-12	Micropile Type I
	18	8	120-810	8.5-37	Micropile Type II
8	19	23	100-1220	8.5-67	SGP Micropile (Type III) or SGP Pile
	20	20	130-660	7-39	MRP Micropile (Type IV) or MRP Pile

(1) Some types may include several sub-types. (2) Some piles subjected to several tests. (3) Minimum and maximum nominal diameter B. (4) Minimum and maximum full embedment depth D. (5) Involving a Single Global Post grouting. (6) With Multiple Repeatable Post grouting.

Hence, it was considered for the CFA piles the "Bored Pile with a single or a double rotation CFA (2 types)", corresponding to type 6 and group 2, whereas for the OMEGA piles was selected the "Screwed Cast-in Place Pile" type number 7 and group 3.

Based on the above mentioned regarding the characteristic of both piles, the match was clear considering that CFA piles have pile type specifically with its name. The OMEGA piles are part of the "Screw Piles" as defined by the European Nomenclature.

Table 4.18 – Pile type Curves (Qi) associated to a certain soil type (Bustamante *et al.*, 2009)

Pile Type No.	Clay, Loam	Sand, Gravel	Chalk	Marl, Limestone	Weathered Rock
1	Q2	Q2*	Q5	Q4	Q6**
2	Q2	Q2	Q5	Q4	Q6**
3	Q1	Q1	Q1	Q2	Q1**
4	Q1	Q2	Q4	Q4	Q4**
5	Q3	Q3*	Q5	Q4	Q6**
6	Q2	Q4	Q3	Q5	Q5**
7	Q3	Q5	Q4	Q4	Q4**
8	Q1	Q2	Q2	Q2	Q2**
9	Q3	Q3**	Q2	Q2**	(a)
10	Q6	Q8	Q7	Q7	(a)
11	Q2	Q3	Q6**	Q5**	(a)
12	Q2	Q2**	Q1	Q2**	(a)
13***	Q2	Q1	Q1	Q2	(a)
14***	Q2	Q2	Q1	Q2**	(a)
15***	Q6	Q8	Q7	Q7	(a)
16***	Q2	Q2	Q1	Q2**	(a)
17	Q1	Q1	Q1	Q2	Q6**
18	Q1	Q1	Q1	Q2	Q6**
19	Q6	Q8	Q7	Q7	Q9**
20	Q6	Q9	Q9	Q9	Q10**

* If ground properties permit. ** Use of a higher value must be proven by a load test. *** Cross section and perimeter estimated according to Fig.3.
(a) For pile groups No.9 – 16 and if rock condition permits penetration, choose the qs value proposed for marl and limestone or a higher one if this can be proven either by a load test or by reference to an existing example in the same local area

The information in Table 4.18 establishes the curve Qi for a certain pile type based on a certain soil crossed. Consequently, "Clay, Loam" corresponds to cohesive layers and "Sand, Gravel" to granular layers. Hence the curves adopted are presented in Table 4.19.

Table 4.19 – Respective curves Qi adopted

	Granular	Cohesive
CFA	Q4	Q2
OMEGA	Q5	Q3

Finally the values of q_{si} are obtained through the analysis of the abacus on Figure 4.7. The results are shown in Table Table 4.20, Table 4.21 and Table 4.22.

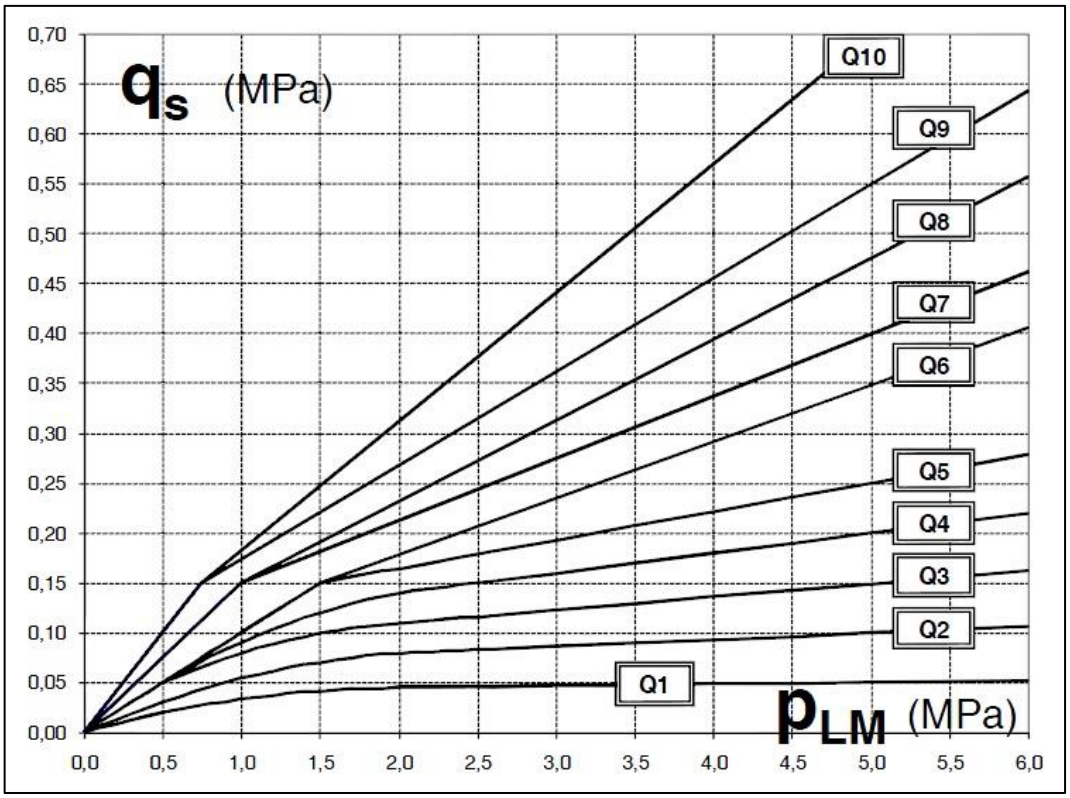

Figure 4.7 – Qi Abacus correlating Ménard Limit Pressure (p_{LM}) with skin friction (q_s) (Bustamante *et al.*, 2009)

Table 4.20 – CPT1 q_{si} values for CFA and OMEGA piles

p_l (MPa)	CFA		OMEGA	
	Tipo	q_s (kPa)	Tipo	q_s (kPa)
3.29	Q4	170	Q5	200
1.31	Q2	70	Q3	90
1.24	Q4	120	Q5	130
0.51	Q2	30	Q3	50
1.25	Q4	120	Q5	130

Table 4.21 – CPT2 q_{si} values for CFA and OMEGA piles

p_l (MPa)	CFA		OMEGA	
	Tipo	q_s (kPa)	Tipo	q_s (kPa)
3.05	Q4	160	Q5	190
2.78	Q2	80	Q3	110
1.92	Q4	135	Q5	160
1.05	Q2	55	Q3	75
2.71	Q4	155	Q5	180

Table 4.22 – CPT3 q_{si} values for CFA and OMEGA piles

p_l (MPa)	CFA		OMEGA	
	Tipo	q_s (kPa)	Tipo	q_s (kPa)
0.98	Q4	100	Q5	150
0.64	Q2	40	Q3	60
1.67	Q4	130	Q5	180

The last version of the LCPC Method does not provide any guidelines regarding an upper limit for the skin friction ($q_{s;max}$). However, when correlated with p_l, the limiting values of q_s are implicitly defined by the evolution of the curves (Figure 4.7).

The side friction load ($R_{s;cal}$) values are shown in Table 4.23, as result of sum of the product of q_{si} by the respective shaft area (A_{si}) of each layer.

Table 4.23 – Side friction force ($R_{s;cal}$) according to LCPC Method

$R_{s;cal}$ (kN)	CFA		OMEGA	
	0.6	0.8	0.4	0.6
CPT1	2430.46	3240.62	1808.43	2712.64
CPT2	2501.05	3334.74	2027.08	3040.62
CPT3	2739.03	3652.04	2503.98	3755.96

The average, $(R_{c;cal})_{mean}$, and the minimum, $(R_{c;cal})_{min}$, pile compressive resistance values are shown in the Table 4.24.

Table 4.24 – Average and minimum values of compressive resistance

[kN]	CFA		OMEGA	
	0.60	0.80	0.40	0.60
$(R_{c;cal})_{mean}$	3545.05	5137.54	3582.33	6463.75
$(R_{c;cal})_{min}$	3431.26	5044.86	3272.56	6048.65

In Table 4.25, the design values are calculated resulting from the application of the LCPC Method.

Table 4.25 – LCPC design total resistance of the piles after the correlation factors

[kN]	CFA		OMEGA	
	0.60	0.80	0.40	0.60
$(R_{c;cal})_{mean}$	3545.05	5137.54	3582.33	6463.75
ξ_3	1.33	1.33	1.33	1.33
$(R_{c;cal})_{min}$	3431.26	5044.86	3272.56	6048.65
ξ_4	1.23	1.23	1.23	1.23
$R_{c;k}$	2665.45	3862.81	2660.62	4859.96
γ_t	1.10	1.10	1.10	1.10
$R_{c;d}$	2423.14	3511.65	2418.74	4418.15

The Table 4.26 summarizes the design values for the ultimate pile bearing capacity, where the LCPC proved to be less conservative than the EC7 Approach. Hereinafter, the design, including the determination of the number of piles, shall be made based on the latter.

Table 4.26 – Comparison between the $R_{c;d}$ obtained by the two methods

$R_{c;d}$ (kN)	CFA		OMEGA	
	0.6	0.8	0.4	0.6
EC7 Approach	1931.39	2626.82	1302.62	2276.03
LCPC Method	2423.14	3511.65	2418.74	4418.15

4.3.3. DTU 13.2 NORM (1992)

The French Norm DTU 13.2 "*Foundations Profondes pour le Bâtiment*" established a criterion for the pile design, apart from the outlined methods that estimate "compressive resistance of the ground against a pile, at the ultimate limit state" (in Eurocode 7). For reinforce concrete piles, the criteria controls the stress level of concrete avoiding the steel yielding and concrete cracking.

The approach defines a conventional concrete compressive strength, f_c* (equation 4.2):

$$f_c^* = \frac{\min(f_{cj}; f_{clim})}{k_1 . k_2} \tag{4.2}$$

where,

f_{cj} is the characteristic compressive cylinder strength of concrete at j days, according to BAEL guidelines;

f_{clim} is a limit strength of concrete depending on pile foundation type (Table 4.27);

k_1 is a coefficient that takes into account the execution method of the pile (Table 4.27);

k_2 is a coefficient that takes into account the difficulty related to the concrete casting of the pile.

Table 4.27 – Relation between the pile type and the respective f_{clim} and k_1 (DTU 13.2, 1992)

Group	Pile Foundation Type	f_{clim}	k_1
A	Borehole piles or precast walls	f_{c28}	1.00
	Pre-stressed tubular piles	f_{cj}	1.15
	Prefabricated piles dynamically driven	f_{cj}	1.15
	Well with vibrated concrete	f_{c28}	1.00
	Well with self-compacting concrete	f_{c28}	1.20
B	Driven Cast-in Place Pile	f_{c28}	1.30
	Pile or Barrette Bored in the dry	f_{c28}	1.30
	Bored and Cased Pile		
	▪ Dry casting	f_{c28}	1.20
	▪ Casting underwater	f_{c28}	1.30
	Pile and Barrette Bored with Slurry (generally bentonite)	f_{c28}	1.30

The k_2 value is determined as follows:

- Elements of Group A, $k_2 = 1$;
- Elements of Group B:
  - $D/l < 1/20 \Rightarrow k_2 = 1.05$;
  - $D \leq 0.60\ m \Rightarrow k_2 = 1.30 - \frac{D}{2}$;
  - Not meeting any of the two above conditions: $k_2 = 1.35 - \frac{D}{2}$;
  - Not meeting any of the precedent conditions: $k_2 = 1$

Analysing the Table 4.27, the "Driven Cast-in Place Pile" type was chosen for both CFA and OMEGA piles since there is no distinction in either of the groups between replacement and displacement piles. The limit strength (f_{clim}) associated to this pile type is f_{c28} equal to 30 MPa bearing in mind that the piles concrete class is C30/37. Therefore, the k_1 is equal to 1.30 for both cases.

The k_2 values for each of the 3 diameters considered are presented in Table 4.28.

Table 4.28 – k_2 values

	0.4	0.6	0.8
l/D	1/30	1/20	1/15
k_2	1.05	1.00	1.00

Hence, the f_c* are equal to (Table 4.29):

Table 4.29 – f_c* values

D (m)	f_c* (MPa)
0.4	21.98
0.6	23.08
0.8	23.08

The norm DTU 13.2 defines that, for serviceability limit states, the following compressive strength of concrete limits (Table 4.30) must be satisfied:

- The maximum compressive strength of concrete should not exceed: $\sigma_{c,max}=0.6f_c$*;
- The average compressive strength of concrete should not exceed: $\sigma_{c,mean}=0.3f_c$*;

Table 4.30 – Concrete compressive strength limits

D (m)	$\sigma_{c.max}$ (MPa)	$\sigma_{c.mean}$ (MPa)
0.4	13.19	6.59
0.6	13.85	6.92
0.8	13.85	6.92

These requirements prevent the piles from inefficient structural behaviour avoiding common problems such as the steel yielding and concrete cracking. Hence, the first condition guarantees a level of stress in steel out of the yielding zone whereas the second assures no cracking in the concrete surface.

The calculated values shall be compared with the obtained through the EC7 Approach Method, so, considering the most unfavourable situation (meeting the second condition, $\sigma_{c,mean}=0.3f_c$*), the $R_{c;DTU}$ are presented in Table 4.31.

Table 4.31 – $R_{c;DTU}$ values

	CFA		OMEGA	
	0.60	0.80	0.40	0.60
$R_{c;DTU}$ (kN)	1957.45	3479.92	828.55	1957.45

4.4. DETERMINATION OF THE NUMBER OF PILES FOR EACH COLUMN

Considering the 74 columns presented on the structural plan view (Figure 4.1 and Figure A.1 in Appendix A) and the loads applied on each of them (Figure 4.8), the number of piles per column (n) is determined by equation 4.3:

$$n = \frac{F_{c;d}}{R_{c;d}} \tag{4.3}$$

where,

$F_{c;d}$ is the design load applied to a certain column, at the ultimate limit state;

$R_{c;d}$ is the design compressive resistance of the ground against a pile, at the ultimate limit state.

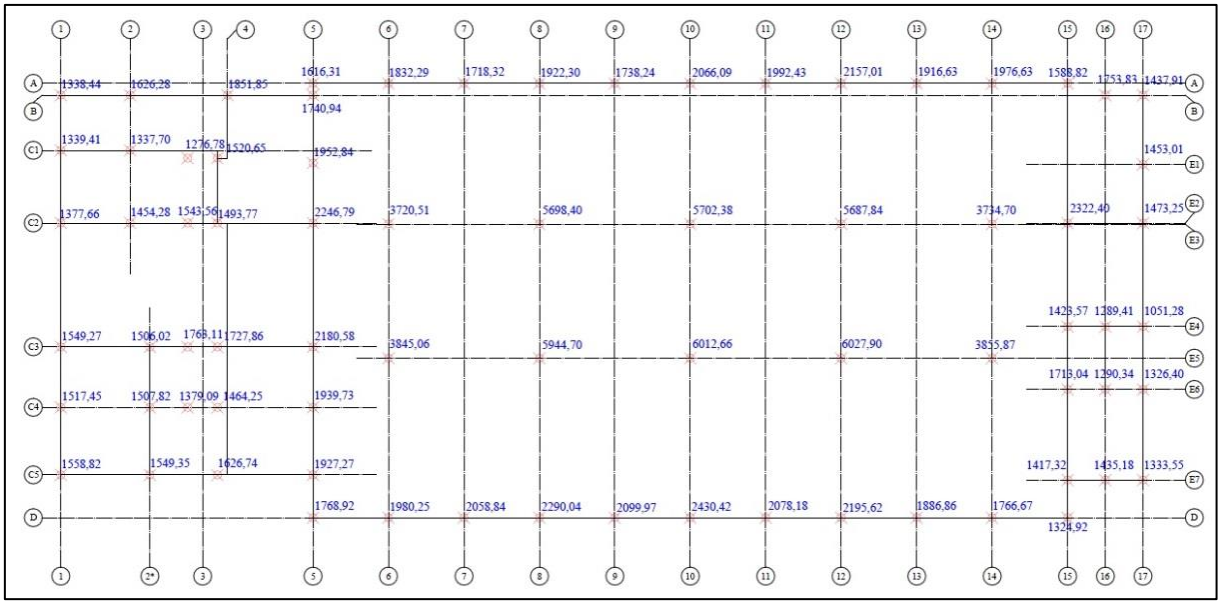

Figure 4.8 – Design loads applied to the columns (Bohn Deep Foundation Ltd)

The $R_{c;d}$ values shall also meet the following criteria (equation 4.4):

$$R_{c;d} = min\{R_{cd;EC7}; R_{cd;DTU}\} \quad (4.4)$$

It should be noted that the resistance values calculated through the application of the DTU 13.2 Norm are characteristic values. Since it was not provided data regarding the load cases, it was considered as conservative estimative a ratio between the design loads and serviceability loads of 1.40. A value between 1.35 (partial factor for permanent action, γ_G) and 1.50 (partial factor for variable action, γ_Q) on the safe side since it is closer to the lower value. Consequently, instead of dividing all the design loads by 1.40, it was decided to multiply the $R_{ck;DTU}$ by 1.4 obtaining the values of $R_{cd;DTU}$ in Table 4.32.

Table 4.32 – Comparative design total resistance of the piles

[kN]	CFA		OMEGA	
	0.60	0.80	0.40	0.60
$R_{cd;EC7}$	1931.39	2626.82	1302.62	2276.03
$R_{cd;DTU}$	2740.44	4871.89	1159.97	2740.44

In order to verify the equation 4.4, the design resistance values used to determine the number of piles per column are shown in Table 4.33.

Table 4.33 – Design total resistance of the piles

[kN]	CFA		OMEGA	
	0.60	0.80	0.40	0.60
R_{cd}	1931.39	2626.82	1159.97	2276.03

The goal is the determination of an optimal solution for a combination of CFA piles and another for OMEGA piles and then, based on the cost of each technique, the choice for one of them. Optimal solution means the choice for the minimum number of piles and smaller diameter meeting at the same time the following inequation (equation 4.5).

$$R_{c;d} \geq F_{c;d} \quad (4.5)$$

The calculation sequence is explained in Figure 4.9 where:

n is the number of piles per column;

$(R_{c;d})_{sd}$ is the design compressive resistance of smaller diameter pile;

$(R_{c;d})_{gd}$ is the design compressive resistance of greater diameter pile.

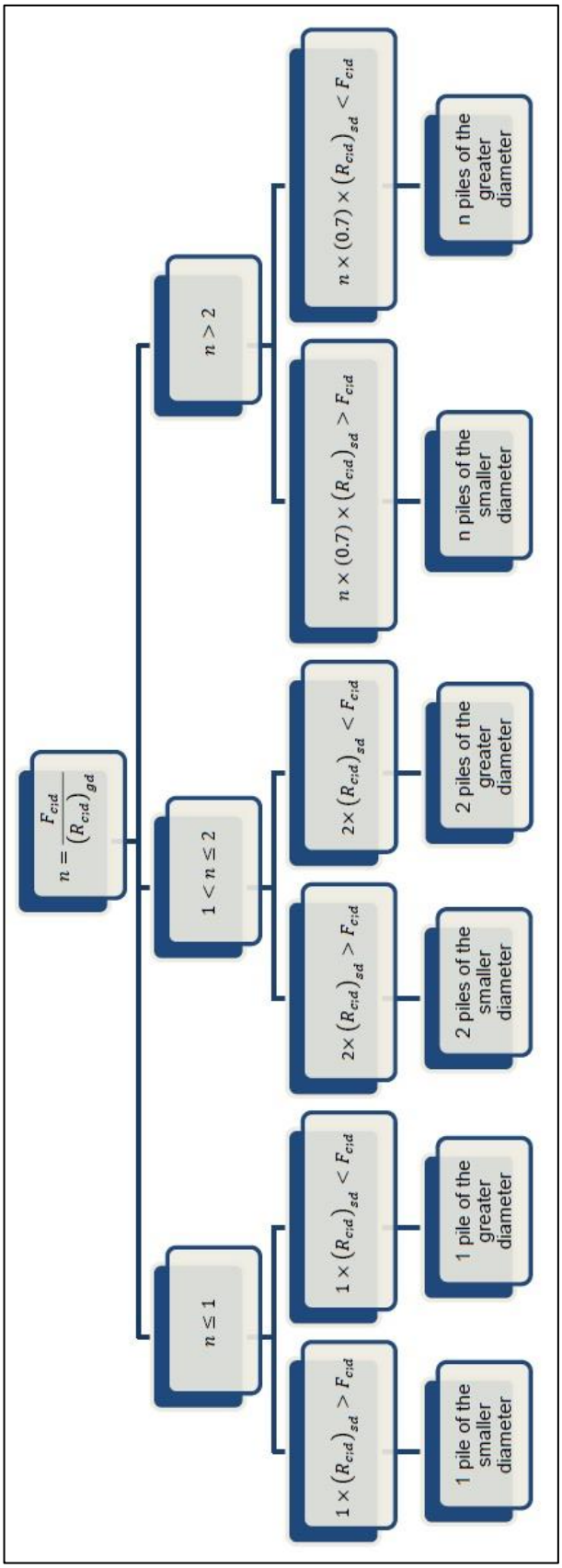

Figure 4.9 – Organizational chart detailing the calculation procedure

Bearing mind the defined stratification defined in 2.5.3, the large soil crossed is granular for which, in case of 3 or more piles, should be applied an interaction factor of 0.7 (Poulos and Davis, 1980) reducing the design resistance of the pile.

Based on provided average prices, in Hungarian forints (Ft), for both piles types and after achieving the optimal solutions for both cases, the choice was the OMEGA solution considering its lower price (Table 4.34).

Table 4.34 – Average price of both CFA and OMEGA piles

Pile Type	D (cm)	Price Range	Average Price	Average Price	Average Price	Optimal Solutions	Total Cost
		Ft/m	Ft/m	€/m	€		€
CFA	60	17000-19000	18000	60.00	720	57	41040
	80	23000-25000	24000	80.00	960	39	37440
						96	78480
Omega	40	11000-13000	12000	40.00	480	3	1440
	60	18000-20000	19000	63.33	760	96	72960
						99	74400

The piles should be placed either in column axis, in the case of only one pile per column, or centered in column axis and separated from axis to axis by 3 diameters (3D). This procedure seeks to minimize the interaction effects between piles. The solution is illustrated in Figure 4.10 where in the countered area is highlighted the overlap of 2 piles corresponding to A5 and B5 columns.

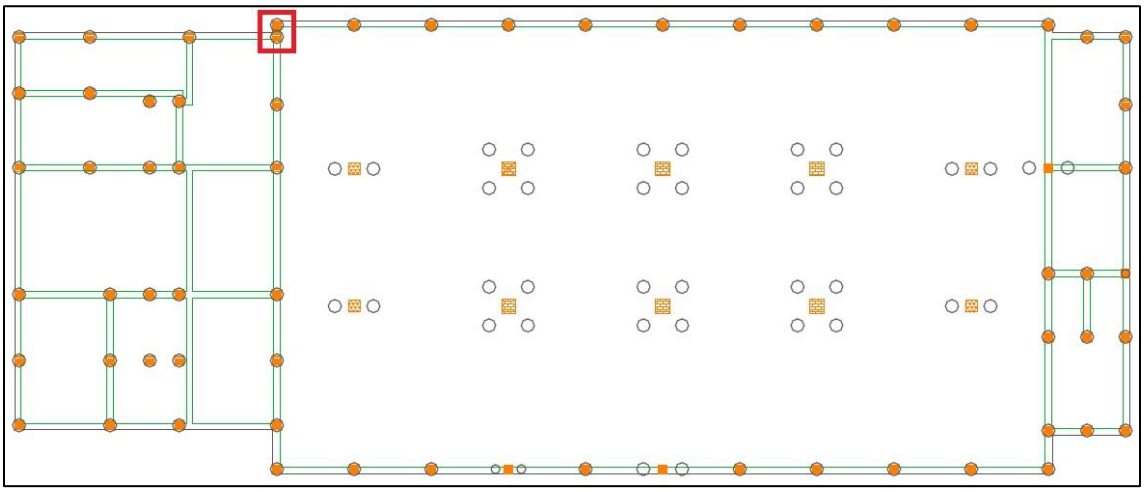

Figure 4.10 – Initial OMEGA piles solution

The overlap detailed is shown in Figure 4.11 and corresponds to a zoom of the red bounded area in the Figure 4.10.

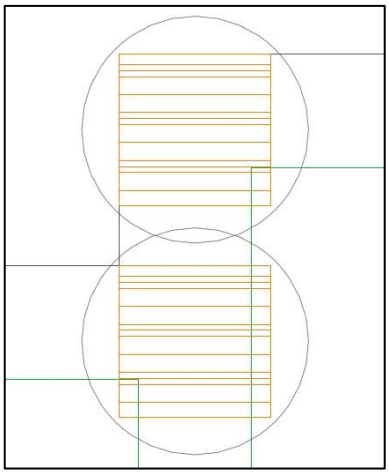

Figure 4.11 – Overlapping piles detail

Hence it was considered only the equivalent resultant, the sum of both applied in the point that would produce the initial forces assuming a local statically determinate problem as it is shown in Table 4.35. The piles were positioned along the y direction (y=20.61 m).

Table 4.35 – Equivalent force application point of the two piles

Column Code	x (m)	y (m)	$F_{c;d}$ (kN)
A5	12.23	20.90	1616.31
B5	12.23	20.34	1740.94
A5+B5	12.23	20.61	3357.25

The final pile location within the rest of the structural elements is presented on Figure 4.12.

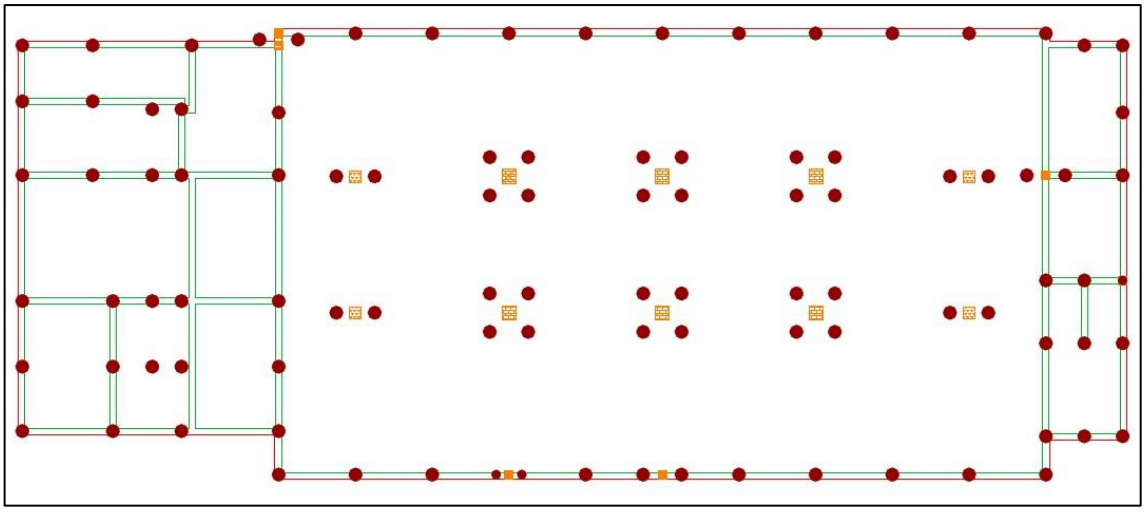

Figure 4.12 – Final OMEGA pile solution

5 ASSESSMENT OF THE SETTLEMENTS

5.1. INTRODUCTION

After reaching the optimal pile foundation system, the settlement assessment was carried out only considering the OMEGA piles and the geometry defined previously (Subchapter 4.4). The deformation analysis was made following two methods of different nature:

- Soil-structure modelling using AxisVM
- Interaction Factor Method (Poulos and Davis, 1980).

All the theoretical background that led to the application of the referred methods was presented in detail in Subchapter 3.3. Therefore, this chapter is firstly intended to present the obtained results followed by the discussion and comparison of them.

5.2. SOIL-STRUCTURE MODELLING USING AXISVM

The program AxisVM is a structural analysis and design software (http://axisvm.eu) being developed by InterCAD Kft. The company is based Budapest, Hungary since 1991. The software used in the scope of this work, AxisVM 11®, is a three-dimensional program based on the finite element method (FEM).

Being a purely structural program, the modelling of this specific geotechnical problem was done through the definition of stiffness parameters that effectively portray the deformability behavior of the piles and the soil. Thus, the assignment of spring constants permitted the simulation of piles and the definition of a continuous 2D element represented the soil stiffness.

5.2.1. PILE FLEXIBILITY ESTIMATION

The spring constant can be defined in the software as a nodal support (Figure 5.1) considering that the pile is a one-dimensional element (FL^{-1}). This value corresponds to the pile flexibility and was determined through the theoretical load-settlement curves, as follows.

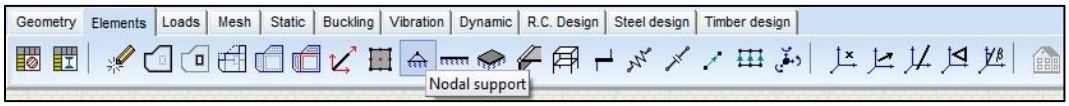

Figure 5.1 – "Nodal support" option in "Elements" menu (adapted from AxisVM)

Assuming the shaft resistance mobilization for 1.5% of pile diameter and the base resistance mobilization for 10% of pile diameter (Table 5.1), the load-settlement curve was defined, for both diameter of 0.4 m and 0.6 m, as the sum of the two components.

Table 5.1 – Settlements associated to resistance mobilization

s (m)	D (m)	
	0.40	0.60
0.015D	0.006	0.009
0.1D	0.040	0.060

Retrieving the Table 4.3 and Table 4.7 with the end bearing force and the side friction force data, respectively and linking the OMEGA values with the settlements established in Table 5.1, it is possible to define a load-settlement curve for each of the CPTU tests studied. Table 5.2 and Table 5.3 present the values of the load-settlement curves for the diameter of 0.4 m and 0.6 m, respectively.

Table 5.2 – Load-settlement curve data for 0.4 m diameter pile

s (m)	R_c (kN)			
	CPT1	CPT2	CPT3	Average
0.000	0.00	0.00	0.00	0.00
0.006	1244.18	1518.60	1352.19	1371.66
0.040	1778.26	2052.67	1886.27	1905.73

Table 5.3 – Load-settlement curve data for 0.6 m diameter pile

s (m)	R_c (kN)			
	CPT1	CPT2	CPT3	Average
0.000	0.00	0.00	0.00	0.00
0.009	1936.96	2348.58	2098.98	2128.17
0.060	3138.62	3550.24	3300.64	3329.83

Associated to the previous tables, the Figure 5.2 and Figure 5.3 illustrate the load-settlement curves for each of the CPTU tests and the average of those results.

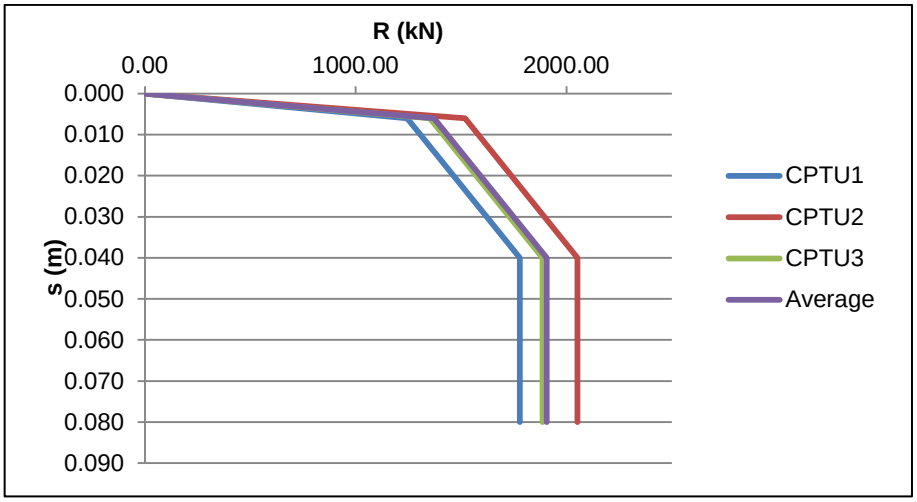

Figure 5.2– Load-settlement curve for 0.4 m diameter pile

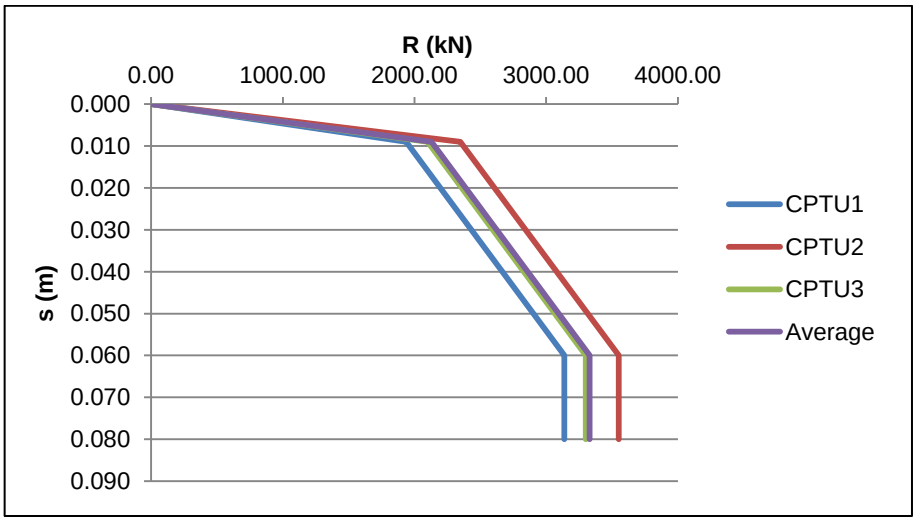

Figure 5.3 – Load-settlement curve for 0.6 m diameter pile

Considering the forces applied to the columns base and subsequently the forces applied to piles bases, presented in Appendix A, the maximum characteristic loads applied on the piles are summarized in Table 5.4:

Table 5.4 – Maximum characteristic loads

D (m)	0.4	0.6
$F_{k,max}$ (kN)	817.87	1604.85

Therefore it can be concluded that all the loads applied on the piles belong to the first line of the theoretical load-settlement curve reflecting that the pile flexibility was simply determined according to equation 5.1:

$$k_P \geq \frac{R(0.015D)}{0.015D}, \qquad kN, m, kN/m \tag{5.1}$$

The input parameters introduced in AxisVM are presented in Table 5.5.

Table 5.5 – Pile flexibility for each diameter

D (m)	0.4	0.6
k_P (MN/m)	228.61	236.46

5.2.2. DETERMINATION OF MODULUS OF SUBGRADE REACTION

The continuous 2D surface support (Figure 5.4) introduced in the program is in fact the modulus of subgrade reaction (Lopes, 2001) or the Winkler (1867) spring stiffness being determined by the equation 5.2:

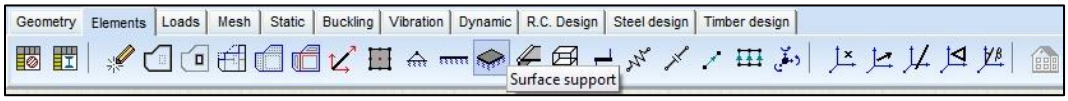

Figure 5.4 – "Surface support" option in "Elements" menu (adapted from AxisVM)

$$k \geq \frac{p}{w}, \qquad kPa, m, kN/m^3 \tag{5.2}$$

where,

p is the raft distributed load;

w is the raft settlement.

The distributed load, p, corresponds exactly to the sum of all the characteristic values divided by the raft area and is equal to 107.06 kN/m^2.

The raft settlement was determined through the Schmertmann method considering an equivalent rectangular raft area (Table 5.6) and the Young's Modulus evolution with depth as defined in equation 2.14. Since the method was developed to predict settlements on sands (which represent 80% of the studied soil profile), the consolidation effects associated to the clayey layers were neglected. However, this assumption does not affect significantly the obtained results.

Table 5.6 – Equivalent rectangular raft dimensions

L (m)	B (m)	L/B	A (m^2)
52	20.35	2.56	1058.2

The calculation of the vertical strain influence factor, I_ε, was done following the Table 3.4 for intermediate L/B between 1 and 10, in which it is proposed an equation that establishes the interpolation. Hence, for each sublayer considered the value I_ε for axisymmetric and for strip (continues) foundation taking the respective $I_{\varepsilon p}$. For the latter, it was considered the unit weights defined in 2.6.1 and the adopted stratigraphy presented in Table 2.2, Table 2.3 and Table 2.4 in order to calculate the effective vertical stress.

The results are presented in the appendix (A.2) to this thesis. The vertical strain influence factor evolution with depth is presented in Figure 5.5.

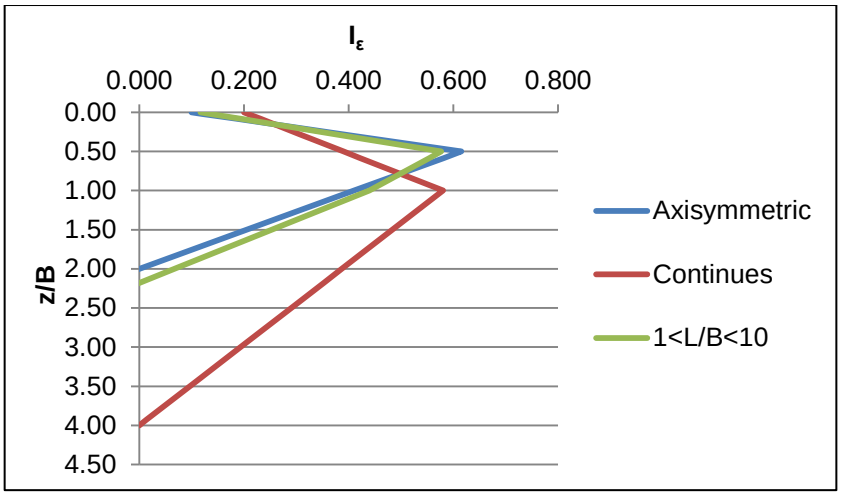

Figure 5.5 – I_ε depth evolution for L/B=2.56

Analysing Figure 5.5, it can be observed that the specific case study (L/B=2.56) is characterized by a slightly smaller peak of I_ε but, on other hand, by a larger starting I_ε (0.12) and a larger influence depth (z/B=2.18) when compared with axisymmetric foundation.

The obtained raft settlements are resumed in Table 5.7, with reduced variations between each of the tests.

Table 5.7 – Raft settlement

CPTU	s (mm)
1	12.45
2	12.45
3	12.36

Consequently, the values for the modulus of subgrade reaction are also close to each other (Table 5.8). For the AxisVM modelling the average value should be computed.

Table 5.8 – Modulus of subgrade reaction

CPTU	k (kN/m^3)
1	8602.57
2	8599.39
3	8662.14
Average	8621.36

Taking into account the simplified calculation carried out for both the pile flexibility and the modulus of subgrade reaction, it was considered appropriate to vary slightly the average values of the referred stiffness parameters. Hence, the following parametric analyses were the defined, in addition to the use of the average values:

- 20% decrease of the pile stiffness ($0.8.k_p$) and 20% increase of the modulus of subgrade reaction ($1.2.k_s$);
- 20% increase of the pile stiffness ($1.2.k_p$) and 20% decrease of the modulus of subgrade reaction ($0.8.k_s$);
- 20% decrease of the pile stiffness ($0.8.k_p$) and 20% decrease of the modulus of subgrade reaction ($0.8.k_s$);

The objective of theses analyses is to study the input parameters influence in the maximum settlements generated, maximum differential settlement and angular distortion.

The Table 5.9 summarizes the nodal and the surface supports associated to each of the 4 studies carried out (including the average and the variations from this).

Table 5.9 – Stiffness parameters input

Case Study	k_p (kN/m)		k_s (MN/m^3)
	D=0.4	D=0.6	
1	228609.84	236463.82	8621.36
2	182887.87	189171.05	10345.64
3	274331.80	283756.58	6897.09
4	182887.87	189171.05	6897.09

5.2.3. MODEL CONSTITUTION

As an initial iteration, a raft of 0.8 m thick of C25/30 concrete class was considered. However, due to the significant discrepancy between the applied loads in different raft zones, an efficient solution to create greater concrete thickness (1.0 m) in the most loaded areas was considered. This decision is conservative in view of the subsequent reinforcement design, reducing the steel ratio.

In order to design a more rigid structure, in addition to the inclusion of 74 columns, it was also modelled the first floor slab of 20 cm thick. The Figure 5.6 exemplifies the considered model.

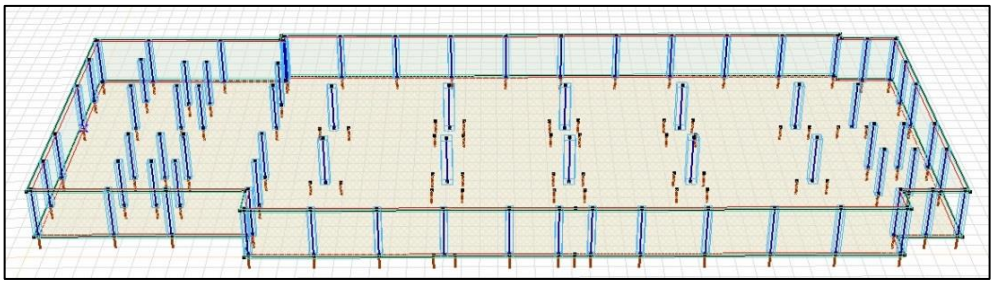

Figure 5.6 – 3D perspective of the defined model (adapted from AxisVM)

In the 3D wireframe (Figure 5.6), the columns are countered by blue and the piles are represented in brown.

For the settlement assessment, the reinforcement is not relevant so it was not specified for this calculation. The mesh is defined by elements of 0.5 m size which can reproduce, considering the significant dimensions of the structure to model, its deformation behaviour fundamentally correct. The model run was performed through a linear static analysis.

5.2.4. AXISVM RESULTS

Taking into account the dimensions of the modelled structure, it becomes impossible to present and study all results obtained by the program. Thus, it is essential to select the most significant results in the scope of this project. When assessing the piled raft settlements, results such as the pile settlement and the differential settlements between piles are very important, as stated above.

Figure 5.7, Figure 5.8, Figure 5.9 and Figure 5.10 represent the 2D isosurfaces obtained by the program associated to displacement in vertical direction (eZ) for each of the 4 cases studied.

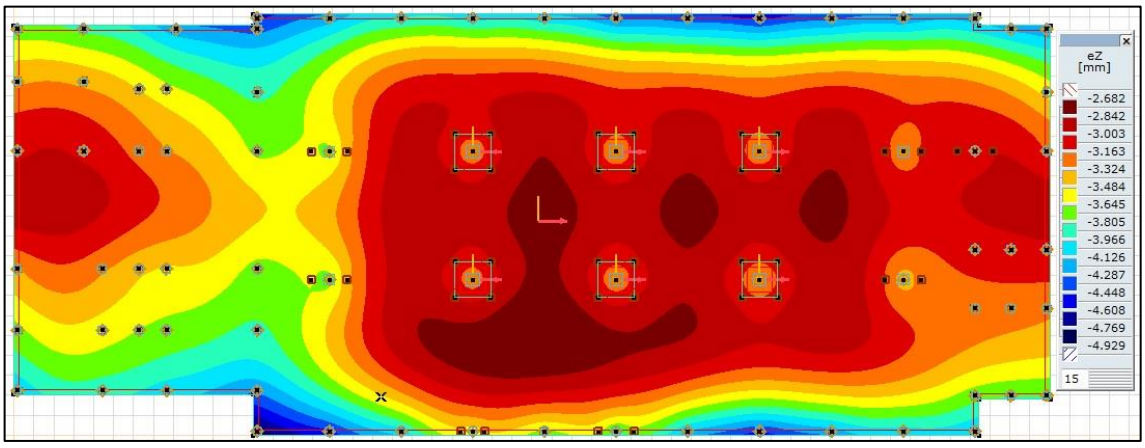

Figure 5.7 – Case study 1 Isosurface 2D (adapted from AxisVM)

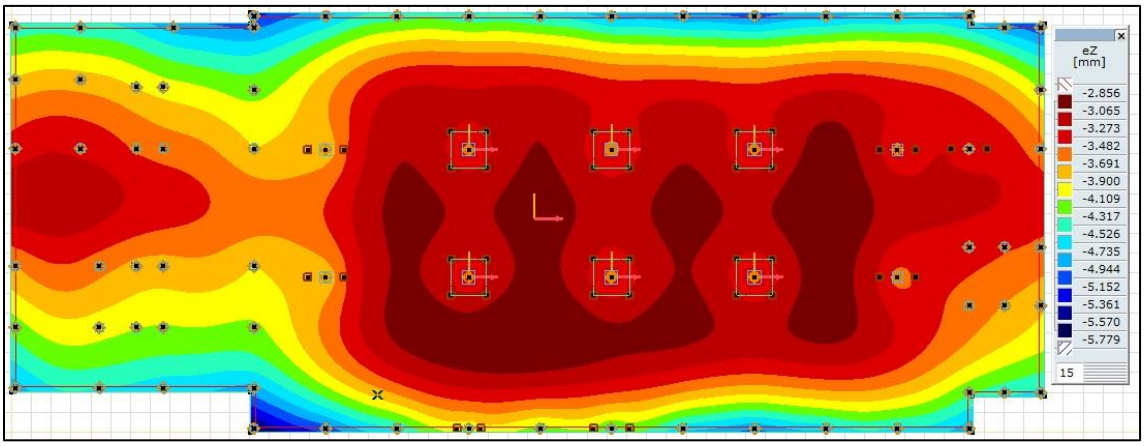

Figure 5.8 – Case study 2 Isosurface 2D (adapted from AxisVM)

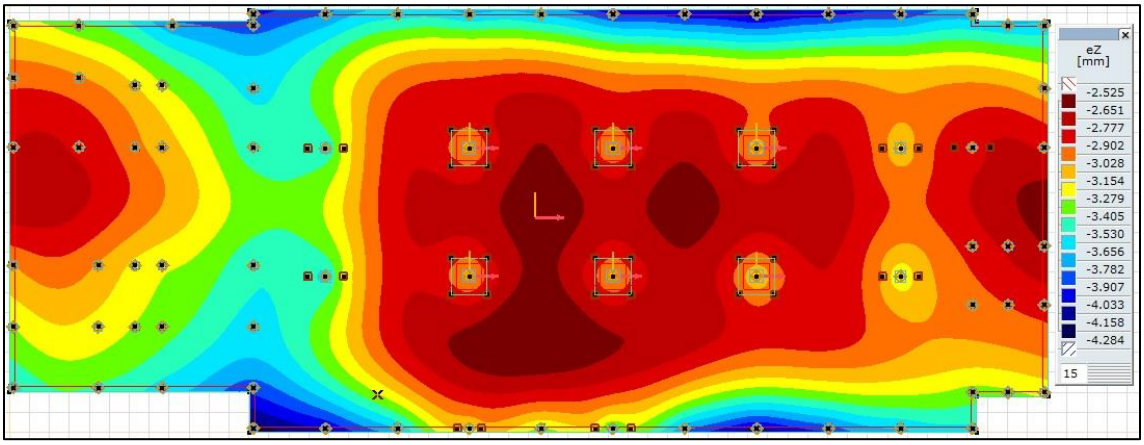

Figure 5.9 – Case study 3 Isosurface 2D (adapted from AxisVM)

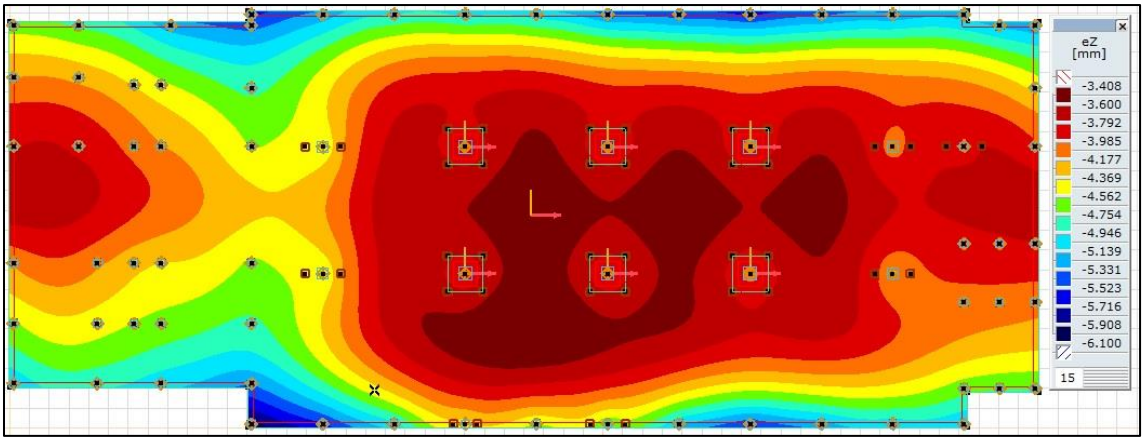

Figure 5.10 – Case study 4 Isosurface 2D (adapted from AxisVM)

As can be seen, the simple observation of the figures above does not allow inferring relevant conclusions regarding the variations imposed. In fact, only slightly differences in the isosurfaces boundaries can be noticed. Thus, it was necessary, in order to understand the relative influence of this

binomial, to analyse specifically the obtained values. Thus, there were interpreted the results for the settlements (s) of each pile and the differential settlement (Δs) and the angular distortion (α= Δs/L) between every pair of piles (separated by L meters), summarized in Table 5.10, Table 5.11 and Table 5.12.

Table 5.10 – Maximum and average settlements

	Case Study			
	1	2	3	4
s_{max} (mm)	4.843	5.649	4.230	6.000
s_{avg} (mm)	3.555	3.957	3.236	4.425
s_{max}/s_{avg}	1.362	1.428	1.307	1.356

Table 5.11 – Maximum and average differential settlements

	Case Study			
	1	2	3	4
Δs_{max} (mm)	1.912	2.521	1.575	2.365
Δs_{avg} (mm)	0.568	0.740	0.474	0.706
$\Delta s_{max}/\Delta s_{avg}$	3.366	3.407	3.323	3.350

Table 5.12 – Maximum and average angular distortions

	Case Study			
	1	2	3	4
α_{max}	1/3597	1/2421	1/4115	1/3049
α_{avg}	1/29412	1/22222	1/34483	2/23256

Through the observation of Table 5.10, it can be concluded that the settlement magnitude is mostly defined by the pile flexibility, when comparing the fluctuations establishing the case study 4 as the base. When increasing the soil spring constant from $0.8k_s$ to $1.2k_s$ (case study 2) while maintaining the pile flexibility, the maximum settlement (produced in any case in the same pile, over the column D5) is just reduced in 6%, whereas the increase of the pile flexibility from $0.8k_s$ to $1.2k_s$ while maintaining the soil spring constant induces a settlement reduction of 30%.

Logically, the higher the ratio s_{max}/s_{avg} the greater the differential settlement, fact corroborated in Table 5.11. Other important aspect resulting of the comparison between the case study 2 and 3 is that the variation of the greater magnitude parameter will control the differential settlement ratio between the maximum and the average.

Regarding the angular distortions, the case study 2 resulted in the largest percentages but still well below the regulatory limits.

5.3. INTERACTION FACTOR METHOD

The hand calculation of the pile group settlements was performed by using the Interaction Factor Method which can be mathematically expressed by the equation 3.16. Regarding the referred equation, some considerations shall be evidenced.

The component of the applied load (P_{av}) is originally the average load on a pile, which means the sum of all the serviceability loads and its subsequent division by the number of piles within the group (scenario 1). In addition to this methodology, a second approach was considered where values applied on each pile came from service loads (scenario 2). This procedure seeks to highlight the effect of different load magnitude applied on piles on the differential settlements. The considered service load on a certain pile is function of the service load – obtained by dividing the design load by 1.4 (Subchapter 4.4) – on the column base. If the column receives only one pile then the service load will be exactly the same. On other hand, if the column receives more than one pile then the service load on each pile will be the column service load divided by the number of piles.

The unit load settlement (s_1) was determined according to equation 3.17 and is equal to 2.065×10^{-6} m/kN with P_t=1; I_ρ=0.156; D=0.6 m (the predominant pile diameter (96 of the 99 piles) was considered instead of calculating an equivalent diameter); E_{sL}=126.20 MPa (corresponds to the soil Young's modulus at the pile tip, z=12 m).

The interaction factor was calculated by the equation 3.25 instead of the equation 3.26, since this one is only valid for a single C and D pair. Thus, 4 possibilities were computed resulting from the combination of the limit values of A and B, as expressed in Table 2.1Table 5.13.

Table 5.13 – A and B combinations

Variable	Combinations			
	1	2	3	4
A	0.98	0.98	0.57	0.57
B	-1.20	-0.60	-1.20	-0.60

For a certain spacing (s=7 m), the returned α values, presented in Table 5.14, are significantly different which led to the adoption of the average of the 4 combinations.

Table 5.14 – α_{ij} values

Variable	Combinations			
	1	2	3	4
α_{ij}	0.0514	0.2244	0.0299	0.1305

Retrieving again equation 3.25, and in accordance with what has been done in the unit load settlement calculation, only the diameter 0.6 m was considered, which means that this parameter becomes a constant. Thus, it was possible to define an interaction power function between the spacing (s) and the average interaction factor ($\alpha_{ij,avg}$) as presented in Figure 5.11.

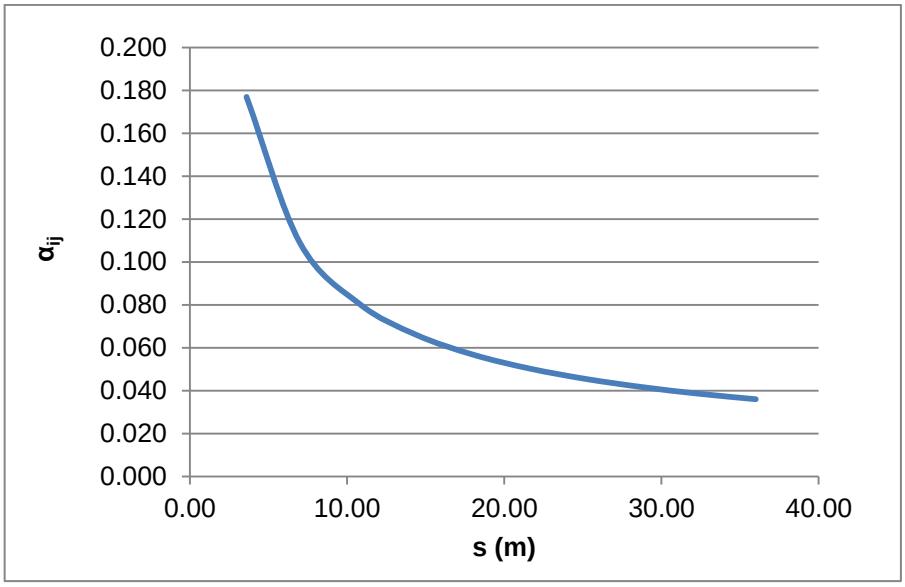

Figure 5.11 – Evolution of the interaction factor with the spacing between piles

The curve represented in Figure 5.11 can be associated to a trendline which was determined with Microsoft Excel® 2010 and is expressed by the equation 5.3:

$$\alpha_{ij} = 0.4198 \times s^{-0.689}, \quad m \tag{5.3}$$

The coefficient of determination (R^2) of the obtained trend line is equal 0.9995 meaning an almost perfect correlation.

5.3.1. Analysis and Results of the Two Studied Scenarios

Similarly to what was done in the presentation of results of AxisVM, the focus was to interpret the results for the settlements (s) of each pile and the differential settlement (Δs) and the angular distortion (α= Δs/L) between piles (separated by L meters). The maximum and the average values are presented, for the 2 scenarios considered, in Table 5.15, Table 5.16 and Table 5.17.

Table 5.15 – Maximum and average settlements

	Scenario	
	1	2
s_{max} (mm)	19.345	19.182
s_{avg} (mm)	17.146	17.166
s_{max}/s_{avg}	1.128	1.117

Table 5.16 – Maximum and average differential settlements

	Scenario	
	1	2
Δs_{max} (mm)	5.150	5.270
Δs_{avg} (mm)	1.559	1.647
$\Delta s_{max}/\Delta s_{avg}$	3.304	3.201

Table 5.17 – Maximum and average angular distortions

	Scenario	
	1	2
α_{max}	1/1779	1/1499
α_{avg}	1/10870	1/10526

The maximum settlements occur when assuming the average load on the piles (Scenario 1), however it is almost an insignificant difference when compared with Scenario 2, taking into account the magnitude in question (tenth of millimetre).

The values of differential settlement are higher in Scenario 2 even though not substantially. The maximum differential settlement stands around 5 mm and the average around 1.6 mm.

Regarding the angular distortions, Scenario 2 had again higher values than Scenario 1, with the average angular distortions in the first being 3% greater than the second. As in the previous analyses the obtained results are well below the regulatory limits.

5.4. COMPARISON AND DISCUSSION OF THE OBTAINED RESULTS

Two different analyses were carried out to assess the pile group settlements, one based on a structural finite element analysis and another based on an analytic calculation with the main objective of comparing and interpret the obtained results. Thus, the last part of the current chapter was meant to discuss and understand the differences registered by both methodologies.

For the comparative analysis, the case study 1 results were chosen in the case of the AxisVM modelling while for the Interaction Factor Method (IFM), the Scenario 2 was chosen. The Table 5.18, Table 5.19 and Table 5.20 summarize, for the referred two cases, the maximum and average results of piles settlement (s), differential settlement (Δs) and angular distortion (α).

Table 5.18 – Maximum and average settlement comparison

	AxisVM	IFM	s_{IFM}/s_{AxisVM}
s_{max} (mm)	4.843	19.182	3.96
s_{avg} (mm)	3.555	17.166	4.83

Table 5.19 – Maximum and average differential settlement comparison

	AxisVM	IFM	$\Delta s_{IFM}/\Delta s_{AxisVM}$
Δs_{max} (mm)	1.912	5.270	2.76
Δs_{avg} (mm)	0.568	1.647	2.90

Table 5.20 – Maximum and average angular distortion comparison

	AxisVM	IFM	$\alpha_{IFM}/\alpha_{AxisVM}$
α_{max}	1/3597	1/1499	2.40
α_{avg}	1/29412	1/10526	2.79

Observing Table 5.18, an emphasis must be made on the discrepancy between the results obtained for both the maximum settlement and for the average settlement. In the case of the latter, the average settlement ratio is almost 5, an excessively wide range between both results and at the same time quite unexpected.

Regarding both the average differential settlements and the average angular distortions, the divergence between both methods is smaller but still significant. The ratio is, in both cases, near 3.

The different nature of analyses can be a cause for the disparate results, since the first analysis is a numeric modelling and the second a simplified empirical method. The other cause, eventually the most significant, is the type of the software used for modelling this interaction, which is not geotechnical code, using a limited structural approach. The geotechnical environment was created by assuming the piles as vertical springs and the soil a 2D support below the raft with certain stiffness. Obviously, the program is not able to reproduce the interaction between the piles since it considers that each of the springs work individually and that that there is no influence of the raft over the soil. In addition to this, the model contained not only the raft foundation but also the structural elements of the first level of the building (columns and first floor slab), creating a stiffer body and reducing the settlements. On the other side, and in order to justify the obtained gap, it must be noted that an empirical method tends to be conservative regarding all the simplifications behind its formulation leading the higher settlements.

6
DESIGN OF THE PILES AND REINFORCEMENT SLAB

6.1. INTRODUCTION

The reinforcement design can be considered as the last step of the geotechnical project. Since the calculation is based on the applied loads and the given structural geometry, no geotechnical parameter intervene in these procedures. Nevertheless, the both the piles and the raft foundation were designed in order to meet the common geotechnical project requirements. Thus, it was considered convenient the calculation of the reinforcement of these two elements. In the case of piles, a hand calculation was carried out whereas for the raft foundation (or reinforcement slab) the software AxisVM was used again.

6.2. PILE DESIGN

Considering the piles are only axially loaded, no reinforced concrete should be designed due to the effects of bending moment or shear force. In this scenario, the Eurocode 2, in 9.8.5, recommends a minimum longitudinal reinforcement area, designated $A_{s,bpmin}$.

Respecting the Table 5.9N from the same section, $A_{s,bpmin}$ is given by equation 6.1:

$$A_{s,bpmin} = A_s = 0.005.A_c \tag{6.1}$$

where,

A_c is the cross sectional area of reinforcement.

Thus, the area of reinforcement for both the 0.4 m and 0.6 m diameter piles is given in Table 6.1, considering the 16 mm as minimum diameter, the minimum of 6 longitudinal bars and a clear distance not exceeding 200 mm.

Table 6.1 – Minimum pile reinforcement area

D (m)	$A_{s,bpmin}$
0.4	7Φ16
0.6	10Φ16

Regarding the transverse reinforcement, EN 1536 suggests, for an helical reinforcement:

$$A_{st} = max\left\{6; 0.25 \times \Phi_{A_{s,bpmin}}\right\} \quad (mm) \tag{6.2}$$

Thus, the diameter for the transverse reinforcement should be 6 mm and the spacing shall not be less than the clear distance obtained in the longitudinal reinforcement (180 mm).

6.3. RAFT FOUNDATION DESIGN

Being a structural software, highly targeted to solve project queries, AxisVM enables a failure calculation, which leads to the reinforced concrete design. The model used to run this calculation is the same used to the settlements assessment, illustrated in Figure 5.6 as well as the geometry of the structural elements defined in subchapter 5.2.3.

The reinforced slab to design is represented in Figure 6.1 as 3D perspective with the 0.8 m raft and the 6 other zones with 1.0 m, identifiable by its salience. The reason for the extra concrete thickness zones is related to the significant applied loads over these areas, as it was pointed out in the previous chapter.

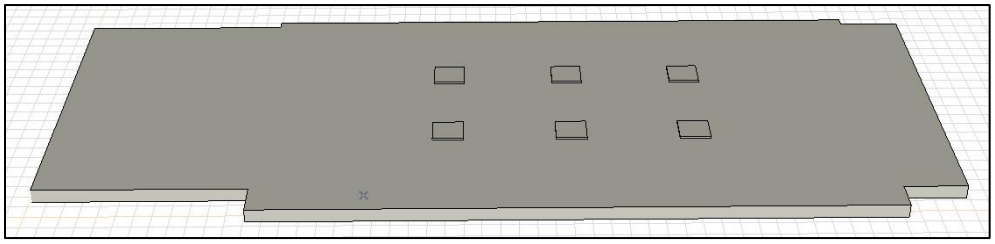

Figure 6.1 – 3D perspective of the raft foundation (adapted from AxisVM)

The concrete class of the slab is C25/30, mentioned above in subchapter 5.2.3, the rebar steel is S500 and associated with the adopted geometry complete the material input.

The model adopted was a linear static type analysis but considering a different load case from the previous analysis. This time, the ultimate limit state was used considering the design values of the applied loads over the piles. The software AxisVM also enables the option of performing the reinforcement calculations under the Eurocode 2 regulations, which was then the code adopted.

The "R.C. Design" menu on AxisVM comprises the "Reinforcement Parameters" and the "Actual Reinforcement". The first is set to introduce the thickness of the material (slab) and its mechanical parameters, in the case of being reinforced concrete, both the concrete and steel classes are defined.

The second is set to define a certain level of reinforcement for the modelled elements, specifically the slab.

Focusing on the actual reinforcement, it should be noted that the software requires the definition of the rebars cover on top and bottom surfaces, which was set as the minimum (26 mm) as shown in Figure 6.2.

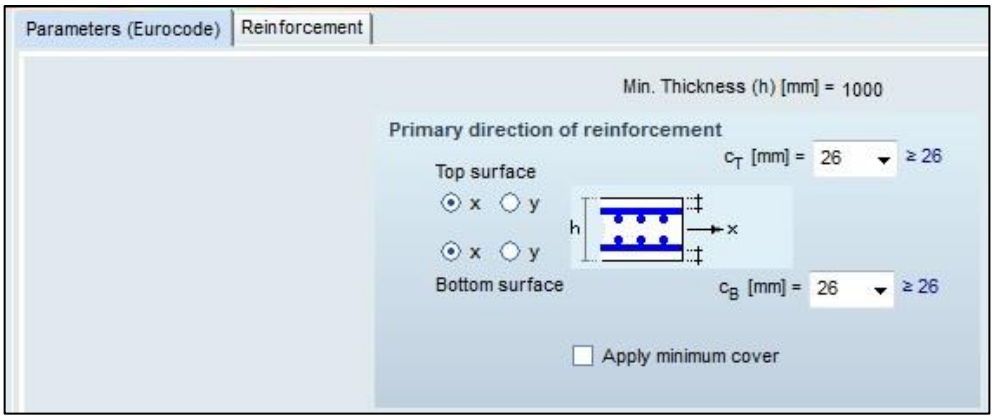

Figure 6.2 – Cover to reinforcement (adapted from AxisVM)

The actual reinforcement is designed in directions x and y, according to Figure 6.3, and on top and bottom of the cross section (Figure 6.4).

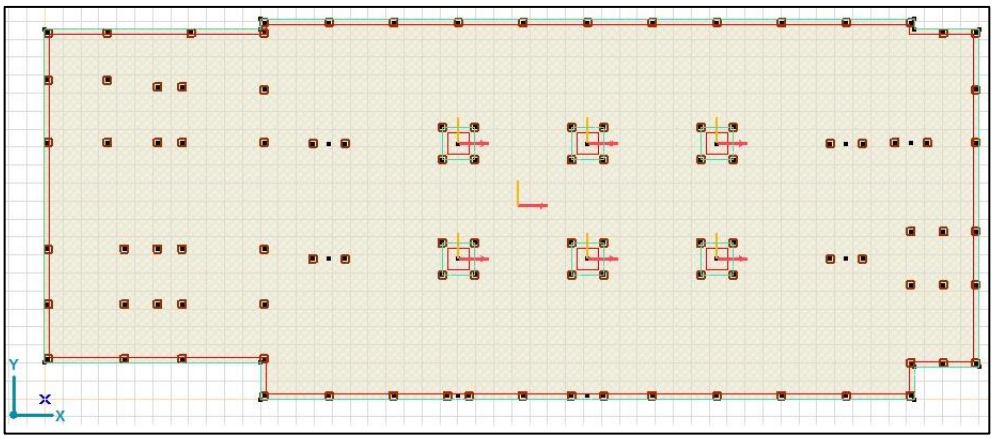

Figure 6.3 – Plan xOy (adapted from AxisVM)

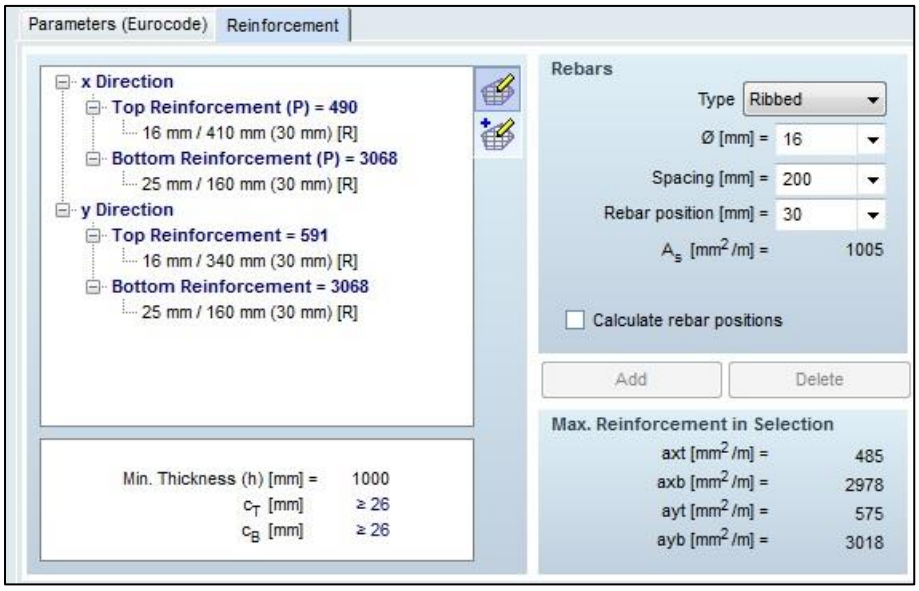

Figure 6.4 – Actual reinforcement window on AxisVM software (adapted from AxisVM)

The level of required reinforcement is defined comparatively with the "reinforcement values" provided by the program, ensuring that the difference between the two is positive. Obviously, the smaller the reinforcement differences the more economic is the solution.

To perform this calculation, it was chosen the Case Study 1 (see 5.2.2) that represents the average values for the pile flexibility (k_p) and the soil stiffness (k_s). The results obtained via AxisVM are summarized in Table 6.2, where the reinforcement is indicated according to the direction and the position. Distinction between the 6 thicker zones (numbered clockwise) and the main slab is made too.

Table 6.2 – Required reinforcement for the raft design

Direction	Position	Extra thick zones												Main slab	
		1		2		3		4		5		6			
		Φ (mm)	s (mm)	Φ (mm)	s (mm)	Φ (mm)	s (mm)	Φ (mm)	s (mm)	Φ (mm)	s (mm)	Φ (mm)	s (mm)	Φ (mm)	s (mm)
x	t	16	330	16	360	16	360	16	420	16	420	16	350	16	100
	b	25	180	25	170	25	170	25	160	25	160	25	170	25	200
y	t	16	260	16	240	16	230	16	330	16	380	16	360	16	230
	b	25	180	25	180	25	180	25	160	25	160	25	160	25	230

*t: top, b: bottom

Observing the Table 6.2, it is possible to conclude that the creation of the extra thick zones led to the decrease of the steel reinforcement ratio in both the top and the bottom surfaces, considering that even being 20 cm thicker, the reinforcement level is still higher than in the main slab. Moreover, the increase of the slab thickness in certain critical zones permitted a more leveled amount of reinforced concrete all over the raft.

To complement the Table 6.2, it was considered suggestive the presentation of the reinforcement differences 2D isosurfaces of the top surface x direction (xt), the bottom surface x direction (xb), the

top surface y direction (yt), the bottom surface y direction (yb), (Figure 6.5, Figure 6.6, Figure 6.7 and Figure 6.8).

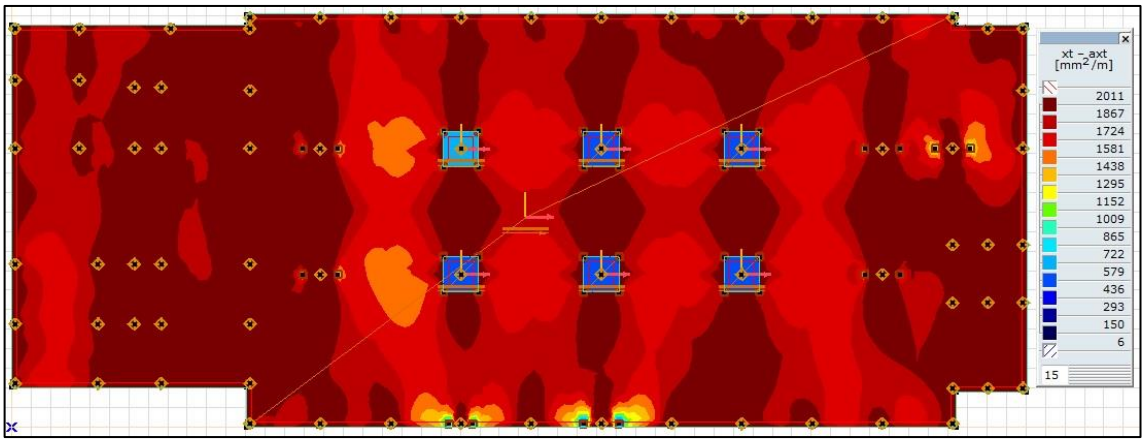

Figure 6.5 – Reinforcement difference xt (adapted from AxisVM)

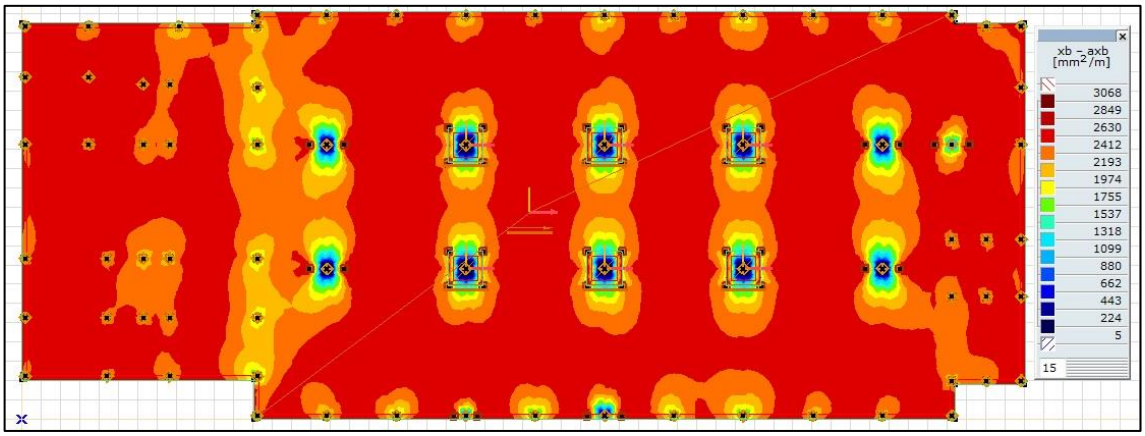

Figure 6.6 – Reinforcement difference xb (adapted from AxisVM)

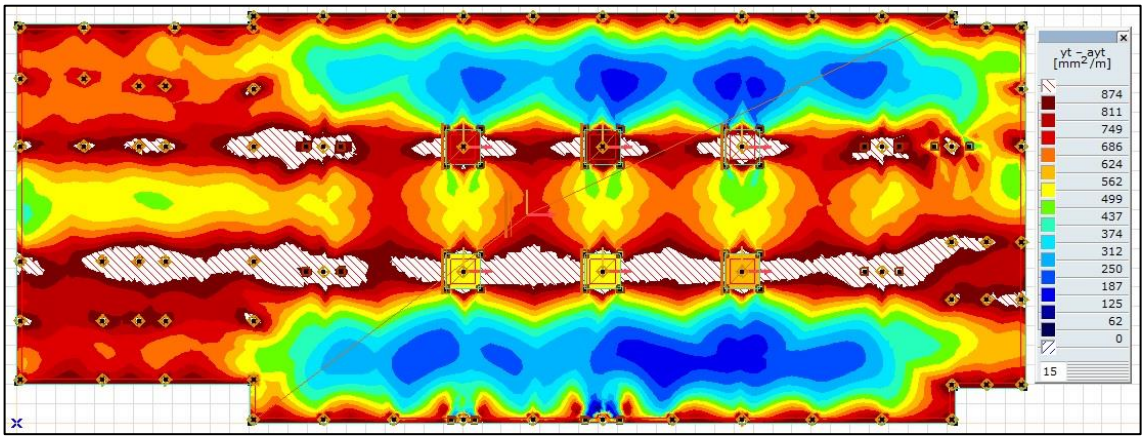

Figure 6.7 – Reinforcement difference yt (adapted from AxisVM)

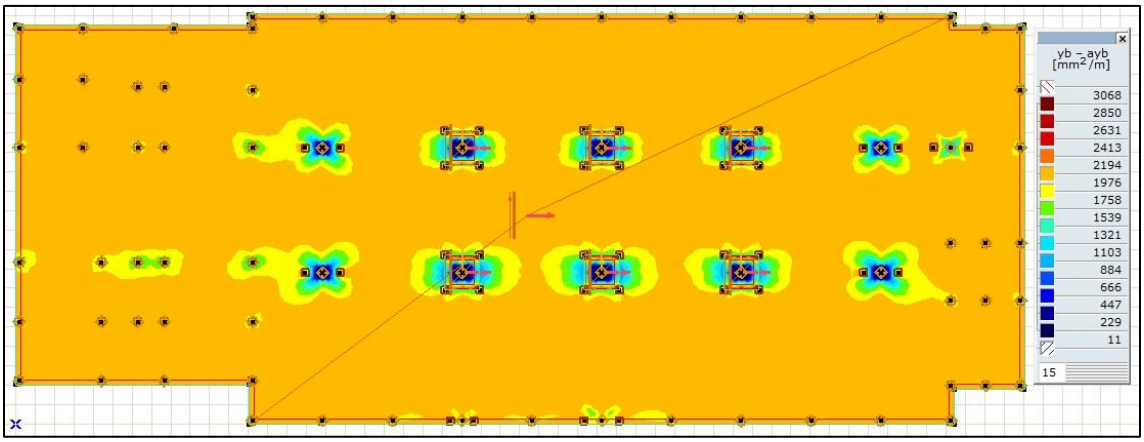

Figure 6.8 – Reinforcement difference yb (adapted from AxisVM)

Figure 6.5, Figure 6.6, Figure 6.7 and Figure 6.8 show the reinforcement differential in both x and y direction combined with the top and the bottom surfaces. According to the colour legend on the right, the more red the scale is the larger the reinforcement differential.

The reinforcement design was carried out assuring that no node, within any of the 7 domains, would have a negative difference between the required and the actual reinforcement. Hence, this permitted the optimization of the more confined domains (6 thicker slabs) and led, at the same time, to a non-economic design of the larger domain (main slab). In order to optimize the latter, more discretized domains should have been created, approaching the differences to zero and eliminating the red coloured surfaces.

7
DESIGN OF THE EXCAVATION DEWATERING SYSTEM

7.1. INTRODUCTION

The groundwater on a particular construction site is caused essentially by heavy rainfall and percolation through permeable soils. The permeability of the soils will govern the water table (or phreatic level) position in the subsoil and its variations.

Within a Civil Engineering work, the reduction of the groundwater level is crucial considering the effects the water has on the strength properties of the soil and the associated deformations that can be induced by the pore water pressure variation, which is the same as the effective stress changes. However in the specific case of a shallow excavation, the increase of soil strength, induced by the reduction of the pore water pressure, cannot be considered relevant when compared with its effects in a deep excavation execution.

In the scope of a shallow excavation execution (Figure 7.1 – Water conditions in the construction site), the high position of the water table *in situ* is more directly affected by the construction methods and consequently its duration and cost. In a long term analysis, the durability of the built structure could be affected and the maintenance costs can be significant (Puller, 2003). Therefore, the control of groundwater gains particular relevance in the geotechnical project planning.

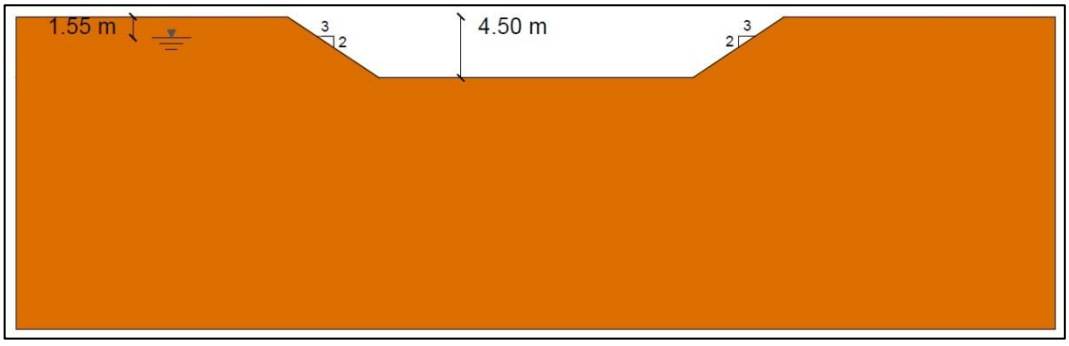

Figure 7.1 – Water conditions in the construction site

In relation to Figure 7.1, the excavation was considered to be 4.50 m, slightly above the measured values in the investigation drillings (see 2.1), fact that will not influence the results, though.

This chapter addresses a possible temporary dewatering system for the executed excavation (Figure 7.1) by creating wells using the program Plaxis 2D and a classical empirical formulation proposed by Mansur and Kaufman (1962).

To run the calculations, it was adopted a simplified stratigraphy based on the 3 CPTU tests as shown in Figure 7.2.

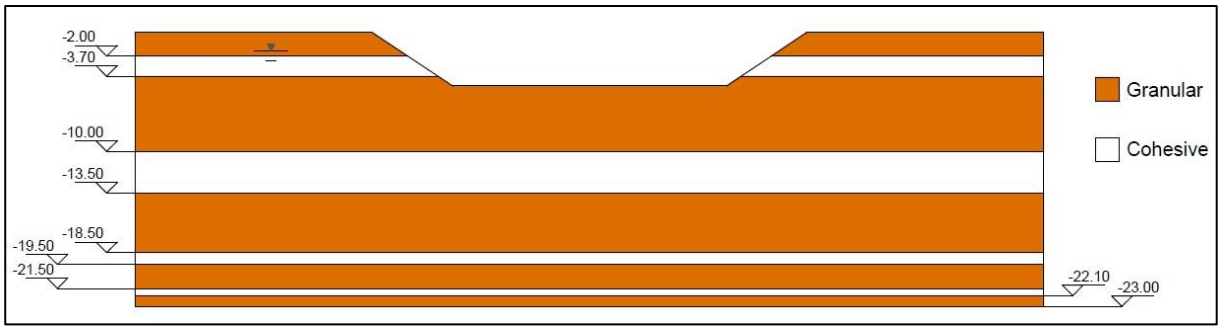

Figure 7.2 – Adopted stratigraphy for the groundwater calculations

7.2. ASSESSMENT OF THE COEFFICIENT OF PERMEABILITY

Recalling the adopted soil stratification, two main soil behaviour types were defined, granular and cohesive. Hence, it was necessary to arbitrate the value of the soil coefficient of permeability (k), considering common sands and clays. In the absence of the grain size distribution curve, which is remarkably the most relevant element for the evaluation of this parameter, the permeability (also called hydraulic conductivity) estimative was done using standard values available in the literature (Matos Fernandes, 2006).

For the granular soils, it was considered $k=10^{-5}$ m/s, whereas for the cohesive strata, it was considered $k=10^{-8}$ m/s.

7.3. PLAXIS 2D MODELLING

The program Plaxis 2D is a Dutch software based on the finite element method intended to solve various geotechnical problems, including hydraulic coupling.

The modelling in the program was done according to Figure 7.2, assigning, according to the strata, its respective characteristics, which, in this case, are the hydraulic conductivity in direction x (k_x) and y (k_y) since it is related to a percolation problem. In addition to this, two narrow trenches (0.50 m each) were created with no domain assigned to represent the wells. The option for this procedure instead of using the *Well* feature offered by the program was due to the boundary condition problems related to cross different layers. The Figure 7.3 represents the modelled structure in Plaxis 2D.

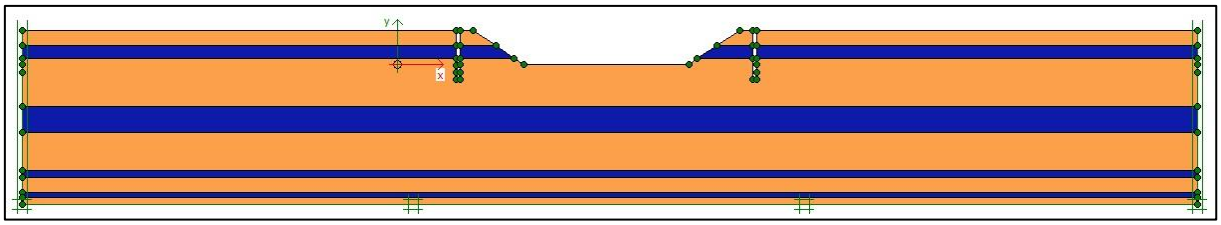

Figure 7.3 – Modelled structure in Plaxis 2D (adapted from Plaxis 2D)

In order to accurately portray the groundwater conditions far from the excavation pit, a wide mesh was created, assuring that near the lateral boundaries the water table remains in the initial level. Moreover, this covers all the variations from the initial conditions until the final lowered water table, close to the wells.

The mesh is composed by triangular elements (Figure 7.4), defined as "Coarse" in the "Global Coarseness" menu.

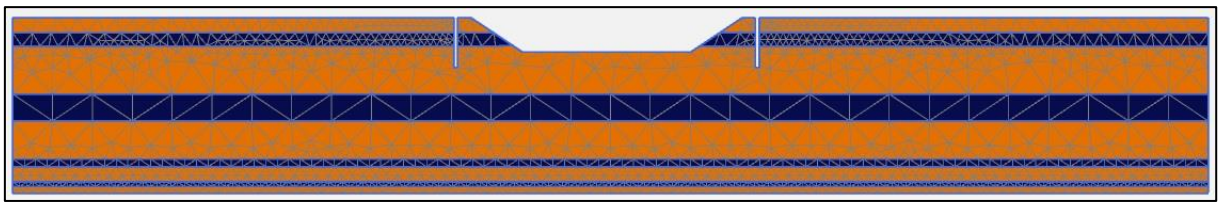

Figure 7.4 – Generated mesh in Plaxis 2D (adapted from Plaxis 2D)

The definition of the water conditions was done through the assignment of the boundary type "Head (user-defined)", where it was necessary to insert, for each of the lateral boundary points, the piezometric head, h_w, in relation to the phreatic level. The Figure 7.5 illustrates the "Boundary Conditions" window.

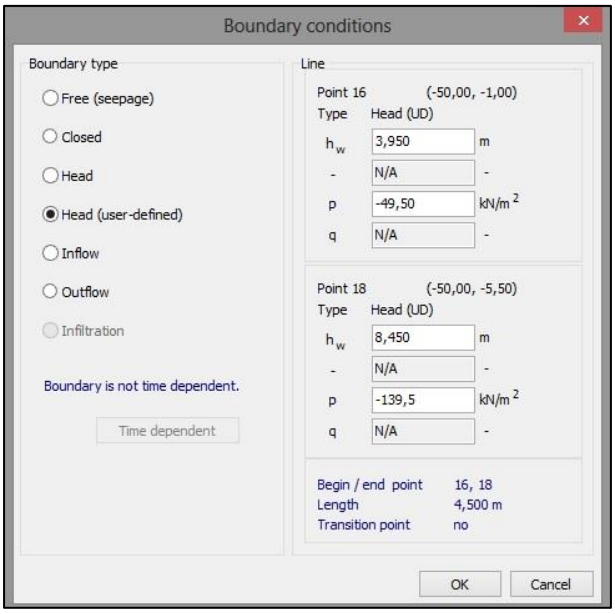

Figure 7.5 – Boundary conditions window in Plaxis 2D (adapted from Plaxis 2D)

The drainage system was simulated using the "Flow Mode" and the calculation type "Groundwater flow – steady state".

The length of the trenches was iterated in order to achieve at least a difference of 1 meter between the groundwater table and the bottom of the excavation (working level), a distance considered reasonable to guarantee satisfactory working conditions and the economy of the well execution.

The optimal solution was found with a pair of trenches with 7.5 m depth and 3.0 m below the working level as shown Figure 7.6. The coloured shades represent the different groundwater heads in the different nodes of the modelled mesh.

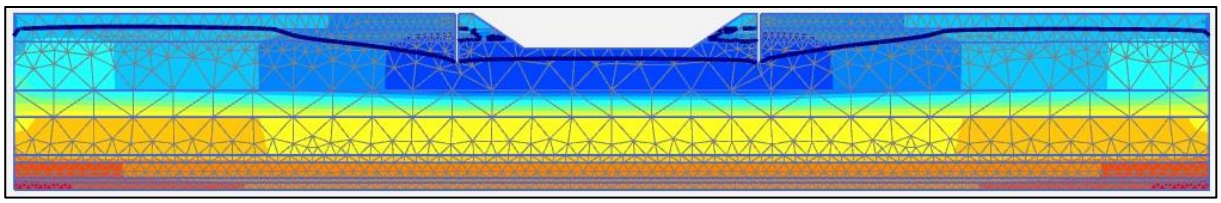

Figure 7.6 – Evolution of the water table position (adapted from Plaxis 2D)

This configuration of the trenches places the water table 1.30 m (z=17.20 m) below the working level (Figure 7.7) from an initial position at 2.95 m, which means a lowering of 4.25 m.

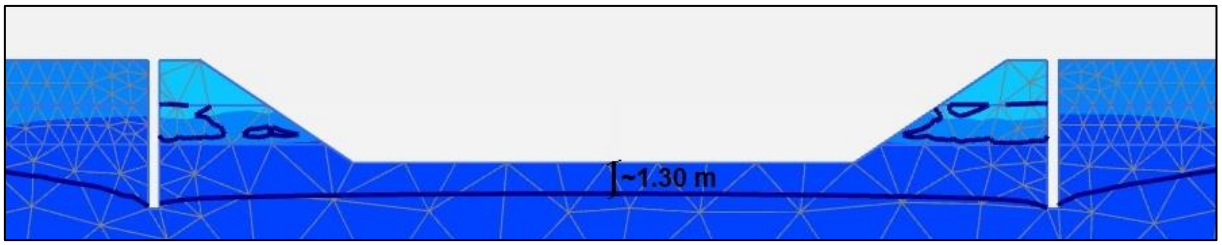

Figure 7.7 – Lowering level obtained with 7.5 length trenches (adapted from Plaxis 2D)

Between the trenches and the slopes, arose some irregular lines, displaying the same label as the water table that the author believes to be due to numeric errors.

Regarding the flow values around the bottom of the trenches, through the stress points it was possible to obtain the absolute mode flow as show in Figure 7.8 and Figure 7.9 and summarized in Table 7.1.

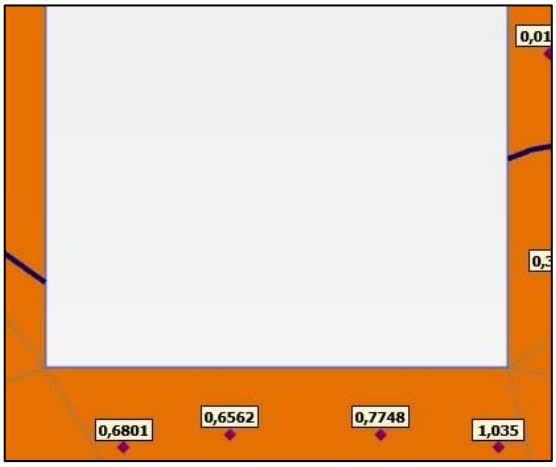

Figure 7.8 – Left trench |q| values (m^3/day/m) (adapted from Plaxis 2D)

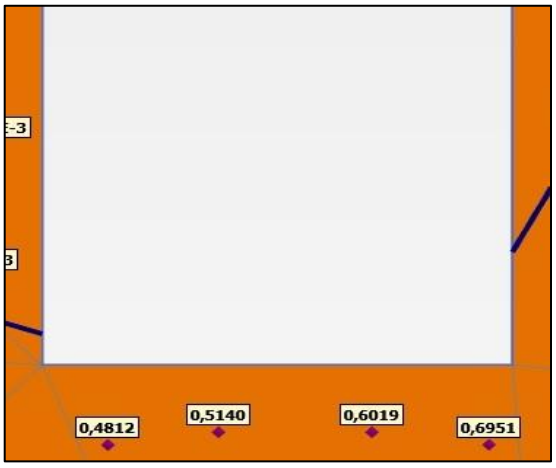

Figure 7.9 – Right trench |q| values (m^3/day/m) (adapted from Plaxis 2D)

Table 7.1 – Right trench |q| values (m^3/day/m)

|q|	Left trench	Right trench	Total
$\|q\|_{avg}$ (m^3/day/m)	0,7865	0,5731	1.3596
$\|q\|_{avg}$ (L/day/m)	786,53	573,05	1359.58
$\|q\|_{avg}$ (m^3/s/m)	9,103E-06	6,633E-06	1.574E-06

7.4. MANSUR AND KAUFMAN WELL FORMULA

The design of dewatering systems requires frequently the definition of complex models, not compatible with an initial estimative always needed in the scope of a project. For this kind of application, the empirical formulae remain very useful, albeit not completely accurate, to predict a possible drainage solution.

In this context, Mansur and Kaufman (1962) proposed various equations for different well configurations to estimate both the discharge Q (equation 7.1) and the maximum residual head h_d (equation 7.2). The presented equations apply to a narrow trench work (Figure 7.10), as the current case study.

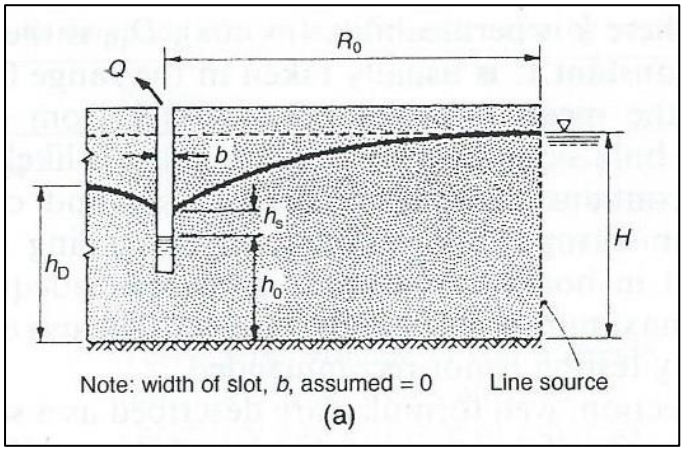

Figure 7.10 – Dewatering for trenchworks (Puller, 2003)

$$Q = \left[\left(0.73 + 0.27\frac{(H - h_0)}{H}\right)\frac{kx}{2R_o}(H^2 - h_0^2)\right], \quad (m^3/s\,/m) \tag{7.1}$$

where,

H is the height of the static water table (m);

h_0 is the height of the water table in wells (m);

k is the soil permeability (m/s)

x is the length of the trench (m);

R_o is the distance of the line source (m)

$$h_D = h_0 \left[\frac{1.48}{R_o}(H - h_0) + 1 \right], \quad (m) \tag{7.2}$$

Being H=21.45 m, h_0=15.5 m (considering there is no water at the bottom of the well), x=1 (discharge per meter out of plane), R_o=60 m (assuming the same influence width introduced in Plaxis 2D) and k_{eq}=7.046x10^{-6} m/s calculated according equation 7.3:

$$k_{eq} = \frac{k_s H_s + k_c H_c}{H_s + H_c} \quad (m/s) \tag{7.3}$$

where,

k_s is the sand coefficient of permeability;

k_c is the clay coefficient of permeability;

H_s is the total height of sand strata;

H_c is the total height of clay strata.

The values of Q and h_D are summarized in Table 7.2.

Table 7.2 – Hand calculation results

Mansur and Kaufman	
Q (m^3/s/m)	1.039E-05
Q (L/day/m)	897.79
h_D (m)	17.77

7.5. COMPARISON AND DISCUSSION OF THE OBTAINED RESULTS

Again, the two analysed methodologies differ from each other mainly on its nature, being the comparison of results a way to frame the obtained results and eventually a validation for the numerical modelling, considering the empirical formulae are based on experimental results. The Table 7.3 present the results obtained through the two methods.

Table 7.3 – Comparison between both methods

	Plaxis 2D	Hand Calculation
Q_{avg} (L/day/m)	679.79	897.79
h_D (m)	17.20	17.77

The hand calculated discharged led to value around 30% higher than the obtained via Plaxis 2D, which can be considered a satisfactory range bearing in mind the different formulations behind the methods.

Regarding the total head between the wells, the values are very similar with the empirical solution being again greater (around 3%).

8
CONCLUSIONS

The present work sought to answer the requirements of a geotechnical project, according to the established objectives of the dissertation.

Initially, a soil characterization was performed using CPTU data, the unique *in situ* test provided. Considering the last approaches (Robertson, 2009) on CPT/CPTU test interpretation, the mechanical and deformability parameters of the soil were estimated, assuming some simplifications in its application. Still in the geotechnical framework, the lack of a load test prevented a more accurate Young's modulus evolution with depth, since no calibration was available to fundament the local correlation for the α parameter.

A bibliographical review was carried out in order to apply some design methodologies to the specific case study. The design approaches are numerous and the choice was done based on its representativeness in the scope of pile design. Actually, a geotechnical study is associated with some unpredictability taking into account the variability of its main object of study, the soil.

In this way, the selected methods for bearing capacity analysis are two (EC7 Approach based on Dutch method and LCPC method) of the most consecrated procedures in the current geotechnical design. Moreover, the calculation by two different ways allowed the perception of the values range and also the sensitivity to understand whether the methodologies are conservative or not. Thus, the EC7 approach proved to be more conservative when compared with the French method and the OMEGA piles solution more economical than CFA.

To assess the piled raft settlements, an empirical geotechnical approach (Interaction Factor Method) was compared with a 3D model defined in structural software AxisVM. Regarding these analyses, some conclusions must be drawn, recalling subchapter 5.4:

- A structural program is not able to reproduce the interaction between the piles imbedded in the soil, neglecting then a percentage of the effective pile settlement;
- An empirical method is naturally conservative considering the simplifications behind its formulation, leading to higher settlements.

The final objective of the thesis was the design of a possible dewatering system, considering the high position of the phreatic level. To perform such calculations, Plaxis 2D and a classic formulation were used. In both cases, the soil permeability was the parameter to be defined. Since no grain size distribution curves were provided, this parameter was determined based on standard values available on specific bibliography.

REFERENCES

AFNOR DTU-13.2 (1992). *Foundations Profondes pour le Bâtiment*. 11-212. (in French)

Almeida Neto, J.A. (2002). *Análise do Desempenho de Estacas Hélice Contínua e Ômega – Aspectos Executivos*. Master Thesis, EPUSP. São Paulo, Brazil. (in Portuguese)

AxisVM – Structural Analysis & Design Software (2013). http://axisvm.eu (Accessed in May 2013).

Begemann, H.K.S. (1965). *The friction jacket cone as an aid in determining the soil profile*. Proceedings of the 6th International Conference on Soil Mechanics and Foundation Engineering, 17-20. Montreal, Canada.

Bustamante, M. and Frank, R. (1999). *Current French design practice for axially loaded piles*. Ground engineering, 38-44.

Bustamante, M. and Gianeselli, L. (1982). *Pile Bearing Capacity Prediction by Means of Static Penetrometer CPT*. Proceedings, 2nd European Symposium on Penetration Testing, Vol. 2, 493-500.

Bustamante, M. and Gianeselli, L. (1996). *Recommandations pour la préparation d'un essai de chargement statique de pieu instrumenté à l'aide d'un extensomètre LPC*. Techniques et méthodes des Laboratoires des Ponts et Chaussées. Méthode. (in French)

Bustamante, M., Gambin, M. and Gianeselli, L (2009). *Pile Design at Failure Using the Ménard Pressuremeter: an Up-Date.* Contemporary Topics in In Situ Testing, Analysis, and Reliability of Foundations, 127-134.

Brown, D.A. (2005). *Practical considerations in the selection and use of continuous flight auger and drilled displacement piles*. Geotechnical Special Publication, ASCE, 129251-129261.

Brown, D.A., Dapp, S.D., Thompson, W.R. and Lazarte, C.A. (2007). *Design and Construction of Continuous Flight Auger Piles*. US Department of Transportation, FHWA.

Campanella, R.G., Gillespie, D. and Robertson, P.K. (1982). *Pore pressures during cone penetration testing*. Proceedings of the 2nd European Symposium on Penetration Testing. A.A. Balkema. 507-512.

CEN (1999). *EN 1536 Execution of special geotechnical work – Bored piles*.

CEN (2004). *EN 1992-1-1 Eurocode 2: Design of concrete structures - Part 1-1: General rules and rules for buildings.*

CEN (2004). *EN 1997-1 Eurocode 7 - Geotechnical design - Part 1: General rules.*

CEN (2007). *EN 1997-2 Eurocode 7 - Geotechnical design - Part 2: Ground investigationand testing.*

de Ruiter, J. and Beringen, F.L. (1979). *Pile Foundations for Large North Sea Structures*. Marine Georesources & Geotechnology, Vol. 3, No. 3, 267-314.

FASCICULE No 62 – Titre V (1993). *Règles techniques de conception et de calcul des fondation des ouvrages de génie civil*. Cahier des clauses techniques générales applicables aux marchés publics de travaux, No 93–3 T.O. (in French)

Fernandes, D. (2011). *Definição de Curvas de Transferência de Carga de Estacas em Solo Residual do Granito*. Master Thesis, FEUP. Porto, Portugal. (in Portuguese)

Gyalog, L. (2005). *Magyarország fedett földtani térképéhez (az egységek rövid leírása)*. Magyar Földtani és Geofizikai Intézet. Budapest, Hungary. (in Hungarian)

Junttan. Respecting Ground (2013). http://www.junttan.com/piling_solutions (Accessed in March 2013).

Kulhawy, F.H. and Mayne, P.W. (1990). *Manual on Estimating Soil Properties for Foundation Design*. Geotechnical Engineering Group, Cornell University. Ithaca, New York, USA.

Lakatos, I. (2011). *Cölöpalapok méretezése az Eurocode 7 követelményei szerint*. PhD Thesis, BME. Budapest, Hungary. (in Hungarian)

Lopes, F.R. (2000). *Design of raft foundations on Winkler springs*. Vol. Design applications of raft foundations.

Lunne, T., Robertson, P.K. and Powell, J.J.M. (1997). *Cone Penetration Testing in Geotechnical Practice*. Blackie Academic & Professional. London, United Kingdom.

Mahler, A. (2007). *Settlement Prediction of CFA Piles Based on CPTu Results*. BME. Budapest, Hungary.

Mandolini, A. and Viggiani, C. (1997). *Settlement of Piled Foundations*. Geotechnique no. 47 (4), 791-816.

Mansur, C. and Kaufman, R. (1962). *Dewatering. Foundation engineering*. Foundation Engineering, 241-350.

Matos Fernandes, M. (2006). *Mecânica dos Solos – Conceitos e Princípios Fundamentais*. FEUP edições. Porto, Portugal. (in Portuguese)

Matos Fernandes, M. (2011). *Mecânica dos Solos – Introdução à Engenharia Geotécnica*. FEUP edições. Porto, Portugal. (in Portuguese)

Mayne, P.W. (2007). *Cone Penetration Testing State-Of-Practice*. Transportation Research Board, Vol. 368.

Mayne, P.W. and Schneider, J.A. (2001). *Evaluating Axial Drilled Shaft Response by Seismic Cone*. Foundations & Ground Improvement, GSP 113, ASCE, 655-669.

Poulos, H.G. (1987). *From theory to practice in pile design*. Vol. 55, No. 9.

Poulos, H.G. (2006). *Pile Group Settlement Estimation – Research To Practice*. Geotechnical Special Publication 153.

Poulos, H.G. and Davis, E.H. (1980). *Pile Foundation Analysis and Design*. No. Monograph.

Puller, M. (2003). *Deep Excavations: a practical manual*. Thomas Telford, ASCE.

Robertson, P.K. (1990). *Soil classification using the cone penetration test*. Canadian Geotechnical Journal, 27(1), 151-158.

Robertson, P.K. (2009). *Interpretation of cone penetration tests-a unified approach*. Canadian Geotechnical Journal 46.11, 1337-1355.

Robertson, P.K. (2012). *Interpretation of in-situ tests – some insights*. Mitchell Lecture - ISC'4 Brazil, Sept., 2012. Gregg Drilling & Testing, Inc. Signal Hill, California, USA.

Robertson, P.K., and Campanella, R.G. (1983). *Interpretation of cone penetration tests – Part I: sand*. Canadian Geotechnical Journal, 20(4), 718-733.

Robertson, P.K. and Cabal, K.L. (2012). *Guide to Cone Penetration Testing for Geotechnical Engineering*. Gregg Drilling & Testing, Inc. Signal Hill, California, USA.

Robertson, P.K., Campanella, R.G., Gillespie, D. and Greig, J. (1986). *Use of piezometer cone data*. Proceedings of the ASCE Speciality Conference In Situ '86: Use of In Situ Tests in Geotechnical Engineering, ASCE, 1263-1280. Blacksburg, Virginia, USA.

Rocscience (2013). http://www.rocscience.com/settlecalc/schmerthelp.html (Accessed in April 2013).

Schmertmann, J.H. (1970). *Static cone to compute settlement over sand*. Journal of the Soil Mechanics Engineering Division, ASCE, Vol. 96, No. 3, 1011-1043.

Senneset, K. and Janbu, N. (1985). *Shear strength parameters obtained from static cone penetration tests. Strength Testing of Marine Sediments: Laboratory and In-Situ Measurements*. Symposium, ASTM Special technical publication, STP 883, 41-54.

Senneset, K. and Nestvold, J. (1992). *Deep Compaction by Vibro Wing Technique and Dynamic Compaction*. Geotechnical Special Publication, ASCE, Vol. 2, No. 30, 889-901.

Viana da Fonseca, A. and Santos, J. (2008). *International Prediction Event on the Behaviour of Bored, CFA and Driven Piles in CEFEUP/ISC'2 Experimental Site – 2003*. Final Report. FEUP edições. Porto, Portugal.

Viana da Fonseca, A, Buttling, S. and Coutinho, R.Q. (2012). *Foundations: Shallow and Deep Foundations, Unsaturated Conditions, Heave and Collapse, Monitoring and Proof Testing*. Vol. Handbook of Tropical Residual Soils Engineering. CRC Press. London, United Kingdom.

Winkler, E. (1867). *Die Lehre von der Elastizitat und Festigkeit*. Dominicus. Prague, Czech Republic. (in German)

Zhang, G., Robertson, P.K. and Brachman, R.W.I. (2002). *Estimating liquefaction-induced ground settlements from CPT for level ground.* Canadian Geotechnical Journal, 39(5), 1168–1180.

APPENDIX A

A.1. CHARACTERISTIC AND DESIGN LOADS

Table A.1 – Piles data

Column Code	Pile Number	Pile Diameter	x (m)	y (m)	E_d (kN)	E_k (kN)
A5	1	0,60	12,23	20,90	1616,31	1154,51
A6	1	0,60	15,84	20,90	1832,29	1308,78
A7	1	0,60	19,44	20,90	1718,32	1227,37
A8	1	0,60	23,04	20,90	1922,30	1373,07
A9	1	0,60	26,63	20,90	1738,24	1241,60
A10	1	0,60	30,23	20,90	2066,09	1475,78
A11	1	0,60	33,83	20,90	1922,43	1373,16
A12	1	0,60	37,43	20,90	2157,01	1540,72
A13	1	0,60	41,03	20,90	1916,63	1369,02
A14	1	0,60	44,63	20,90	1976,63	1411,88
A15	1	0,60	48,23	20,90	1588,82	1134,87
B1	1	0,60	0,20	20,34	1338,44	956,03
B2	1	0,60	3,50	20,34	1626,28	1161,63
B4	1	0,60	8,15	20,34	1851,85	1322,75
B5	1	0,60	12,23	20,34	1740,94	1243,53
B16	1	0,60	50,03	20,34	1753,83	1252,74
B17	1	0,60	51,83	20,34	1437,91	1027,08
C11	1	0,60	0,20	17,71	1339,41	956,72
C12	1	0,60	3,50	17,71	1337,70	955,50
C13	1	0,60	6,30	17,34	1276,78	911,99
C14	1	0,60	7,67	17,34	1520,65	1086,18
C15	1	0,60	12,23	17,19	1952,84	1394,89
C21	1	0,60	0,20	14,25	1377,66	984,04
C22	1	0,60	3,50	14,25	1454,28	1038,77
C23	1	0,60	6,30	14,25	1543,56	1102,54
C24	1	0,60	7,67	14,25	1493,77	1066,98
C25	1	0,60	12,23	14,25	2246,79	1604,85
C26	1	0,60	14,94	14,20	1860,26	1328,75
	2	0,60	16,74	14,20	1860,26	1328,75

C28	1	0,60	22,14	15,10	1424,60	1017,57
	2	0,60	23,94	15,10	1424,60	1017,57
	3	0,60	23,94	13,30	1424,60	1017,57
	4	0,60	22,14	13,30	1424,60	1017,57
C210	1	0,60	29,33	15,10	1425,60	1018,28
	2	0,60	31,13	15,10	1425,60	1018,28
	3	0,60	31,13	13,30	1425,60	1018,28
	4	0,60	29,33	13,30	1425,60	1018,28
C212	1	0,60	36,53	15,10	1421,96	1015,69
	2	0,60	38,33	15,10	1421,96	1015,69
	3	0,60	38,33	13,30	1421,96	1015,69
	4	0,60	36,53	13,30	1421,96	1015,69
C214	1	0,60	43,73	14,20	1867,35	1333,82
	2	0,60	45,53	14,20	1867,35	1333,82
C215	1	0,60	47,33	14,24	1161,20	829,43
	2	0,60	49,13	14,24	1161,20	829,43
C217	1	0,60	51,83	14,24	1473,25	1052,32
C31	1	0,60	0,20	8,34	1549,27	1106,62
C32*	1	0,60	4,45	8,34	1506,02	1075,73
C33	1	0,60	6,30	8,34	1763,11	1259,36
C34	1	0,60	7,67	8,34	1727,86	1234,19
C35	1	0,60	12,23	8,34	2180,58	1557,56
C41	1	0,60	0,20	5,27	1517,45	1083,89
C42*	1	0,60	4,45	5,27	1507,82	1077,01
C43	1	0,60	6,30	5,27	1379,09	985,06
C44	1	0,60	7,67	5,27	1464,25	1045,89
C45	1	0,60	12,23	5,27	1939,73	1385,52
C51	1	0,60	0,20	2,24	1558,82	1113,44
C52*	1	0,60	4,45	2,24	1549,35	1106,68
C54	1	0,60	7,67	2,24	1626,74	1161,96
C55	1	0,60	12,23	2,24	1927,27	1376,62
D5	1	0,60	12,23	0,20	1768,92	1263,51
D6	1	0,60	15,84	0,20	1980,25	1414,46
D7	1	0,60	19,44	0,20	2058,84	1470,60
D8	1	0,40	22,44	0,20	1145,02	817,87
	2	0,40	23,64	0,20	1145,02	817,87
D9	1	0,60	26,63	0,20	2099,97	1499,98
D10	1	0,60	29,33	0,20	1215,21	868,01
	2	0,60	31,13	0,20	1215,21	868,01
D11	1	0,60	33,83	0,20	2078,18	1484,41
D12	1	0,60	37,43	0,20	2195,62	1568,30
D13	1	0,60	41,03	0,20	1886,86	1347,76
D14	1	0,60	44,63	0,20	1766,67	1261,91
D15	1	0,60	48,23	0,20	1324,92	946,37
E117	1	0,60	51,83	17,19	1453,01	1037,86
E415	1	0,60	48,23	9,31	1423,57	1016,84
E416	1	0,60	50,03	9,31	1289,41	921,01
E417	1	0,40	51,83	9,31	1051,28	750,91
E56	1	0,60	14,94	7,80	1922,53	1373,24
	2	0,60	16,74	7,80	1922,53	1373,24

E58	1	0,60	22,14	8,70	1486,18	1061,55
	2	0,60	23,94	8,70	1486,18	1061,55
	3	0,60	23,94	6,90	1486,18	1061,55
	4	0,60	22,14	6,90	1486,18	1061,55
E510	1	0,60	29,33	8,70	1503,17	1073,69
	2	0,60	31,13	8,70	1503,17	1073,69
	3	0,60	31,13	6,90	1503,17	1073,69
	4	0,60	29,33	6,90	1503,17	1073,69
E512	1	0,60	36,53	8,70	1506,98	1076,41
	2	0,60	38,33	8,70	1506,98	1076,41
	3	0,60	38,33	6,90	1506,98	1076,41
	4	0,60	36,53	6,90	1506,98	1076,41
E514	1	0,60	43,73	7,80	1927,94	1377,10
	2	0,60	45,53	7,80	1927,94	1377,10
E615	1	0,60	48,23	6,36	1713,04	1223,60
E616	1	0,60	50,03	6,36	1290,34	921,67
E617	1	0,60	51,83	6,36	1326,40	947,43
E715	1	0,60	48,23	2,00	1417,32	1012,37
E716	1	0,60	50,03	2,00	1435,18	1025,13
E717	1	0,60	51,83	2,00	1333,55	952,54

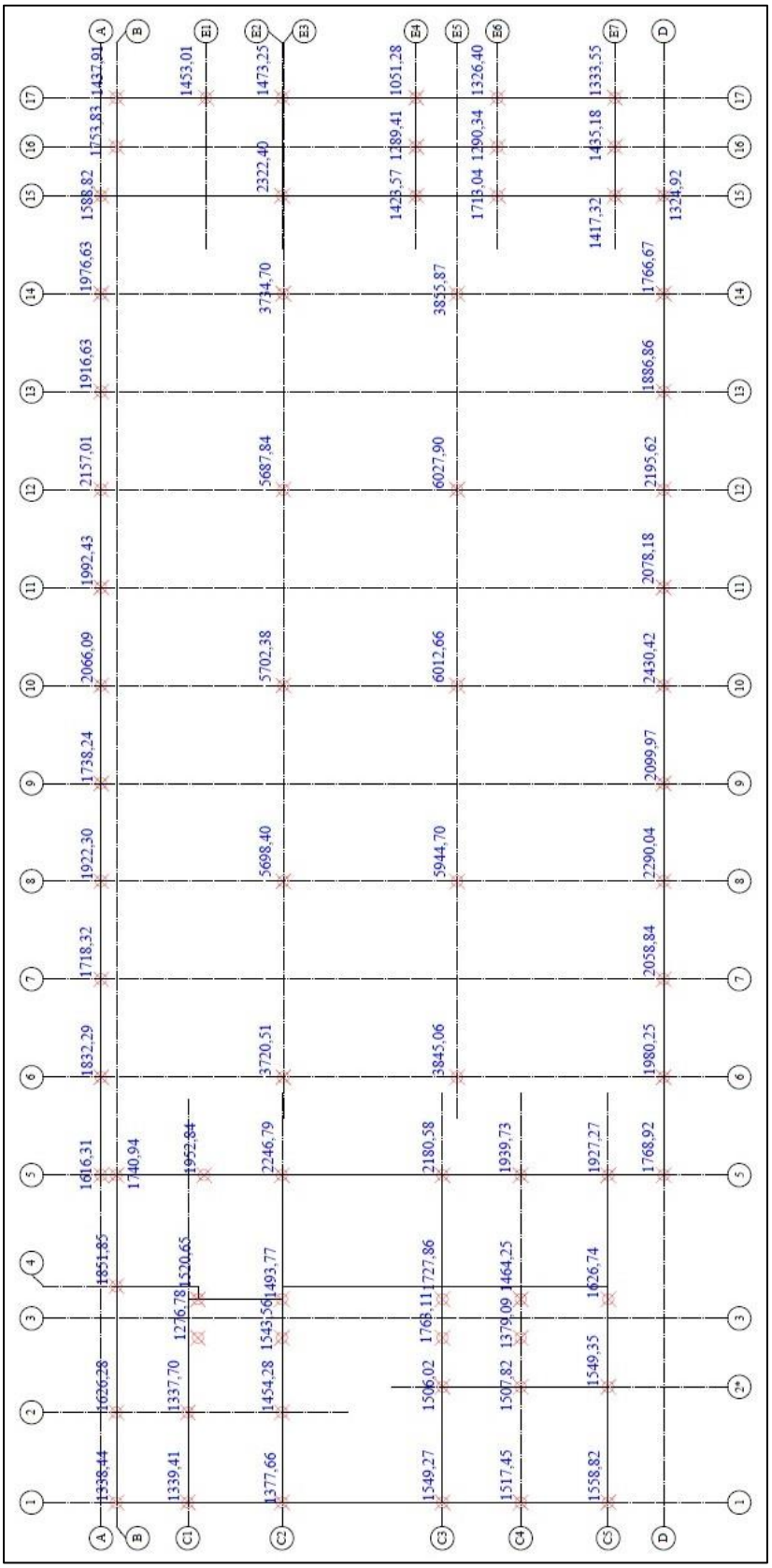

Figure A.1 – Representation of the design loads over the respective column

A.2. SCHMERTMANN METHOD RESULTS

Table A.2 – Schmertmann Method results for CPT1

z (m)	z/B	γ (kN/m^3)	σ'$_{vp}$ (kPa)	$I_{\varepsilon p,s}$	$I_{\varepsilon s}$	$I_{\varepsilon p,c}$	$I_{\varepsilon c}$	I_{ε}	$I_{\varepsilon med}$	h_j (m)	E (MPa)	s_j (m)
0.000	0.00	18	0.00	0.615	0.100	0.581	0.200	0.117				
									0.204	0.400	33.69	0.0003
0.400	0.02	18	3.28	0.615	0.120	0.581	0.207	0.135				
									0.220	1.300	40.35	0.0008
1.700	0.08	16.7	12.23	0.615	0.186	0.581	0.232	0.194				
									0.271	4.200	61.91	0.0020
5.900	0.29	18	46.63	0.615	0.399	0.581	0.310	0.384				
									0.320	1.000	82.30	0.0004
6.900	0.34	16.7	53.52	0.615	0.450	0.581	0.329	0.429				
									0.360	3.275	99.05	0.0013
10.175	0.50	18	80.34	0.615	0.615	0.581	0.390	0.577				
									0.406	1.695	118.54	0.0006
11.870	0.58	18	94.23	0.615	0.582	0.581	0.422	0.554				
									0.501	8.480	158.42	0.0029
20.35	1.00	18	163.68	0.615	0.410	0.581	0.580	0.440				
									0.484	20.350	271.44	0.0039
40.70	2.00	18	330.34	0.615	0.000	0.581	0.387	0.067				
									0.370	3.640	365.48	0.0004
44.34	2.18	18	360.15	0.615	-0.073	0.581	0.352	0.000				
											s (mm)	12.45
											k (kN/m^3)	**8602.57**

Table A.3 – Schmertmann Method results for CPT2

z (m)	z/B	γ (kN/m^3)	σ'$_{vp}$ (kPa)	$I_{\varepsilon p,s}$	$I_{\varepsilon s}$	$I_{\varepsilon p,c}$	$I_{\varepsilon c}$	I_{ε}	$I_{\varepsilon med}$	h_j (m)	E (MPa)	s_j (m)
0.000	0.00	18	0.00	0.618	0.100	0.582	0.200	0.117				
									0.204	0.400	33.69	0.0003
0.400	0.02	18	3.28	0.618	0.120	0.582	0.208	0.135				
									0.217	1.000	39.18	0.0006
1.400	0.07	16.7	10.17	0.618	0.171	0.582	0.226	0.181				
									0.268	4.500	60.74	0.0021
5.900	0.29	18	47.02	0.618	0.400	0.582	0.311	0.385				
									0.343	3.500	92.10	0.0014
9.400	0.46	16.7	71.14	0.618	0.578	0.582	0.376	0.543				
									0.384	0.775	108.85	0.0003
10.175	0.50	18	77.48	0.618	0.618	0.582	0.391	0.578				
									0.407	1.695	118.54	0.0006
11.870	0.58	18	91.37	0.618	0.584	0.582	0.423	0.556				
									0.502	8.480	158.42	0.0029
20.35	1.00	18	160.82	0.618	0.412	0.582	0.581	0.441				
									0.484	20.350	271.44	0.0039
40.70	2.00	18	327.48	0.618	0.000	0.582	0.387	0.067				
									0.370	3.640	365.48	0.0004
44.34	2.18	18	357.29	0.618	-0.074	0.582	0.353	0.000				
											s (mm)	12.45
											k (kN/m^3)	**8599.39**

Table A.4 – Schmertmann Method results for CPT3

z (m)	z/B	γ (kN/m^3)	σ'$_{vp}$ (kPa)	$I_{\varepsilon p,s}$	$I_{\varepsilon s}$	$I_{\varepsilon p,c}$	$I_{\varepsilon c}$	I_{ε}	$I_{\varepsilon med}$	h_j (m)	E (MPa)	s_j (m)
0.000	0.00	18	0.00	0.615	0.100	0.581	0.200	0.117				
									0.206	0.600	34.47	0.0004
0.600	0.03	18	4.91	0.615	0.130	0.581	0.211	0.144				
									0.219	0.800	39.96	0.0005
1.400	0.07	16.7	10.43	0.615	0.171	0.581	0.226	0.180				
									0.308	8.775	77.49	0.0037
10.175	0.50	18	82.29	0.615	0.615	0.581	0.390	0.577				
									0.406	1.695	118.54	0.0006
11.870	0.58	18	96.18	0.615	0.582	0.581	0.422	0.554				
									0.501	8.480	158.42	0.0029
20.35	1.00	18	165.63	0.615	0.410	0.581	0.580	0.440				
									0.484	20.350	271.44	0.0039
40.70	2.00	18	332.29	0.615	0.000	0.581	0.387	0.067				
									0.370	3.640	365.48	0.0004
44.34	2.18	18	362.10	0.615	-0.073	0.581	0.352	0.000				
											s (mm)	12.45
											k (kN/m^3)	**8662.14**